



# Primary cilia on colonic mesenchymal cells regulate DSS-induced colitis and inflammation associated colon carcinogenesis

Ruizhi Tang

## ► To cite this version:

Ruizhi Tang. Primary cilia on colonic mesenchymal cells regulate DSS-induced colitis and inflammation associated colon carcinogenesis. Human health and pathology. Université Montpellier, 2017. English. NNT : 2017MONTT020 . tel-01680051

**HAL Id: tel-01680051**

**<https://theses.hal.science/tel-01680051>**

Submitted on 10 Jan 2018

**HAL** is a multi-disciplinary open access archive for the deposit and dissemination of scientific research documents, whether they are published or not. The documents may come from teaching and research institutions in France or abroad, or from public or private research centers.

L'archive ouverte pluridisciplinaire **HAL**, est destinée au dépôt et à la diffusion de documents scientifiques de niveau recherche, publiés ou non, émanant des établissements d'enseignement et de recherche français ou étrangers, des laboratoires publics ou privés.

# THÈSE

Pour obtenir le grade de  
**Docteur**

**Délivré par l'Université de Montpellier**

**Préparée au sein de l'école doctorale Science  
Chimiques et Biologiques de la Santé  
Et de l'unité de recherche L'institut de  
Génétique Moléculaire de Montpellier**

**Spécialité : Biochimie et biologie moléculaire**

**Présentée par Ruizhi TANG**

**Primary cilia on colonic mesenchymal cells  
regulate DSS-induced colitis and inflammation  
associated colon carcinogenesis**

**Soutenue le 4 juillet 2017 devant le jury composé de**

Mr Jean-Paul Borg, Dr, CRCM

Mr Jean-Paul Borg, Dr, CRCM

Mr Giorgio Stassi, Dr, University of Palermo

Mr Carsten JANKE, Dr, Institut Curie

Mr Michael HAHNE, Dr, IGMM

Présidente du Juy

Rapporteur

Rapporteur

Examineur

Directeur de thèse



**Titre en français :** Régulation de la colite induite par DSS et de la carcinogenèse du côlon associée à l'inflammation par les cils primaires des cellules mésenchymateuses du côlon

**Résumé en français**

La glycylation, une modification post-traductionnelle des microtubules, est cruciale dans le maintien des cils primaires. Notre groupe a précédemment identifié un rôle inattendu de la tubuline glycyrase TTLL3 dans la régulation de l'homéostasie du colon et de la tumorigénèse. Plus précisément, une diminution du nombre de cils primaires a été observée chez les souris déficientes pour la glycyrase TTLL3, qui est la seule glycyrase exprimée dans le côlon. Les souris TTLL3 - / - ne présentent pas d'anomalie évidente à l'état stationnaire. Cependant, lorsqu'elles sont exposées à une carcinogenèse du côlon chimiquement induite, les souris TTLL3 - / - sont plus sensibles à la formation de tumeurs. Il est important de noter que les niveaux d'expression de TTLL3 sont significativement réduits dans les carcinomes primaires et métastases colorectales chez l'homme comparativement au tissu de côlon sain, ce qui suggère un lien entre la régulation des cils primaires par TTLL3 et le développement du cancer colorectal.

L'objectif de mon projet de thèse était d'explorer l'effet de la modulation des cils primaires sur la carcinogenèse du côlon. J'ai ainsi démontré que le

nombre de cils primaires diminue lors de la carcinogénèse du côlon chimiquement induite chez la souris. Notamment, j'ai découvert que les cils primaires du côlon sont principalement exprimés par les cellules mésenchymateuses. Pour mieux caractériser le rôle des cils primaires dans le côlon murin, j'ai étudié les conséquences de leur perte dans les cellules mésenchymateuses intestinaux. Pour cela, j'ai utilisé deux modèles de souris KO conditionnelles, pour la kinesin-3A (Kif3A) et le transport intra-flagellaire 88 (Ift88), deux molécules essentielles pour la formation des cils. Leur délétion spécifique dans les cellules mésenchymateuses intestinaux est obtenue par croisement des souches de souris Kif3A<sup>fl/fl</sup> et Ift88<sup>fl/fl</sup> des souris transgéniques collagène VI-cre. Bien que le promoteur collagène VI ne soit actif que dans un sous-ensemble de cellules mésenchymateuses coliques, j'ai constaté que la diminution du nombre de cils primaires dans ces derniers favorise la colite chimiquement induite et la carcinogénèse. L'analyse par séquençage ARN des cellules mésenchymateuses coliques isolées de souris mutantes suggère un déclenchement de la signalisation Wnt et Notch chez les souris ColVIcre-Kif3A<sup>fl/fl</sup>. Nous confirmons actuellement ces résultats par qPCR et immunohistochimie.

**Titre en anglais:** Primary cilia on colonic mesenchymal cells regulate DSS-induced colitis and inflammation associated colon carcinogenesis

### **Résumé en anglais**

Glycylation, a posttranslational modification of microtubules, is crucial in the maintenance of PC. Our group previously identified an unexpected role of the tubulin glycyclase TTLL3 in the regulation of colon homeostasis and tumorigenesis. Specifically, a decreased number of primary cilia (PC) was observed in mice deficient for the glycyclase TTLL3, which is the only glycyclase expressed in the colon. TTLL3<sup>-/-</sup> mice display no obvious abnormalities in the steady state. However, when exposed to chemically induced colon carcinogenesis, TTLL3<sup>-/-</sup> mice are more susceptible to tumor formation. Importantly, TTLL3 expression levels were significantly downregulated in human primary colorectal carcinomas and metastases as compared to healthy colon tissue, suggesting a link between TTLL3 regulation of PC and colorectal cancer development.

The aim of my thesis project was to explore the relation of PC and colon carcinogenesis. In fact, I could demonstrate that the number of PC decreases during chemically induced colon carcinogenesis in mice. Notably, I discovered that PC in the colon are mostly expressed by fibroblasts. To better characterize the role of PC in murine colon, I

studied the consequences of a loss of PC in intestinal fibroblasts. For this, I used two independent ciliary conditional knockout mice, kinesin-3A (Kif3A) and intraflagellar transport 88 (Ift88), both essential for cilia formation. Specific deletion in intestinal fibroblasts is obtained by crossing with colVI-cre transgenic mice. Though the colVI promoter is only active in a subset of colonic mesenchymal cells I found that the decreased number of PC in colonic mesenchymal cells promotes chemically induced colitis and carcinogenesis. RNAseq on isolated colonic mesenchymal cells of mutant mice suggests a triggering of *Wnt* and *Notch* signaling in ColVIcre-*Kif3a*<sup>flx/flx</sup> mice. We are presently validating these findings by qPCR and immunohistochemistry. Taken together, I discovered that PC are expressed by at least a subset of colonic mesenchymal cells, which has not been described before. Decreased numbers of those PC renders mice more susceptible to colitis and colitis associated carcinogenesis.

# Index

<b>1. Introduction.....</b>	<b>7</b>
<b>1.1. Primary cilia (PC) .....</b>	<b>7</b>
<b>1.1.1. Structure of PC .....</b>	<b>7</b>
<b>1.1.2. Intraflagellar transport.....</b>	<b>8</b>
<b>1.1.3. Microtubules (MTs).....</b>	<b>9</b>
<b>1.2. PC and cell cycle.....</b>	<b>13</b>
<b>1.3. PC and signaling pathways.....</b>	<b>16</b>
<b>1.4. PC and disease .....</b>	<b>19</b>
<b>1.5. Colon carcinoma .....</b>	<b>21</b>
<b>1.5.1. Colonic crypts and cell interactions .....</b>	<b>23</b>
<b>1.6. Mouse models for CRC .....</b>	<b>26</b>
<b>1.6.1. APC mouse model.....</b>	<b>26</b>
<b>1.6.2. AOM/DSS.....</b>	<b>27</b>
<b>2. Objectives .....</b>	<b>28</b>
<b>3. Results .....</b>	<b>34</b>
<b>3.1. Colonic mesenchymal cells express primary cilia (PC).....</b>	<b>34</b>
<b>3.2. Number of colonic PC decreases during murine colon carcinogenesis .....</b>	<b>39</b>
<b>3.3. Number of PC may increase in colorectal cancer (CRC) patient samples.....</b>	<b>42</b>
<b>3.4. Generation of mice deficient for PC in intestinal cell subsets..</b>	<b>45</b>

<b>3.5. Validation of mice deficient for PC in intestinal mesenchymal cells</b>	<b>48</b>
<b>3.6. Phenotype of mice deficient for PC in intestinal mesenchymal cells</b>	<b>51</b>
<b>3.7. Decreased number of PC in colonic mesenchymal cells promotes CAC</b>	<b>55</b>
<b>3.8. Decreased number of PC in colonic mesenchymal cells promotes DSS-induced colitis .....</b>	<b>58</b>
<b>3.9. ColVICre-Kif3a<sup>flx/flx</sup> colonic mesenchymal cells display an altered molecular signature.....</b>	<b>60</b>
<b>3.10. ColVICre-Ift88<sup>flx/flx</sup> display less colonic PC and increased susceptibility to DSS-induced colitis .....</b>	<b>62</b>
<b>4. Discussion .....</b>	<b>65</b>
<b>5. Material and Methods .....</b>	<b>74</b>
<b>6. Reference .....</b>	<b>87</b>
<b>7. Annex.....</b>	<b>97</b>
<b>7.1. RNA seq analysis.....</b>	<b>97</b>
<b>7.2. CV .....</b>	<b>107</b>
<b>7.3. Involvement in other projects during my PhD.....</b>	<b>110</b>



# **1. Introduction**

## **1.1. Primary cilia (PC)**

### **1.1.1. Structure of PC**

Cilia are cell-extruding organelles based on a scaffold of microtubules (MTs), the axoneme, extruding mammalian cells (Figure 1). There are two types of cilia: motile and PC (also known as immotile cilia). Although the majority of motile cilia possess the 9+2 arrangement, and most PC have the 9+0 arrangement, but there are exceptions include '9+0' motile cilia in ependymal cells of zebrafish or '9+2' PC in inner ears of mice (Gerdes et al., 2009).

Motile cilia are expressed on specific cells such as airway epithelial cells. Their capacity to beat allows them to transport fluids across cells for example mucus on lung epithelial cells. In contrast, PC are expressed on most eukaryotic cells except immune cells. Generally, one cell expresses only one PC that is anchored to the cell via a basal body. Among different cell types, the length of the primary cilium can vary between 1 and 9  $\mu\text{m}$  (Dummer et al., 2016).

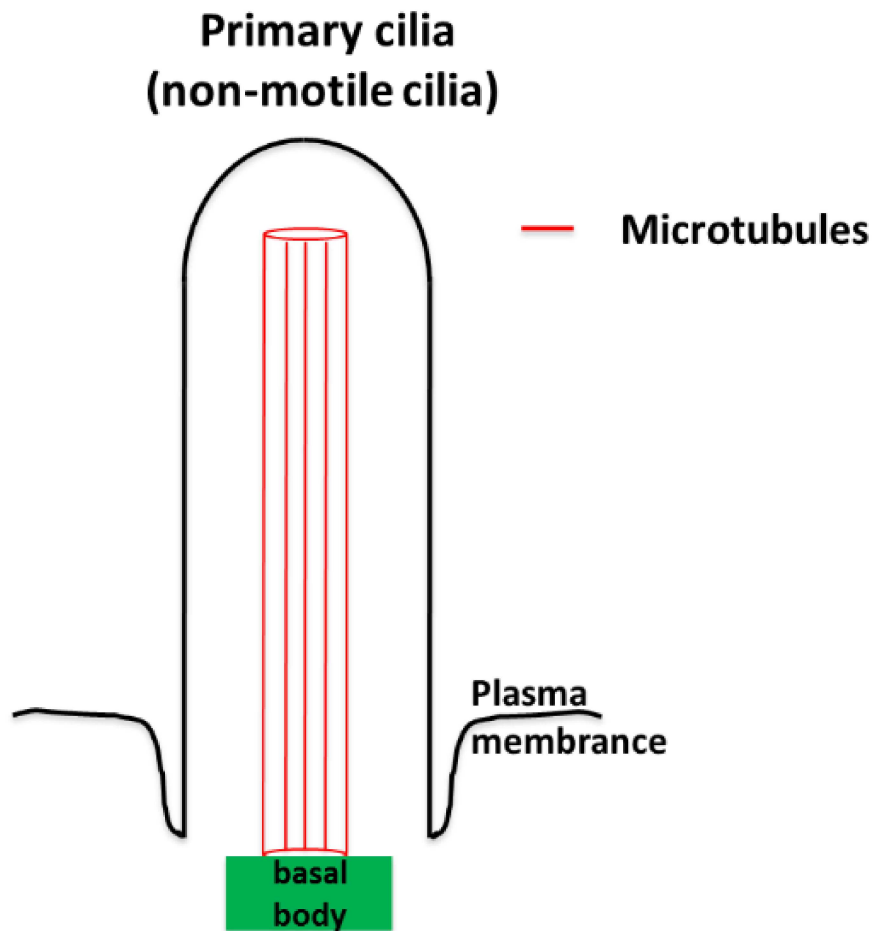
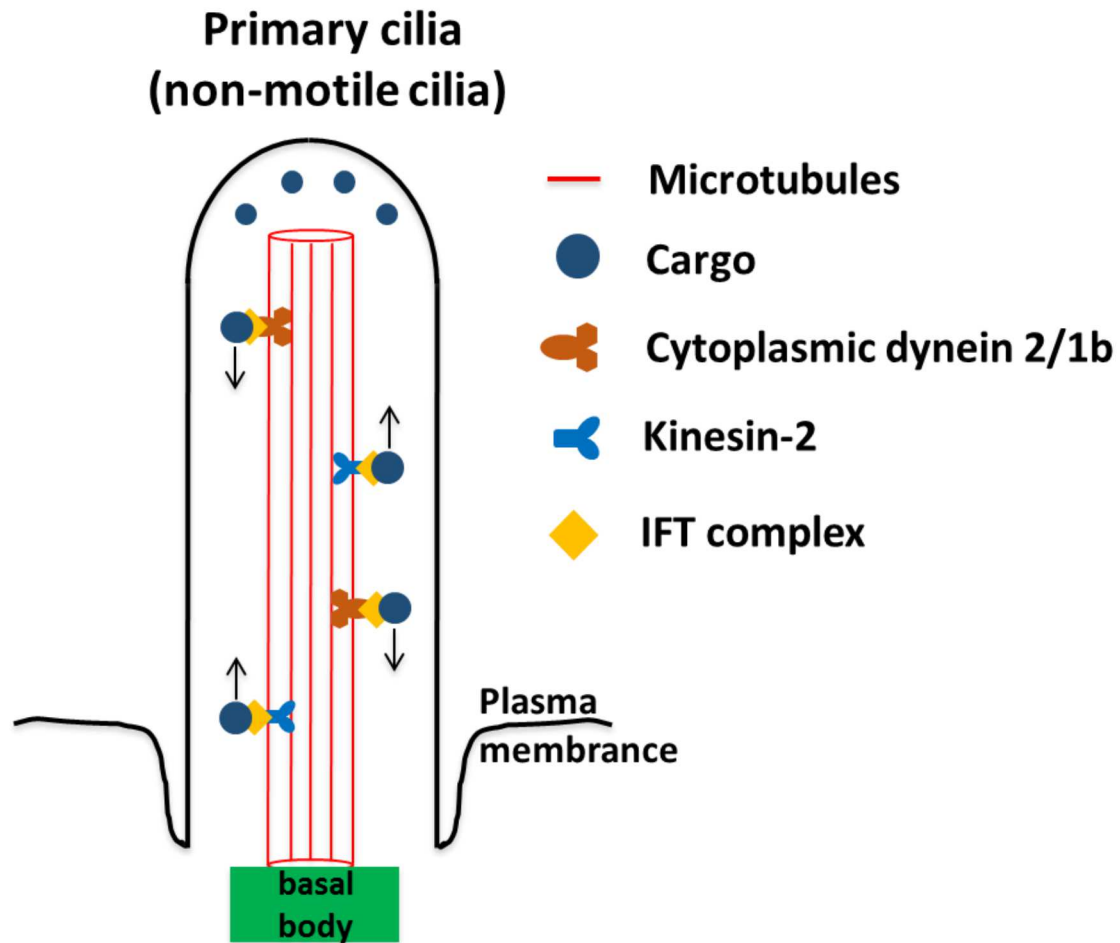


Figure 1 Structure of PC

### 1.1.2. Intraflagellar transport

Cilia are generated and maintained by IFT (intraflagellar transport) in which IFT cargoes are transported along axonemal microtubules by kinesin-II (anterograde) and cytoplasmic dynein 1 B (retrograde) (Figure 2). Deletion of KIF3A (subunit of kinesin) and IFT88 (subunit of IFT) are commonly used for PC knock-out (KO) mouse models.



**Figure 2** Movement of protein complex in PC

### **1.1.3. Microtubules (MTs)**

Besides regulating intracellular signaling via PC, MTs are essential for many physiological cellular functions, such as cell migration, cell division (i.e. proliferation) and the release of soluble factors. All these functions are involved in tumorigenesis, and MTs are a prime target in cancer chemotherapy. In fact, tubulin-binding agents are successfully employed to treat a range of solid cancers (Dumontet and Jordan, 2010).

MTs are formed by polymerized dimers that consist of an alpha and beta chain. The existence of different alpha and beta chains are thought to contribute to the large range of functions executed by MTs. MTs are very dynamic and have in general a half-life of about several minutes(Janke, 2014). Posttranslational modifications (PTMs), including acetylation, glycylation, detyrosination, glutamylation, are important regulators of function of MTs (Figure 3). Histone deacetylase 6 (HDAC6) catalyzes  $\alpha$ -tubulin deacetylation and is overexpressed in different tumor types and HDAC6 inhibitors are in the development for treatment of cancer patients.

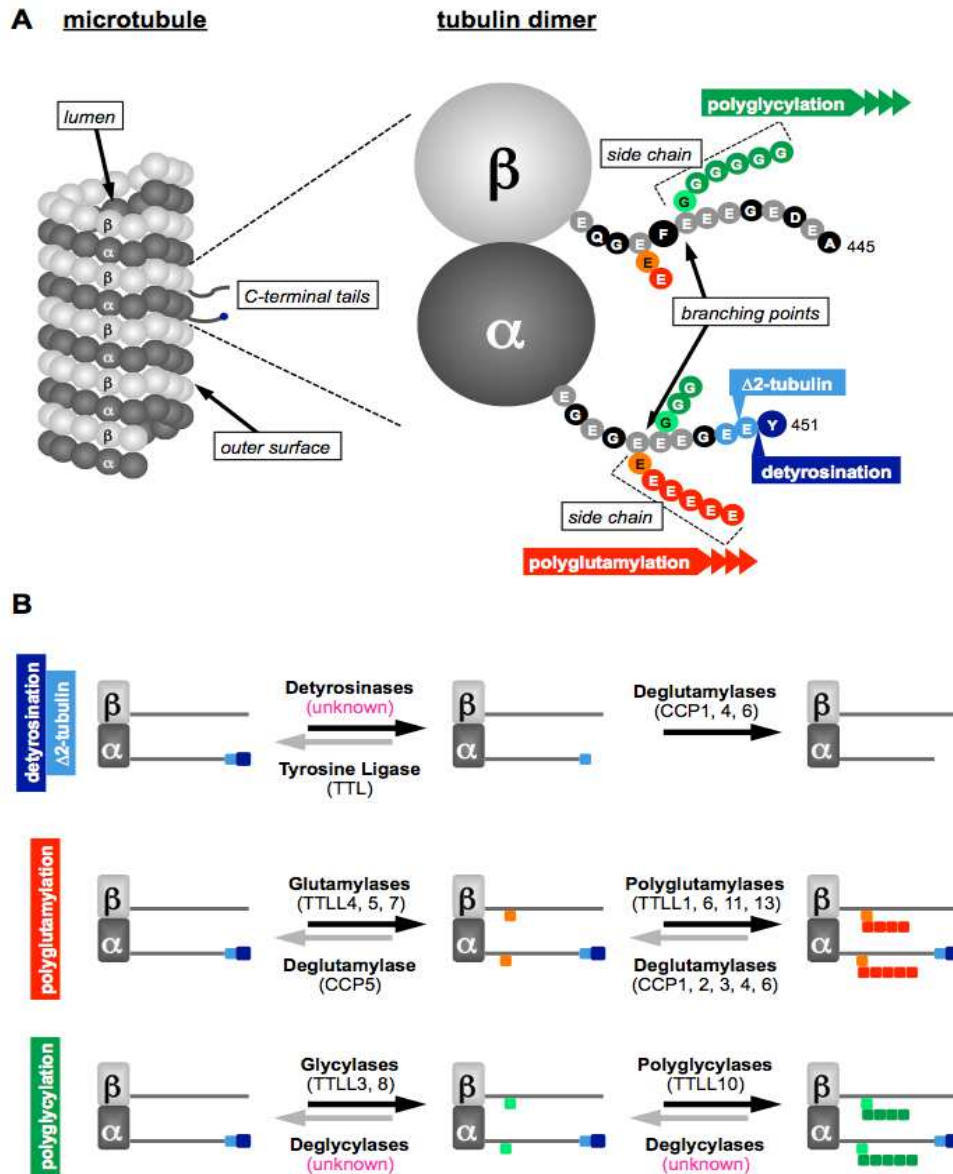


**Figure 3 Tubulin modifying enzymes and their specific PTM determine the tubulin code** (modified from Magiera and Janke, 2014).

(A) Schematic representation of the  $\alpha$ -tubulin- $\beta$ -tubulin dimer and its PTM. The carboxy-terminal tails of both tubulins are represented as amino acid sequences (which correspond to mouse  $\alpha$ 1A-tubulin (from residue 441 to the end) and  $\beta$ 2B-tubulin (from 432 to the end)). Both  $\alpha$ -tubulin and  $\beta$ -tubulin can be modified by polyglutamylation and polyglycylation on different Glu residues within those tails. Together with detyrosination at the C-terminus and the subsequent removal of the penultimate Glu residue (which generates  $\Delta$ 2-tubulin), these modifications are specific to the C-terminal tails of tubulin.

(B) Schematic representation of the enzymes involved in the generation and removal of tubulin PTM shown in A. All PTM are depicted using the color code detailed in A. For all represented PTM, the forward (modification) reactions take place on polymerized microtubules, whereas the reverse reactions (which remove PTM) occur on the soluble tubulin dimer. CCP, cytosolic carboxypeptidase; TTL, tubulin Tyr ligase; TTLL, TTL-like.

Tubulin posttranslational modifications can be visualized with specific antibodies (Magiera and Janke, 2013). PC have a high level of PTMs, in fact anti-acetylation and detyrosination antibodies are established markers for the identification in immunofluorescence (IF) analysis (Figure 4).

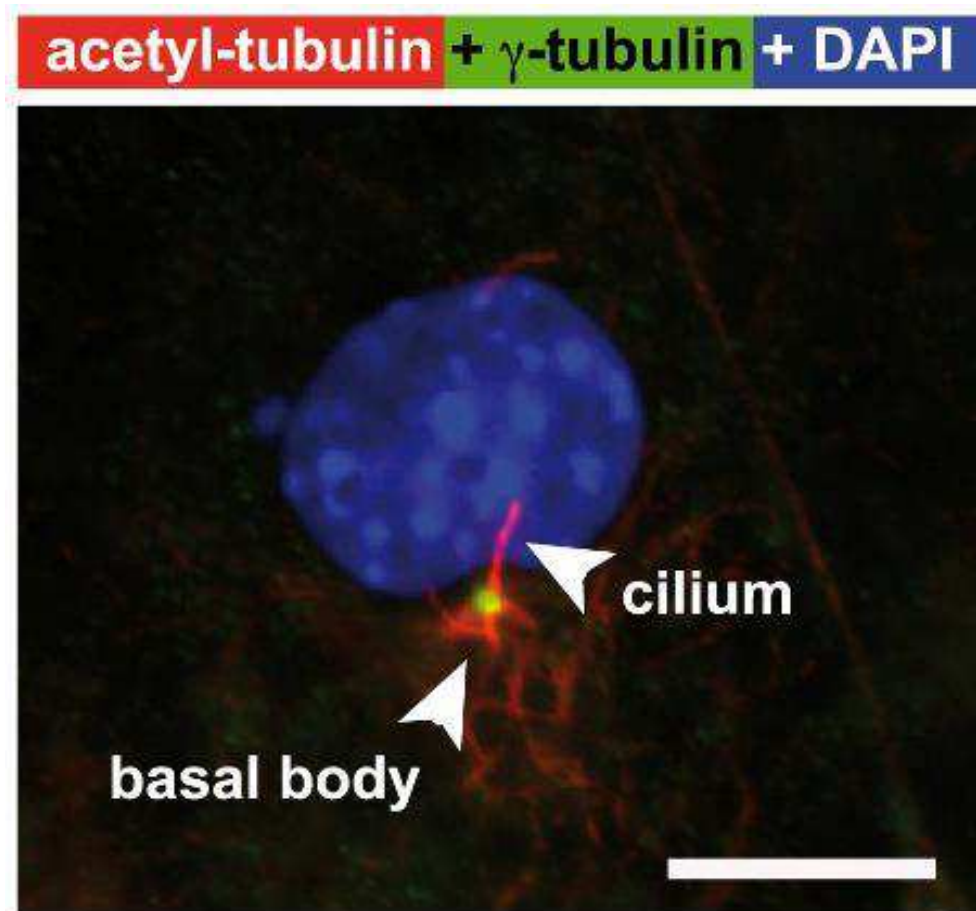


**Figure 4 Primary cilium in wild-type MEFs.** Cells were serum-starved for 2 days and labeled with anti-acetylated tubulin (red) and anti- $\gamma$ -tubulin (green) antibodies, and nuclei were stained with DAPI (blue). Scale bar is 10  $\mu$ m. (Rocha et al., 2014a).

## **1.2. PC and cell cycle**

The cell cycle duplicates large amounts of DNA in chromosomes during the S phase, and then segregates duplicated chromosomes precisely into two genetically identical daughter cells during the M phase. Most cell cycles (G1, S, G2, M phase) have two gap periods, G1 and G2. When environments are unfavorable for cell proliferation, cells delay their cell cycle progression through the G1 phase, and this resting state is known as the G0 phase.

Formation of PC typically starts at the G1/G0 phase and begins to disassemble when cells re-enter the cell cycle (Kim and Tsiokas, 2011) (Figure 5). Upon cell cycle exit, migration of the centrosome to the cell surface represents the first regulatory event of ciliogenesis, during which the mother centriole forms a basal body to nucleate ciliary axoneme (Kobayashi and Dynlacht, 2011). How exactly PC and cell cycle are regulating each other is not fully understood, but some components have been identified.

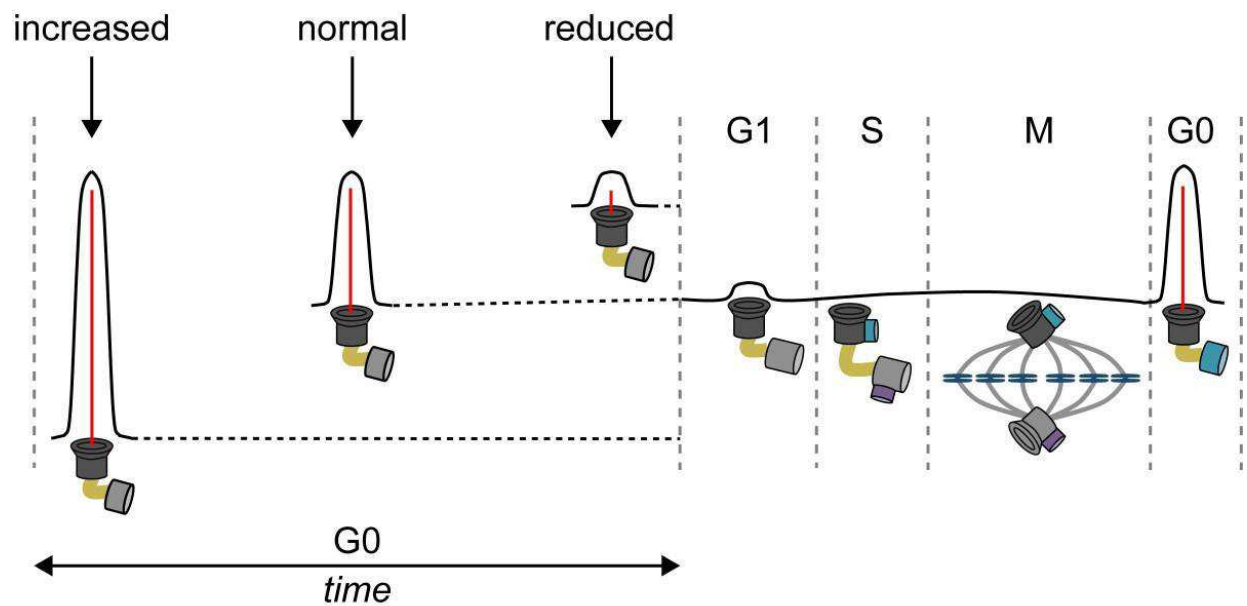


**Figure 5** Cilia length in relation to cell cycle progression (Basten and Giles, 2013).

For example, the NudE Neurodevelopment Protein 1 (NDE1) has been reported to be involved in PC resorption in cultured non-neuronal cells (Kim et al., 2011). Depletion of NDE1 results in a potent block of the G1-to-S transition, associated with a significant increase in PC length (Doobin et al., 2016). Furthermore, Aurora A kinase has been shown to stimulate cilia retraction and cell cycle progression. Inactivation of histone deacetylase 2 (HDAC2) in pancreatic ductal adenocarcinoma (PDAC) cells, results in decreased Aurora A expression, which restore formation of PC (Lancaster et al., 2011).

PC can also modulate cell cycle. Depletion of IFT88, an important component of PC (see above), induces mitotic defects in Hela cells, mouse kidney cells and zebrafish embryos. But IFT88 is also required for spindle orientation in mitosis (Delaval et al., 2011a). Increased



proliferation was observed by staining with the proliferation marker Ki67 in skin epithelial cells from mice deficient for KIF3A (Wong et al., 2009a).

### **1.3. PC and signaling pathways**

PC act as sensory antennae allowing a cell to respond to environmental signals. Many signaling pathways, such as Wnt (Corbit et al., 2008) (Lancaster et al., 2011), Hedgehog (HH) (Wong et al., 2009a) (Han et al., 2009a) (Ho et al., 2013), Notch (Ezratty et al., 2011) and PDGF signaling (Schneider et al., 2005) (Clement et al., 2013) (Umberger and Caspary, 2015), have been shown to be associated with PC. Wnt and HH are important regulators of cell proliferation, differentiation and homeostasis.

Some reports suggest that PC negatively modulate Wnt signaling pathways. For example it has been shown that PC dampen Wnt signaling by limiting  $\beta$ -catenin nuclear entry, and that this regulation is disrupted during cancer cell proliferation (Lancaster et al., 2011). In agreement with this, loss of PC was shown to enhance Wnt activity by  $\beta$ -catenin stabilization and nuclear accumulation (Corbit et al., 2008).

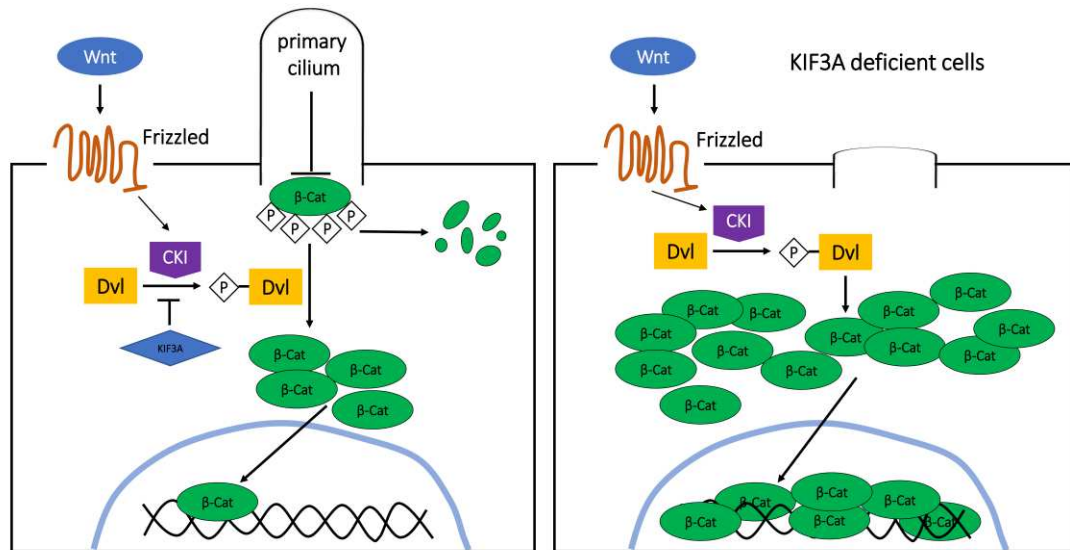


**Figure 6** Loss of PC enhances nuclear accumulation of  $\beta$ -catenin (modified from Corbit et al., 2008).

PC are essential for HH signaling during development, but can either negatively or positively regulate the HH signaling pathway. PC were shown to inhibit Hh signaling in neoplastic chondrocytes, as activation of HH signaling by partial loss of ciliogenesis was able to induce benign cartilage tumors (Ho et al., 2013). PC have a dual role in medulloblastoma formation. Deletion of PC blocked tumor formation driven by active Smoothed protein (Smo). However, removal of PC was required for tumor growth triggered by active glioma-associated oncogene family zinc finger-2 (Gli2) (Han et al., 2009a). A similar dual function of PC on the regulation of HH signaling was described for human basal cell carcinomas (Wong et al., 2009a).

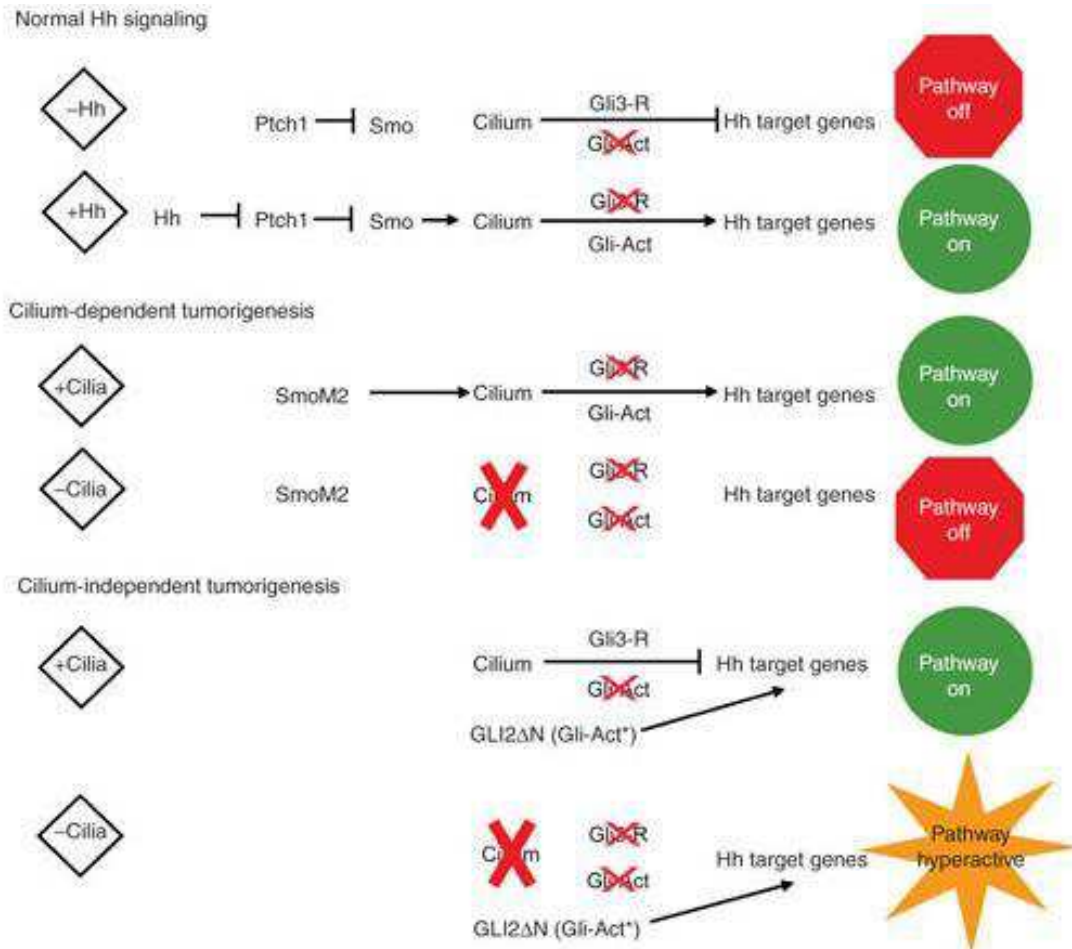


**Figure 7 The dual role of PC in Hedgehog signaling pathway in basal cell carcinoma (Wong et al., 2009a).**

In normal conditions: with the absence of HH ligand, the primary cilium suppress HH via Gli3-R (a repressor of downstream HH target genes), while with the presence of HH ligand, Ptch1-mediated inhibition of Smo is suppressed, which allows Smo to inhibit formation of Gli3-R then induce Gli activators (Gli-Act), finally this turns on the HH pathway.

In cilium-dependent tumorigenesis, the primary cilium is essential for formation of Gli-Act. But in cilium-independent tumorigenesis, even the primary cilium restrains tumorigenesis through production of Gli3-R, however the HH pathway is still turned on by constitutively active GLI2 (Gli-Act\*). Loss of the primary cilium inhibits Gli3-R, inducing hyperactive HH pathways to promote tumorigenesis.

#### **1.4. PC and disease**

Dysfunction of cilia results in severe diseases, which are known as ciliopathies, such as: Joubert syndrome (JBTS), Bardet–Biedl syndrome (BBS), Leber’s congenital amaurosis (LCA), orofaciogigital syndrome type 1 (OFD1), Senior–Løken syndrome (SLS), Alström syndrome (ALS), Meckel–Gruber syndrome (MKS), Jeune asphyxiating thoracic dystrophy (JATD), Ellis–van Creveld syndrome (EVC), nephronophthisis (NPHP) and sensenbrenner syndrome (cranioectodermal dysplasia [CED]) (Waters and Beales, 2011).

More recently, PC were also associated with tumor development, as their numbers were found to be decreased or lost in several types of cancer. Immunohistological analysis of normal breast tissues displayed frequent expression of PC in fibroblasts and myoepithelial cells, whereas PC were not detected in 25 of 26 breast cancer biopsies (Yuan et al., 2010). Another study found that PC were lost early in breast cancer development in cancer cells and surrounding stromal cells. In agreement with this, gene profiling revealed a downregulation of expression levels of genes associated with ciliogenesis and/or ciliopathies in human breast cancers (Menzl et al., 2014).

In prostate cancer, both decreased numbers of ciliated cells as well as decreased cilia length in PC expressing cells were observed in prostatic

intraepithelial neoplasia and invasive cancer compared to normal tissue (Hassounah et al., 2013a).

Another report described a lack of PC expression on the colon cancer cell line DLD1, which carries a mutation on APC, whereas PC were detectable on the normal colon cell line CCD841 (Lancaster et al., 2011).

A gene profile analysis also showed downregulation of cilia genes in colon adenocarcinoma (Shpak et al., 2014a). All these findings suggest a link between loss of PC and tumorigenesis.

## 1.5. Colon carcinoma

Colorectal cancer is the development of cancer from the colon or rectum. Nearly all intestinal epithelial cells are replaced within one week that puts great demands on the cellular organization of this tissue, and also puts it at serious risk of malignant conversion. Indeed, it is the third most commonly diagnosed cancer in males and the second in females (Jemal et al., 2011) with an estimated 400 000 new cases in Europe every year. Colorectal cancer is particularly associated with lifestyle factors including obesity, red and processed meat, alcohol, etc. Its incidence is very high in countries with a diet high in calories and animal fat, such as Slovakia and Hungary (Stewart and Wild, 2014).

CRC development is a long-term process including the transition from normal epithelial cells via aberrant crypts and progressive adenoma stages to carcinomas in situ and finally metastasis (Figure 8).

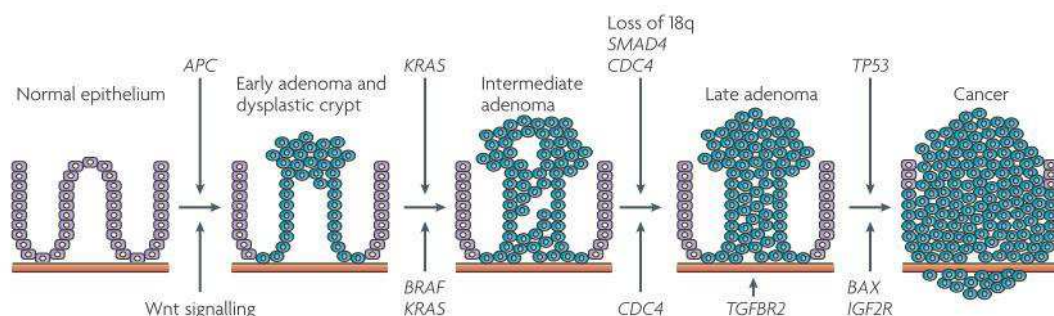


Figure 8 A sequence model for colorectal cancer (Walther et al., 2009).

The most common spontaneous mutations in early stage colorectal cancer are in the adenomatosis polyposis coli (APC) tumor suppressor gene and

the  $\beta$ -catenin proto-oncogene (Miyoshi et al., 1992) (Morin et al., 1997). These lead to hyperactivation of the Wnt pathway, marked by accumulation of transcription factor  $\beta$ -catenin in the nucleus (Morin et al., 1997). Besides, heterozygous somatic mutations in the APC gene are known as well and are called familial adenomatous polyposis (FAP). Patients with FAP develop hundreds of colonic polyps early on in life, and their lifetime risk of developing CRC is almost 100%.

The Wnt signaling pathway plays a critical role in maintenance of tissue homeostasis and is best illustrated in the gut, where a gradient of Wnt signaling activity is regulating homeostasis of intestinal epithelium. Activation of the Wnt signaling pathway results in translocation of  $\beta$ -catenin into the nucleus, where it associates with the T-cell factor/lymphoid enhancer factor (TCF/LEF) family of transcription factors to activate specific Wnt target genes. Intestinal stem cells are at the bottom of intestinal crypts, while proliferating and differentiating cells migrate up in the crypt. Differentiated epithelial cells are finally shed into the lumen while undergoing apoptosis. Notably, nuclear localization of  $\beta$ -catenin is only detectable in the crypt bottom (van de Wetering et al., 2002). This organization is rapidly disturbed upon mutations activating the Wnt pathway and expansion of the proliferative pool occurs. In fact, it has been shown that intestinal epithelial stem cells



regulated by Wnt signaling pathway are the origin of intestinal cancers (Barker et al., 2009).

Much of our understanding of the histopathologic and molecular processes underlying the transition from a normal epithelium to an invasive adenocarcinoma relies on the fundamental work of Fearon and Vogelstein (Fearon and Vogelstein, 1990). They have described the so-called “adenoma-carcinoma sequence”, as the stepwise accumulation of genetic changes in oncogenes and tumor suppressor genes. This sequential acquisition of mutations during CRC is shown in Figure 8 and includes KRAS and p53.

### **1.5.1. Colonic crypts and cell interactions**

The epithelial layer of the human colon is made up of a single sheet of columnar epithelial cells, which form finger-like invaginations into the underlying connective tissue of the lamina propria to form the crypt (Figure 8).

The differentiated epithelial cell types include absorptive cells, mucus-secreting goblet cells and peptide hormone-secreting endocrine cells. Epithelial turnover happens every 5 days (Barker, 2014). The lamina propria contains fibroblasts, subepithelial myofibroblasts, pericytes of the capillaries, mesenchymal stem cells, lymphatic lacteal

associated smooth muscle and the muscularis mucosae(Powell et al., 2011). Within the colon, there are millions of crypts containing the stem-cell population at the base of the crypt. The stem cell niche is formed by the stem cells themselves and myofibroblasts that surround the crypt base (Figure 9).

Colon homeostasis in steady state is tightly regulated by the crosstalk between epithelial and mesenchymal cells. Several signaling pathways have been identified regulating the cellular organization in the colon, including hedgehog (HH), bone morphogenetic protein (BMP), and Wnt and Notch (Figure 9).

Within the zones of proliferation and differentiation, HH ligands produced by differentiated epithelial cells trigger mesenchymal BMP synthesis. Active BMP signaling within differentiated cells are able to maintain differentiation state and quiescence of proliferation. Notch directs enterocyte differentiation due to downregulation of WNT activity towards the top of the crypt(Fre et al., 2005)(van Es et al., 2005)(Es et al., 2010). Furthermore, activation of the Notch signaling results in goblet cell depletion, whereas its inhibition induce proliferation of goblet cells(Fre et al., 2005)(van Es et al., 2005).

Within the stem cell niche, lack of HH signaling leads to decreased mesenchymal BMP synthesis(Brink, 2007). Secretion of Wnt proteins at

the base of crypt, in addition to promoting self-renewal of intestinal stem cells, may also induce synthesis and secretion of BMP antagonists by the underlying myofibroblasts(Klapholz-Brown et al., 2007). Notch also directs cell proliferation due to high WNT activity(Sato et al., 2011). BMP antagonists in this area would further enhance Wnt signaling(Kosinski et al., 2007).

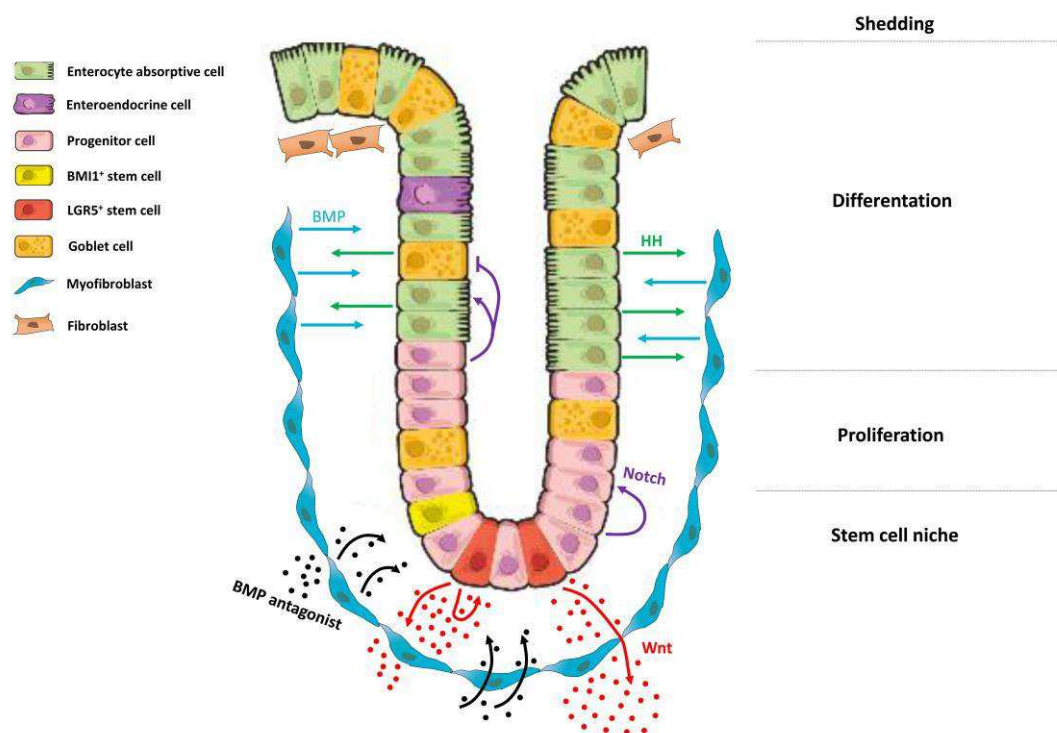


**Figure 8 Schematic representation of colonic cell types and related signaling pathways. This figure is modified from (Medema and Vermeulen, 2011) (Powell et al., 2011).**

Colonic stem cells present in the bottom of the crypt can proliferate and move then upward, when they differentiate. Cell turnover in the colonic crypt takes 5 days and is regulated by Wnt, Notch and BMP and Hedgehog signaling pathways. Myofibroblasts, which express alpha smooth muscle actin, play an important role in constituting the stem cell niche.

## 1.6. Mouse models for CRC

A variety of models of CRC have been developed to mimic human tumors.

### 1.6.1. APC mouse model

APC loss is the cause of familial adenomatous polyposis (FAP), a human autosomal dominant syndrome, in which patients develop numerous colorectal polyps. Based on the high prevalence of APC mutation in colorectal cancer, the first mouse model for CRC was developed in 1990 (Moser et al., 1990). This is the multiple intestinal neoplasia (MIN) model, which is also known as *APC<sup>min/-</sup>* mouse model. Since obtained in 1990, this model has been used for a broad range of research.

*APC<sup>min/-</sup>* mice develop multiple intestinal neoplasia, and they mimic the rapid tumor development seen in FAP patients and model the process of polyp growth and progression. Tumors in *APC<sup>min/-</sup>* mice are predominately found in the small intestine, but extremely rare in the colon (Moser et al., 1990). In average *APC<sup>min/-</sup>* mice die at the age of 3-4 month.

The loss of the APC prevents binding and degradation of  $\beta$ -catenin, which constitutively activates the Wnt-pathway and deregulates growth in tumor cells. But no K-ras mutations or inactivation of p53 have been reported in this mouse model (Smits et al., 1997).

### 1.6.2. AOM/DSS

This is a chemically inducible model (Figure 10). It requires a single injection of azoxymethane (AOM), followed by an inflammatory insult using dextran sodium sulfate (DSS). AOM is a pro-carcinogen, that is metabolized to methylazoxymethanol (MAM), then alkylates macromolecules in the liver and colon, and operates the addition of methyl groups at the O6 position of guanine in DNA (Sohn et al., 2001).

DSS is added in the drinking water and induces specifically inflammation in the colon. In the classical protocol mice receive three administrations of DSS and mice are sacrificed 60 days after the initial AOM injection. First signs of dysplasia are detectable after about 1 month. Tumor lesions in AOM/DSS treated mice or rats have frequently mutations in  $\beta$ -catenin and K-Ras (Tanaka, 2012) (Tanaka et al., 2003a) (Erdman et al., 1997) (Bolt et al., 2000). The former leads to increased activity of the Wnt signaling pathway due to accumulation of  $\beta$ -catenin in the nuclei. The AOM/DSS model therefore mimics well the human disease, though Apc and p53 mutations are less frequently found (De Filippo et al., 1998) (Erdman et al., 1997).

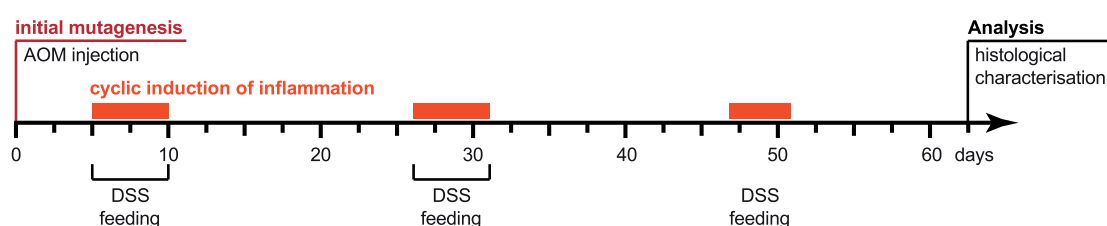


**Figure 10 Protocol for AOM/DSS administration**

## 2. Objectives

In 2006, two CRC patients were identified with two distinct somatic mutations in the tubulin tyrosine ligase-like 3 gene (*TTLL3*)(Sjöblom et al., 2006). The TTLL3 protein was later determined, by the group of C Janke, to catalyse the posttranslational glycylation of microtubules. Moreover, they demonstrated that both mutations in these patients cause loss of TTLL3 enzymatic activity, suggesting that the absence of enzymatic activity is directly involved in the development of colorectal cancer(Rogowski et al., 2009). Therefore, our group together with the Janke team started to investigate the role of tubulin glycylation in CRC development.

We discovered a significant down-regulation of *TTLL3* expression in primary colorectal carcinomas and matched metastases of tumour samples from patients that had not received prior treatment, confirmed the link between TTLL3 and CRC(Rocha et al., 2014a). We also discovered that TTLL3 is the only enzyme that catalyses glycylation in colon, whereas most of the other tissues analysed (murine and human) express the complementary glycyclase, TTLL8(Rocha et al., 2014a). Consequently, the decrease in TTLL3 expression observed in CRC should result in the absence of, or at least a decrease in glycylation activity in colon cells(Rocha et al., 2014a).

To elucidate the role of TTLL3 in the colon, our group analyzed TTLL3-deficient mice and found a reproducible and significant decrease in the number of PC (PC) in colon crypts in *ttll3*<sup>-/-</sup> mice (Figure 11).

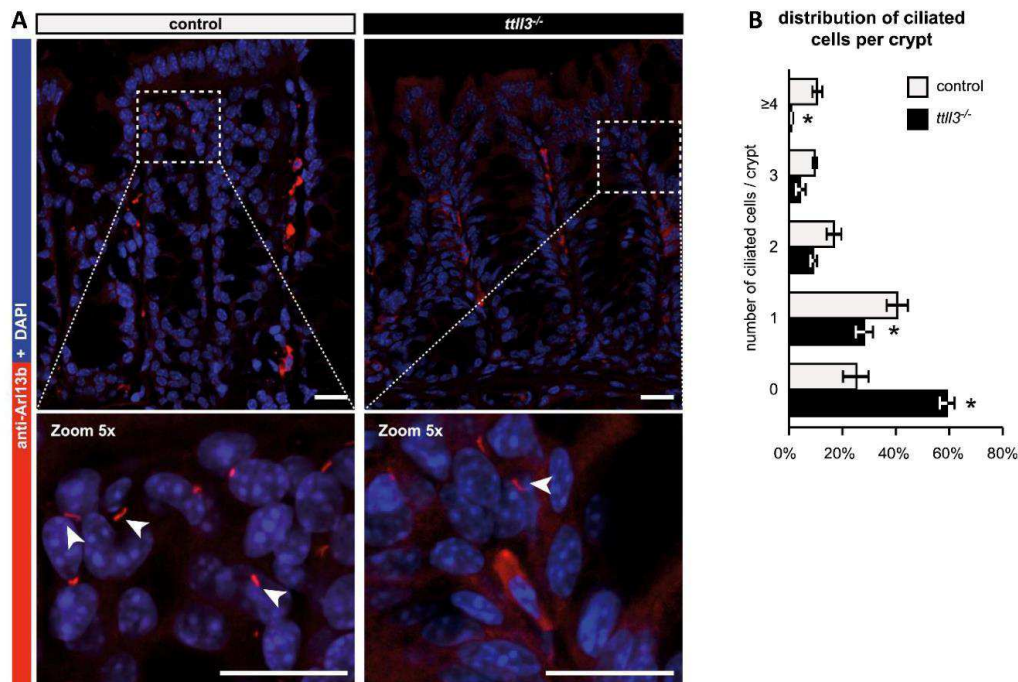


**Figure 11 Decreased PC in TTLL3-deficient colon**(Rocha et al., 2014a).

(A) Confocal images (maximum projection) of cryo-sections from colon stained with the antibody Arl13b (red) and DAPI (blue). Arl13b specifically labels PC (arrowheads). Cytoplasmic staining of stromal cells is non-specific, as Arl13b is a membrane protein. The selected image shows a particularly high density of detectable PC. Scale bars are 20  $\mu$ m.

(B) Quantification of the number of clearly detectable Arl13b-positive ciliated cells per crypt. The relative numbers of crypts with 0, 1, 2, 3, 4 and more ciliated cells are represented as mean values  $\pm$  SEM between individual mice (control n = 7; *ttll3*<sup>-/-</sup> n = 4). Total number of analyzed crypts: control = 259, *ttll3*<sup>-/-</sup> = 198.

This was an important discovery, since it was the first observation of PC in intact colon tissues. Since PC are proposed to play a role in cell proliferation, the proliferative activity and turnover of colon epithelial cells was assessed by quantifying the uptake of bromodeoxyuridine (BrdU) that is incorporated in DNA during S phase. The rate of

proliferation was higher in the colon of *TTLL3*-deficient mice, coupled with a faster turnover of epithelial cells in the crypts (Figure 12).

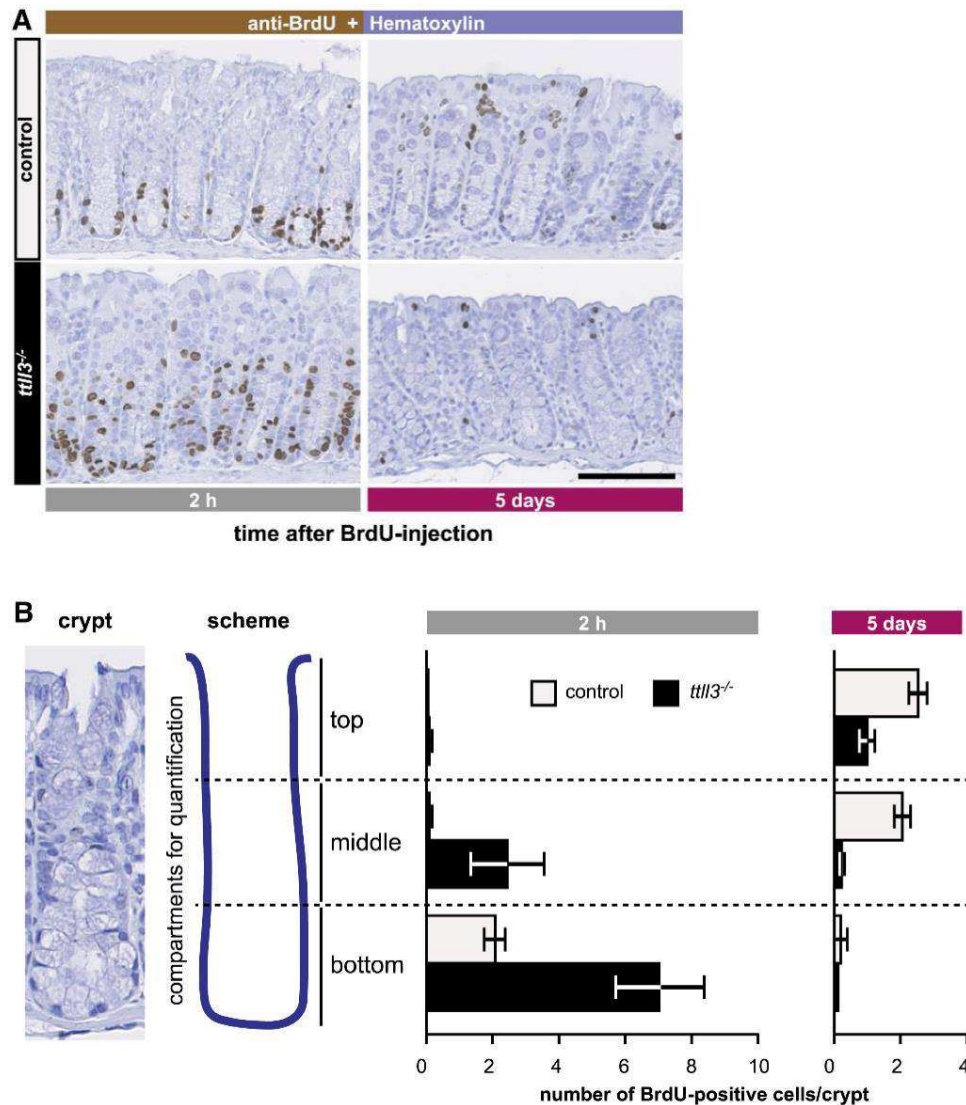


**Figure 12** Loss of *TTLL3* results in increased proliferation of colon epithelium (Rocha et al., 2014a).

(A) Cell proliferation in colon crypts was analyzed by incorporation of BrdU. Representative pictures of BrdU immunohistochemistry (brown) 2 h and 5 days after intraperitoneal injection of BrdU. Paraffin-embedded colon sections from control and *ttll3*<sup>-/-</sup> mice were stained with anti-BrdU antibody and hematoxylin. Scale bar is 100  $\mu$ m.

(B) Quantification of BrdU-positive cells in three compartments of the crypts (see scheme) 2 h and 5 days post-injection. At least 30 crypts per mouse were counted in three (2 h) and four (5 days) independent experiments (number of mice: 2 h control n = 3; 2 h *ttll3*<sup>-/-</sup> n = 3; 5 days control n = 4; 5 days *ttll3*<sup>-/-</sup> n = 4).

Increased cell proliferation in the colon of *ttll3*<sup>-/-</sup> mice did not visibly alter colon morphology (confirmed by the pathologists Prof. Mauro,



University of Chieti, Italy). It thus appears that efficient shedding of colon tissue counterbalances the increased proliferation of colon epithelial cells, resulting in the maintenance of normal colon architecture. However, employing a well-established mouse model of colitis-associated carcinogenesis (see above) the absence of TTLL3 promoted the transformation of the colon epithelium into neoplastic lesions resulting in an increase in the number and size of lesions (Figure 13). Taken together, previous results from our group strongly suggest that decreased numbers of PC in the colon promote cell proliferation and render colon tissue more susceptible to carcinogenesis.

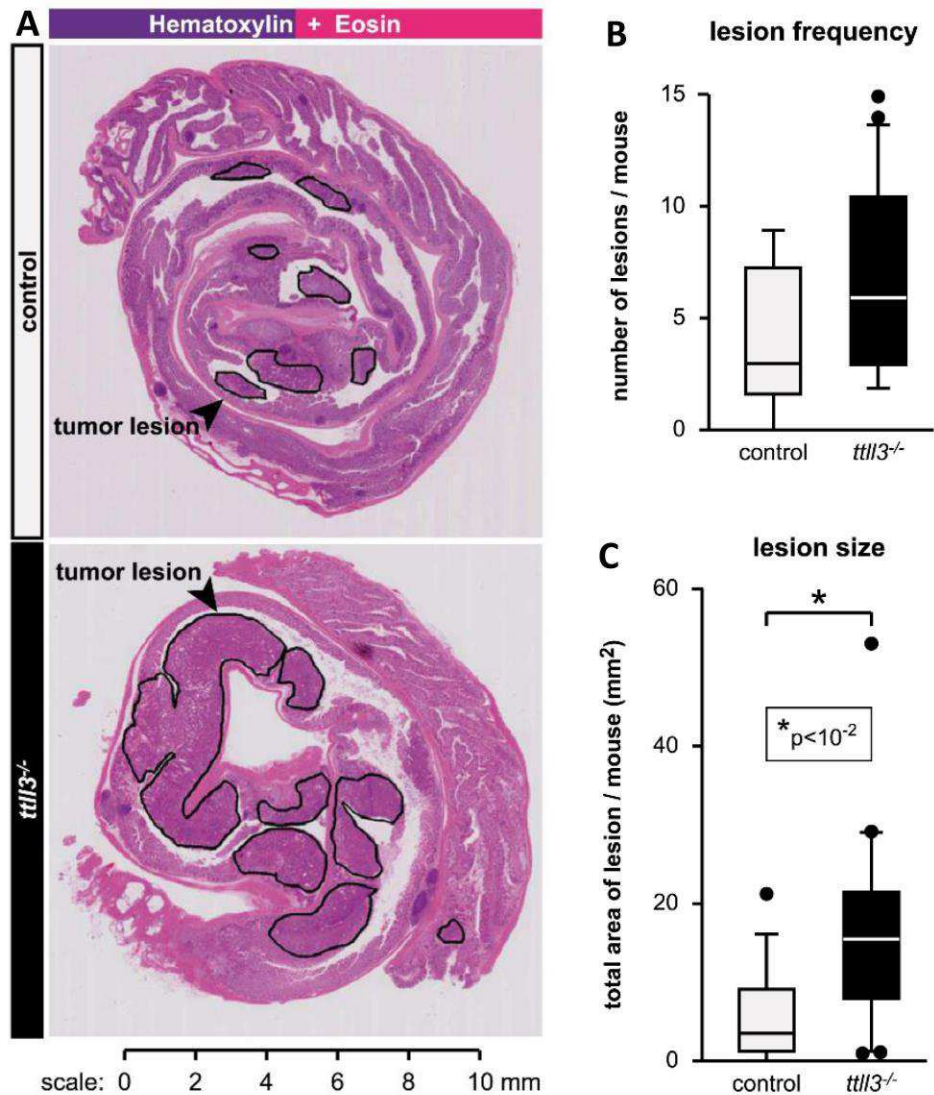


**Figure 13 Loss of TTLL3 promotes colon carcinogenesis.**

(A) Representative images of hematoxylin and eosin staining of paraffin-embedded colon sections prepared as “Swiss rolls”. Single tumors are delimited by black lines.

(B, C) Box plots of the average number of tumors per mouse (B) and the average total area of lesions per mouse (C) with a line indicating the median values. Dots represent values lower than 10% and > 90% of the mean values. Error bars are SD. \*P < 10<sup>-2</sup>.

In order to elucidate PC putative role in the development of cancer, I used two different approaches to delete PC, in two murine models systems, i.e. two conditionally knock out mice for genes involved in the transport machinery involved in cilia formation: *Ift88* (intraflagellar transport protein 88 homolog) and *Kif3a* (a subunit of the heterotrimeric motor

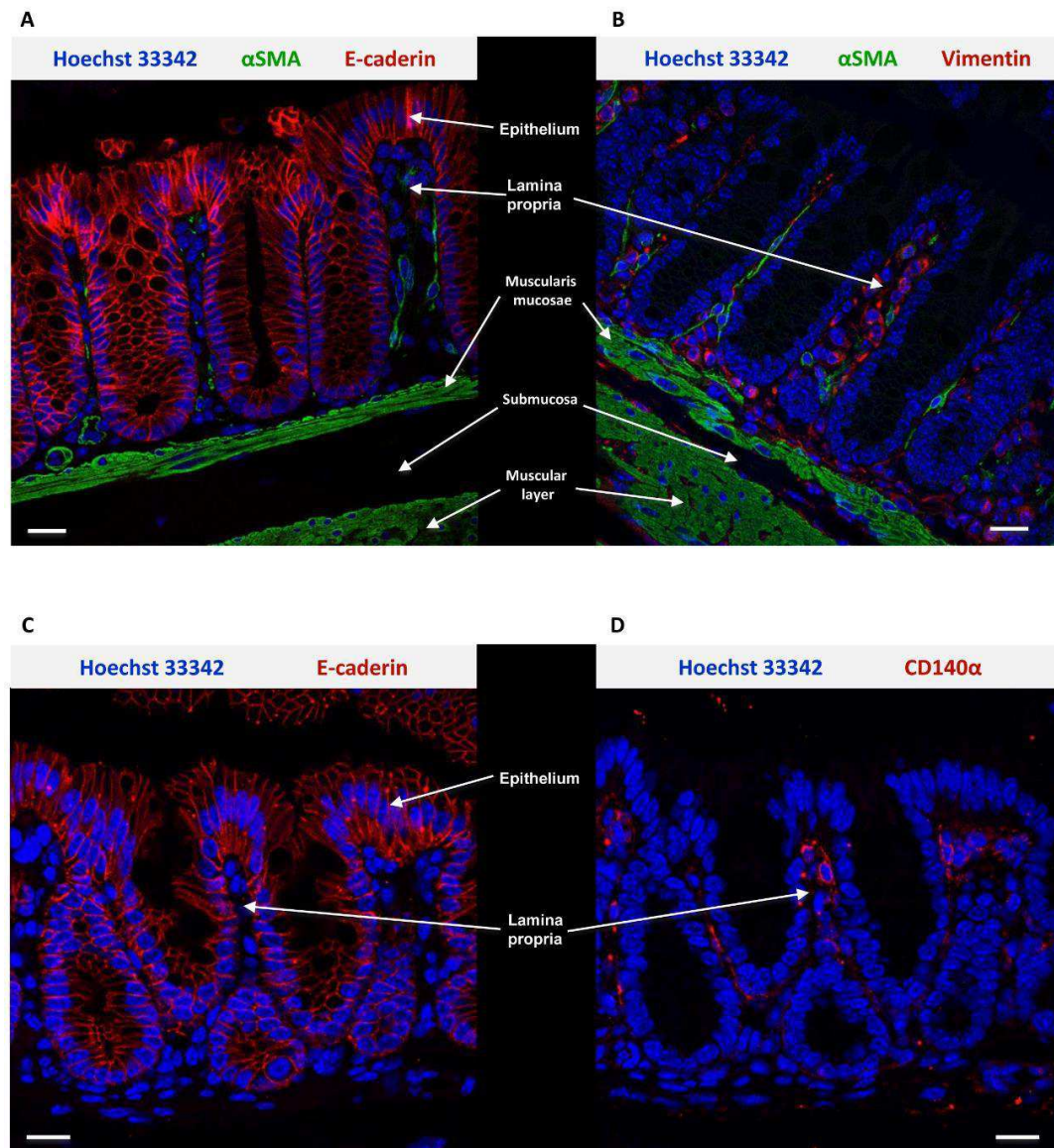
protein, kinesin-2). This has been shown to lead to a complete suppression of cilia (Marszalek et al., 1999a) (Haycraft et al., 2007a). Since total mutants are embryonic lethal, I used tissue-specific promoters to drive their deletion in either colon or brain (see below). *Kif3a* and *Ift88* mutant mice have been extensively studied by others. The Spassky team has already used them to study the role of PC in the hippocampus and cerebellum (Spassky et al., 2008) (Bosch Grau et al., 2013) (Han et al., 2008). However, in addition to their role in PC formation, IFT88 and KIF3a were reported to promote cilia-independent functions, such as spindle orientation or mother centriole appendage formation (Kodani et al., 2013a) (Delaval et al., 2011a). Therefore, different mutants, in which PC are defective must be studied to determine whether a particular phenotype is truly cilia-dependent.

### 3. Results

#### 3.1. *Colonic mesenchymal cells express primary cilia (PC)*

To characterize which cells in the intact colon express PC, I performed co-staining with markers for epithelial cells and mesenchymal cells, i.e. E-cadherin, vimentin, alpha smooth muscle actin ( $\alpha$ SMA) and CD140 $\alpha$  (platelet-derived growth factor receptor alpha). Staining for vimentin and  $\alpha$ SMA allows to distinguish fibroblasts from myofibroblasts, muscularis mucosae, or musculus layer (Figure 14A and 14B), whereas CD140 $\alpha$  characterizes a recently described vimentin<sup>low</sup>SMA<sup>-</sup> subpopulation of fibroblasts present on the upper parts of the crypts (Kurahashi et al., 2013) (Figure 14C, 14D, 15D, 15E). Interestingly, we noted that PC in the intact colon are mainly expressed by E-cadherin negative mesenchymal stromal cells (Figure 15). Most stromal cells in the lamina propria expressing PC were vimentin or CD140 $\alpha$  positive (Figure 15C and 15E), though a few PC were also detectable on  $\alpha$ SMA positive mesenchymal cells (Figure 16 and 17).

**Figure 14. Cell markers in normal mouse colon**



(A) Double staining of E-cadherin (red) and  $\alpha$  smooth muscle actin ( $\alpha$ SMA, green)

(B) Double staining of vimentin (red) and  $\alpha$ SMA (green)

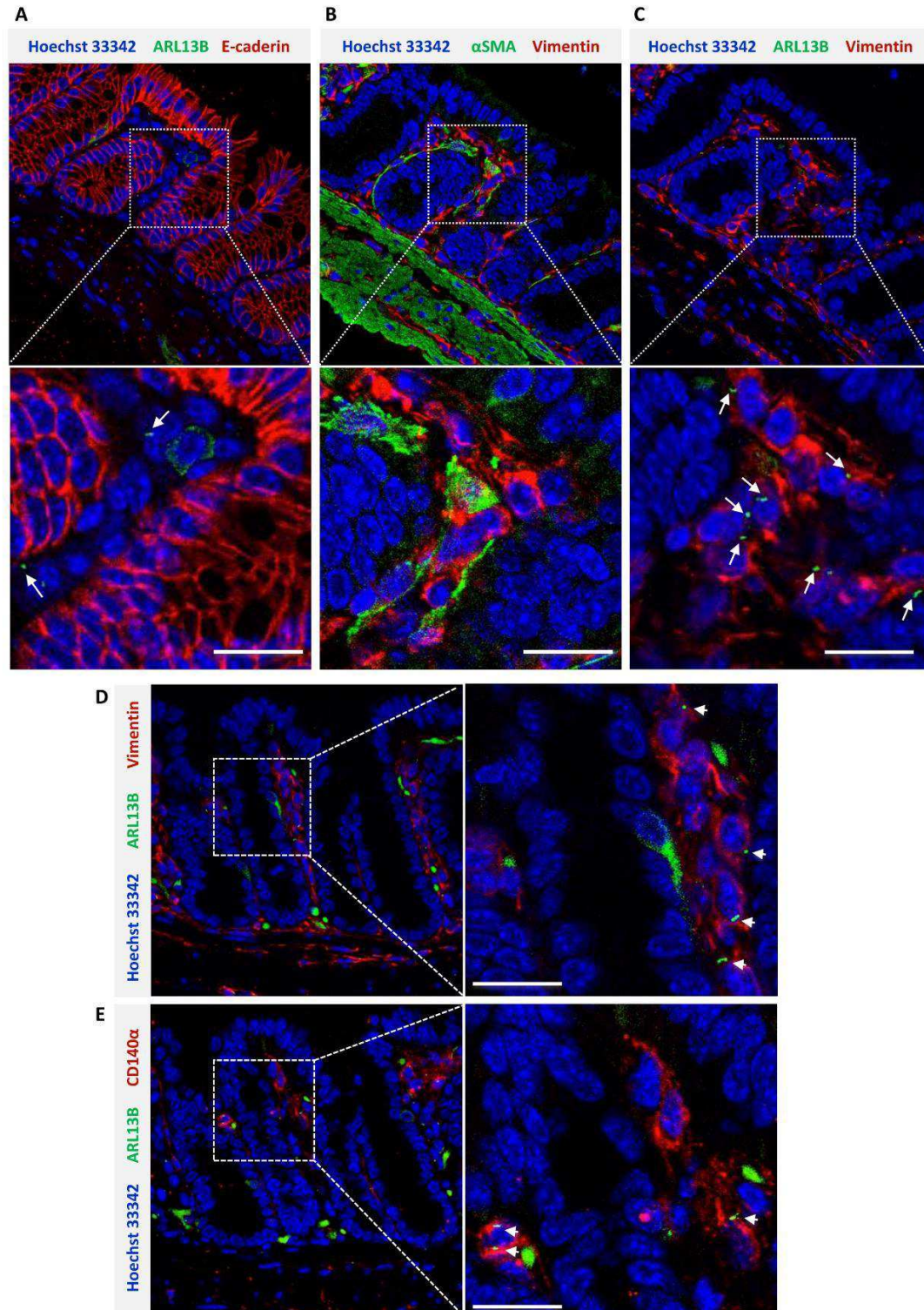
(C) Single staining of E-cadherin (red)

(D) Single staining of CD140 $\alpha$  (red) on a serial section next to (C)

All stainings were performed on sections of colon from *Kif3a<sup>fl/fl</sup>* mice. Nuclei were labelled by Hoechst 33342 (blue). Components of colon are labeled by white arrows. All Scale bars represent 20  $\mu$ m.



**Figure 15 Majority of PC are expressed by vimentin<sup>+</sup> fibroblasts in mouse colon**



(A) Double staining of E-cadherin (red) and ARL13B (green)

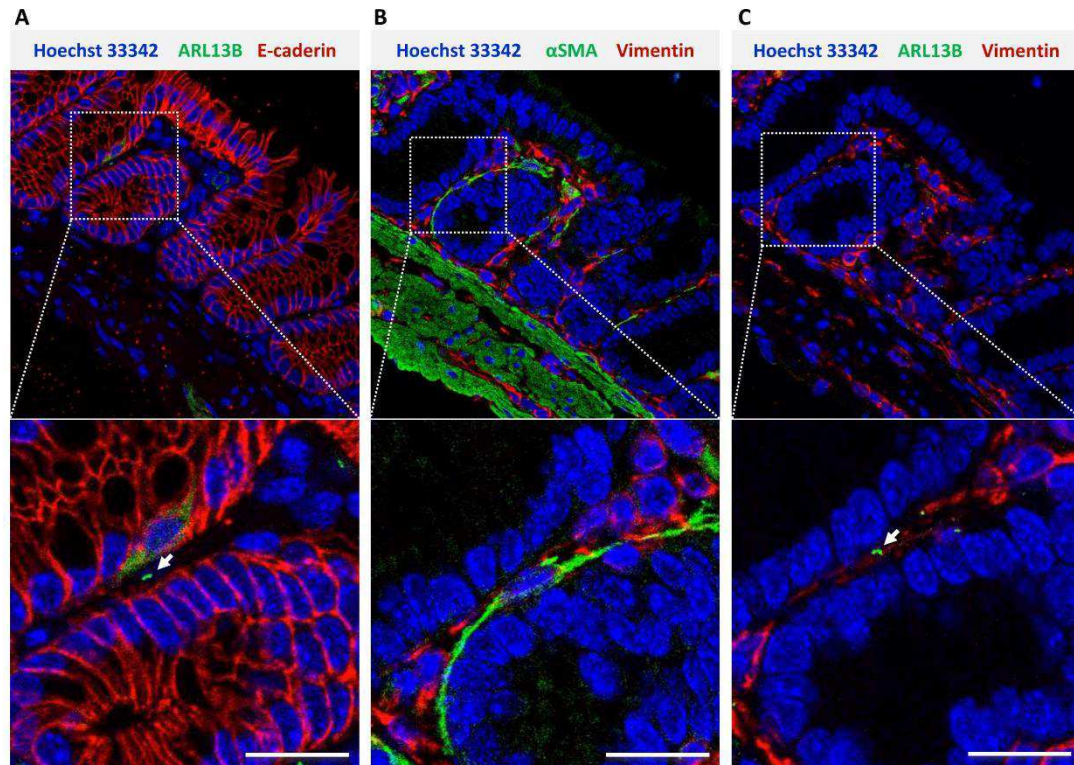
(B) Double staining of vimentin (red) and αSMA (green)

(C) and (D) Double staining of vimentin (red) and ARL13B (green)

(E) Double staining of CD140α (red) and ARL13B (green)

All stainings were performed on serial sections (A - C, D - E) from *Kif3a<sup>fl/fl</sup>* mice. Nuclei were labeled by Hoechst 33342 (blue). PC are indicated by white arrows. All Scale bars represent 20 μm.

**Figure 16 Few PC were detected in  $\alpha$ SMA<sup>+</sup> cells in lamina propria**



(A) Double staining of E-cadherin (red) and ARL13B (green)

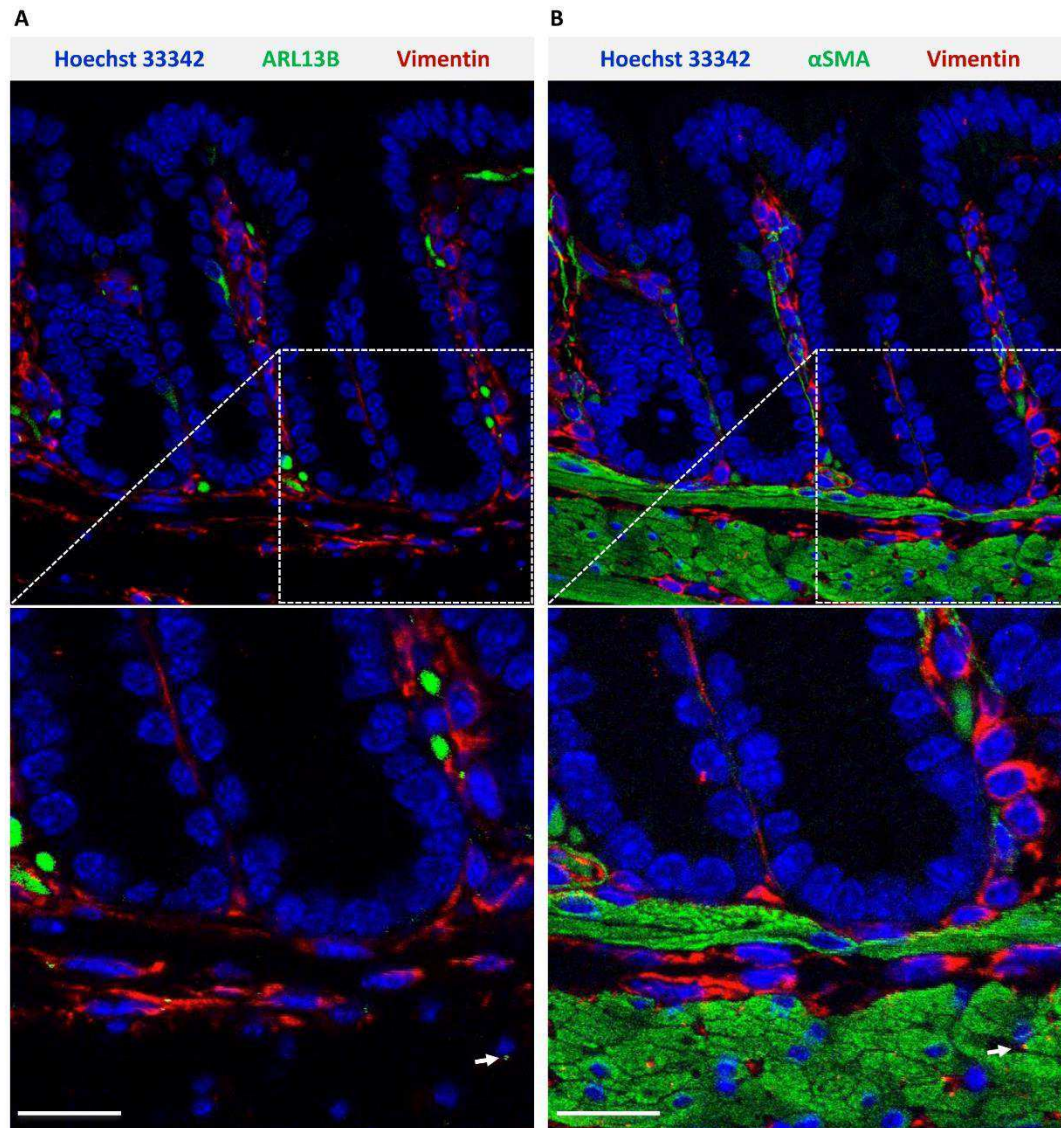
(B) Double staining of vimentin (red) and  $\alpha$ SMA (green)

(C) Double staining of vimentin (red) and ARL13B (green)

All stainings were performed on serial sections from *Kif3a<sup>fl/fl</sup>* mice. Nuclei were labeled by Hoechst 33342 (blue). PC are indicated by white arrows. All Scale bars represent 20  $\mu$ m.



**Figure 17 Few PC were detected in  $\alpha$ SMA<sup>+</sup> cells in muscle layer**



(A) Double staining of vimentin (red) and ARL13B (green)

(B) Double staining of vimentin (red) and  $\alpha$ SMA (green)

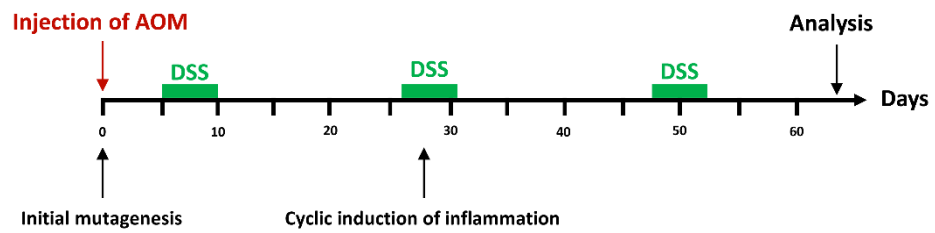
All stainings were performed on serial sections from *Kif3a<sup>fl/fl</sup>* mice. Nuclei were labeled by Hoechst 33342 (blue). PC are indicted by white arrows. All Scale bars represent 20  $\mu$ m.



### **3.2. *Number of colonic PC decreases during murine colon carcinogenesis***

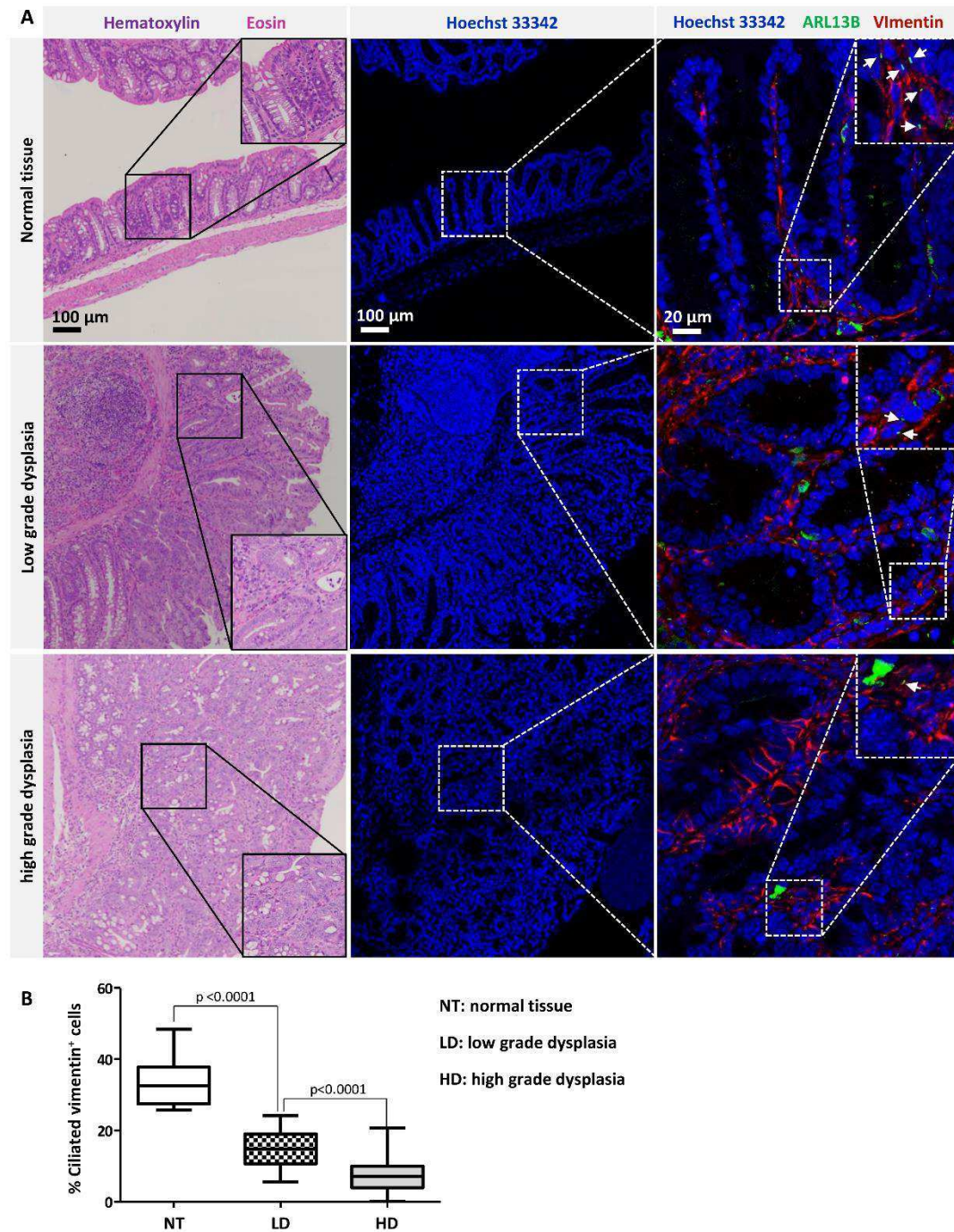
Studies on mouse models described that removal of PC can either block or promote medulloblastoma and basal cell carcinoma (BCC) formation depending on the initiating oncogenic event (Han et al., 2009b)(Wong et al., 2009b). I analyzed the presence of PC in a mouse model that mimics colitis-associated colon carcinogenesis (CAC) (Tanaka et al., 2003b) (Suzuki et al., 2004). This model depends on administration of the mutagen azoxymethane (AOM) and the subsequent induction of inflammation with dextrane sodium sulfate (DSS) (Figure 18). DSS is toxic to mucosal epithelial cells in the colon, and the eventual destruction of the mucosal barrier leads to inflammation. For the detection of PC I established a previously described protocol in our lab that allows detection of PC on paraffin embedded tissue (Hassounah et al., 2013b). Colonic crypts displayed a lower number of PC in tumor lesions compared to adjacent normal tissue (Figures 19). Remarkably, lesion areas with high grade dysplasia showed significant lower numbers of PC than those with low grade dysplasia. This supports our initial hypothesis that the down-regulation of PC supports CAC.

**Figure 18 Illustration of AOM/DSS mouse model**



Briefly, after intraperitoneal injection of AOM, mice were treated by three cycles of DSS administration in water. More details are described in ‘Methods’.

**Figure 19 Decreased colonic PC during murine colon carcinogenesis**



(A) Histological analysis, nuclei staining and double staining were performed on three serial sections. PC in fibroblasts were labeled by ARL13B antibody (green) and vimentin antibody (red). Nuclei were labeled by Hoechst 33342.

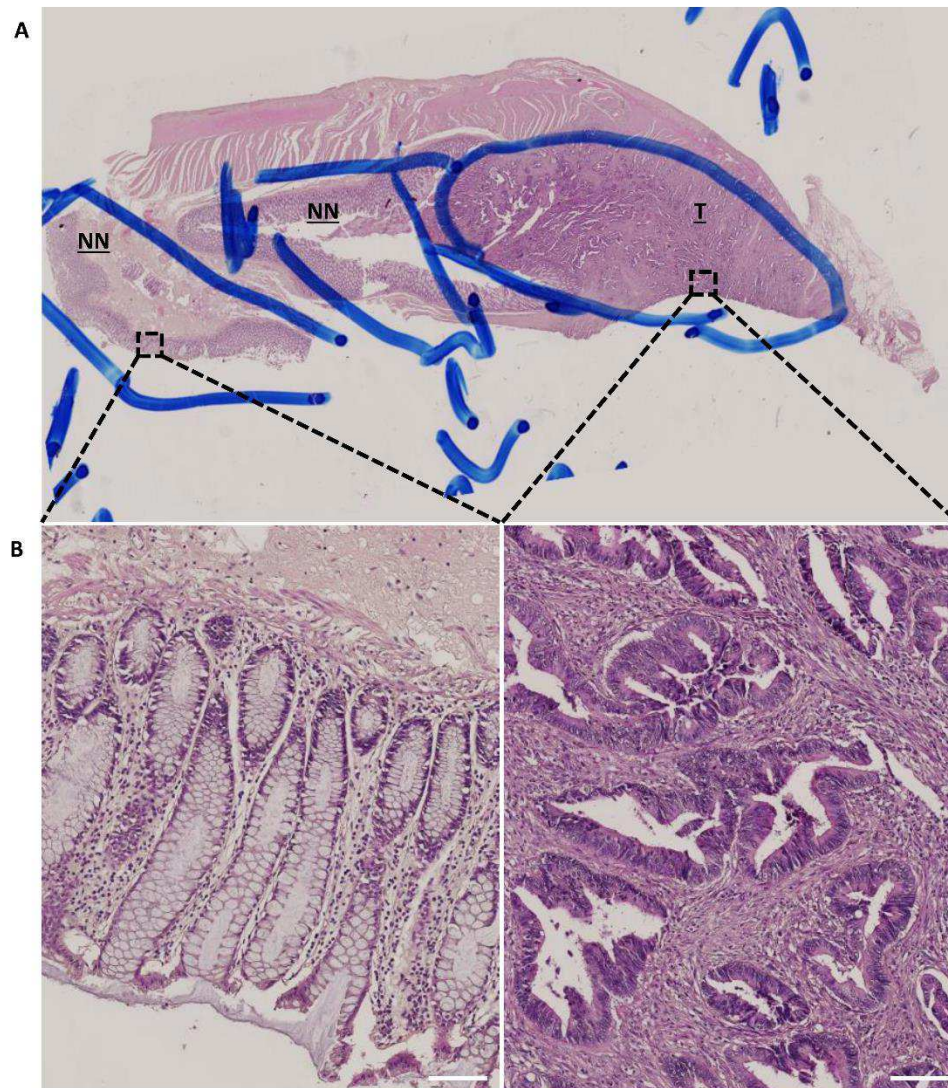
(B) Quantification of PC were made on images from 4 areas of normal tissue (NT) from 3 control mice, 10 areas of low grade dysplasia (LD) from 6 control mice and 10 areas of high grade dysplasia (HD) from 7 control mice. 2-14 images were taken for each area.

### ***3.3. Number of PC may increase in colorectal cancer (CRC) patient samples***

To test if PC are also downregulated during human colon carcinogenesis, I examined two samples we obtained from our collaborators from the University of Chieti (Figure 20). Surprisingly, PC were nearly undetectable on adjacent non-neoplastic colon mucosa (Figure 21A and 21C), but highly expressed on tumor area (Figure 21B and 21D). It has been described that expression of PC might vary in different subtypes of cancer (Han et al., 2009c). For example, ciliary genes were reported to be upregulated in rectal adenocarcinoma, but downregulated in colon adenocarcinoma (Shpak *et al*, 2014). In fact, one of our samples derived from sigmoid colon, the other one from rectum. To understand the expression or function of PC in CRC patients, more samples need to be analyzed.

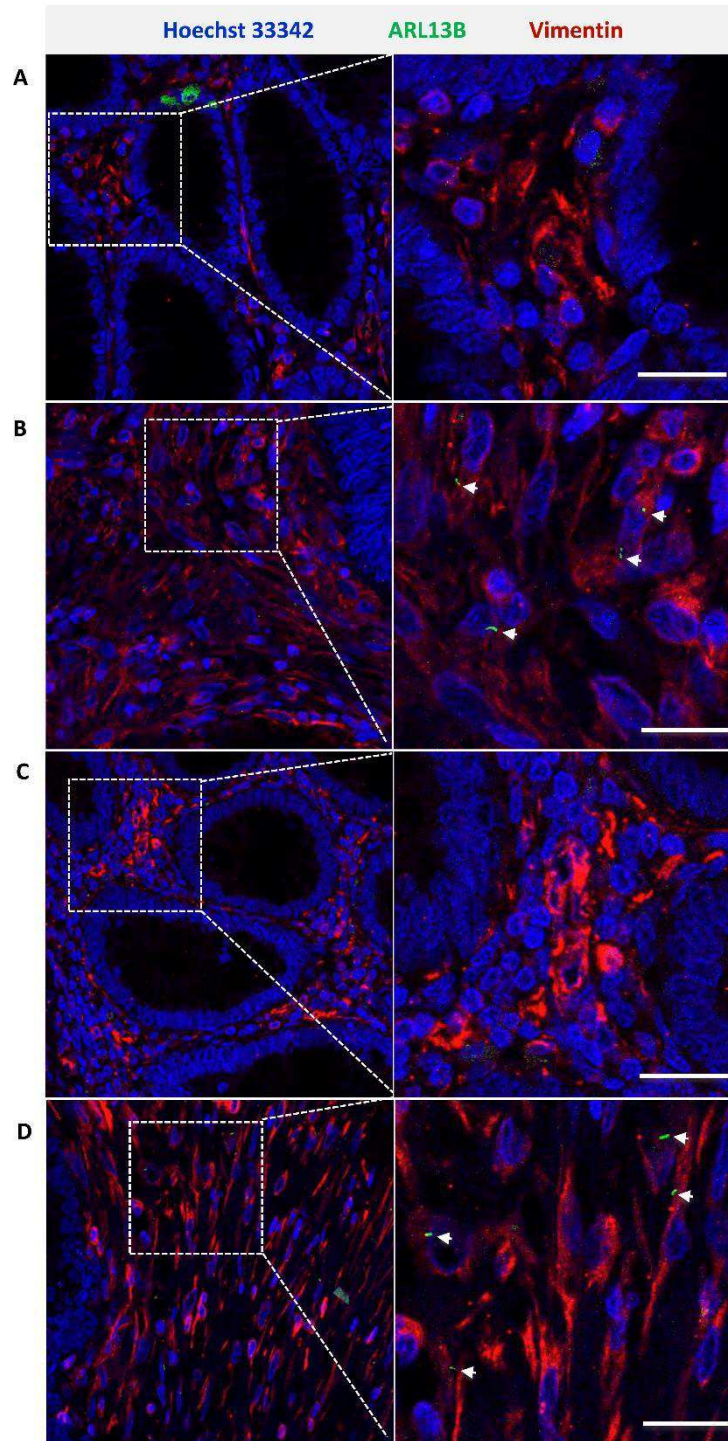


**Figure 20 Histology of patient samples**



Histological analysis was made by pathologists from University of Chieti (A). 'NN' stands for non neoplastic colon mucosa adjacent to tumor area (B left), 'T' stands for primary colorectal cancer (B right). All scale bar represent 100  $\mu$ m

**Figure 21 Expression of PC in biopsies of CRC patients**



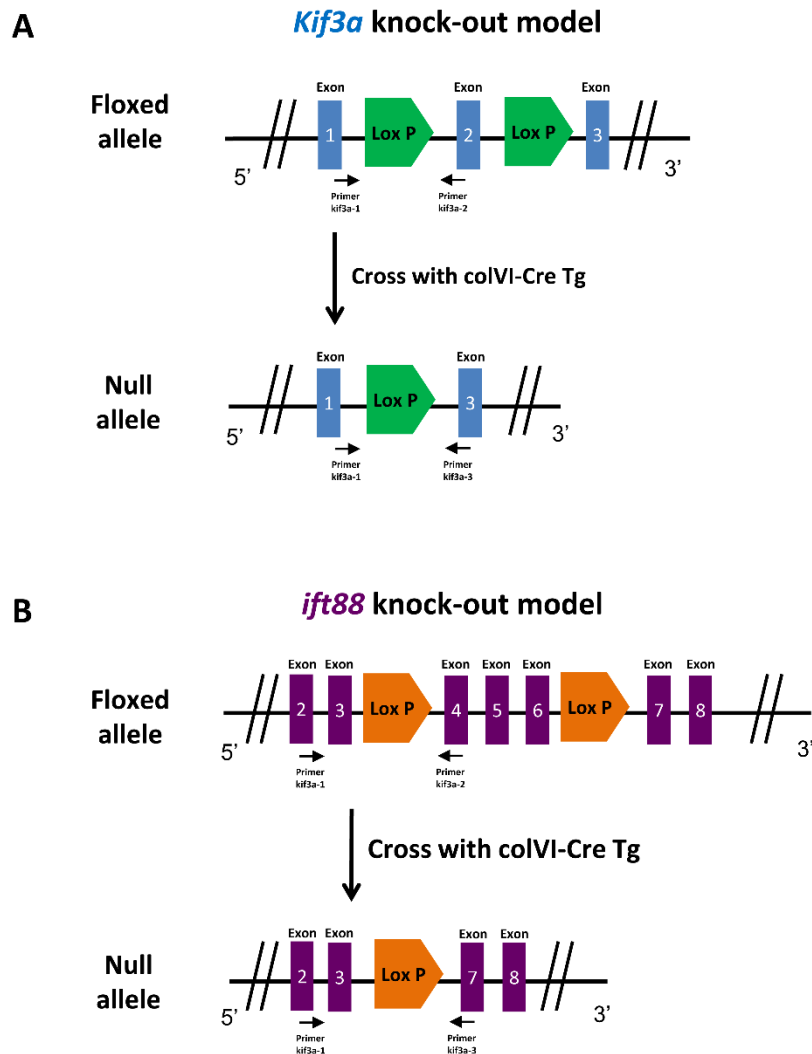
Double staining of ARL13B (green) and vimentin (red) were performed in patient samples. One sample (A and B) derived from rectum, and the other (C and D) from sigmoid colon. Images were taken in NN (A and C) and T (B and D). All scale bar represent 20  $\mu$ m.

### ***3.4. Generation of mice deficient for PC in intestinal cell subsets***

Mouse strains carrying the conditional knockout (KO) alleles for the kinesin family member 3A (*Kif3a<sup>flx/flx</sup>*) (Marszalek et al., 1999b) or intraflagellar transport 88 (*Ift88<sup>flx/flx</sup>*) (Haycraft et al., 2007a), are commonly used for study in PC, but these two proteins are not just essential for cilia formation (Kodani et al., 2013a) (Haycraft et al., 2007a). In this study we employed both mouse strains as this would allow to conclude the role of PC in colonic mesenchymal cells when phenotypes overlap.

Tissue specific deletion of conditional alleles was obtained by crossing the conditional KO mice with transgenic mice for cre-recombinase under the control of a collagenase VI promoter (*colVIcre*) targeting mesenchymal cells, including colonic mesenchymal cells (Armaka et al., 2008a) (Koliaraki et al., 2015a)(Figure 21). Homozygous *ColVIcre-Kif3a<sup>flx/flx</sup>* and *ColVIcre-Ift88<sup>flx/flx</sup>* mice were acquired in the way described in Figure 22.

**Figure 21 Illustration of the two conditional knock-out mouse models used**

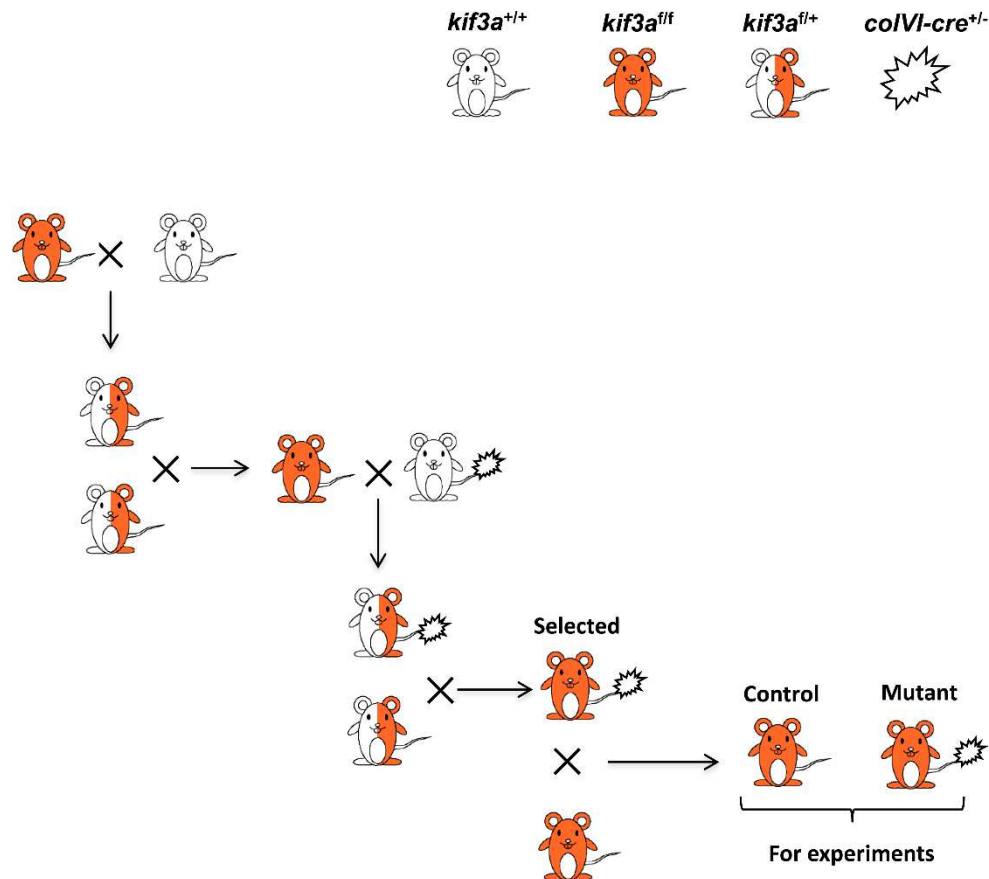


(A) Illustration of the targeting construct and the *Kif3a* genomic region, showing the location of the exons, the loxP sites and the primers(Marszalek et al., 1999a) (Qiu et al., 2012). Three primers were used for genotyping by PCR.

(B) Illustration of the targeting construct and the *Ift88* genomic region, showing the location of the exons, the loxP sites and the primers(Haycraft et al., 2007a). Three primers were used for genotyping by PCR.



**Figure 22 Breeding strategy**



Both mouse models were bred using the same strategy.

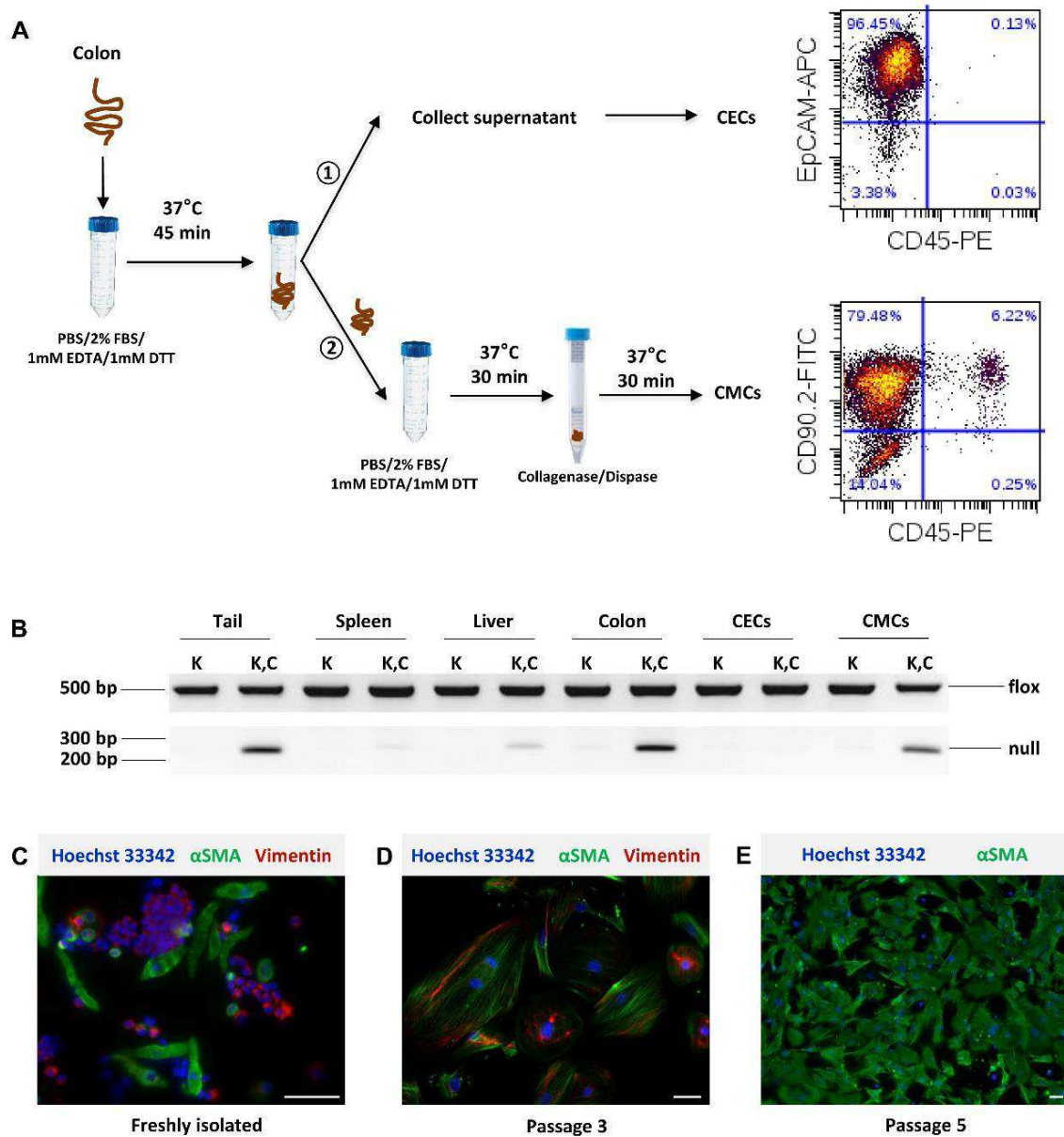
*ColVI-kif3a*<sup>flf</sup> were named mutant mice, and *kif3a*<sup>flf</sup> were considered as control animals.

### 3.5. *Validation of mice deficient for PC in intestinal mesenchymal cells*

Colonic epithelial cells (CECs) and colonic mesenchymal cells (CMCs) were isolated (Figure 23A). The deletion was indeed only detectable in intestinal mesenchymal cells, but not epithelial cells (Figure 23B). To further characterize colVI-deficient colonic mesenchymal cells, I purified cells from intact tissue and kept them in culture. When I took colonic mesenchymal cells in culture, we observed an important increase of  $\alpha$ SMA<sup>+</sup> cells during early passaging. While initially ~50 % of colonic mesenchymal cells expressed  $\alpha$ SMA, a myofibroblast marker, but over 90 % of cells expressed this marker after 2 Passages (Figure 15B, 23C-E). This is in line with a previous report (Koliaraki et al., 2015b). We believe that this change reflects a significant alteration of cell specificity and that *in vitro* analysis of colonic mesenchymal cells are of limited value. We focused therefore our functional studies on PC on *in vivo* experiments, not *in vitro*.

As expected, significantly less PC were detectable in the colon of *ColVIcre-Kif3a<sup>flx/flx</sup>* mice, though the depletion of PC on vimentin<sup>+</sup> or CD140 $\alpha$ <sup>+</sup> colonic mesenchymal cells was about 30-40% (Figure 24). This is in line with a previous report that the ColVI promoter is active in only a part of vimentin<sup>+</sup> or CD140 $\alpha$ <sup>+</sup> colonic mesenchymal cells (Koliaraki et al., 2015a).

**Figure 23 Validation of *colVI-kif3a<sup>fl/fl</sup>* mice in colonic epithelial cells (CECs) and colonic mesenchymal cells (CMCs)**

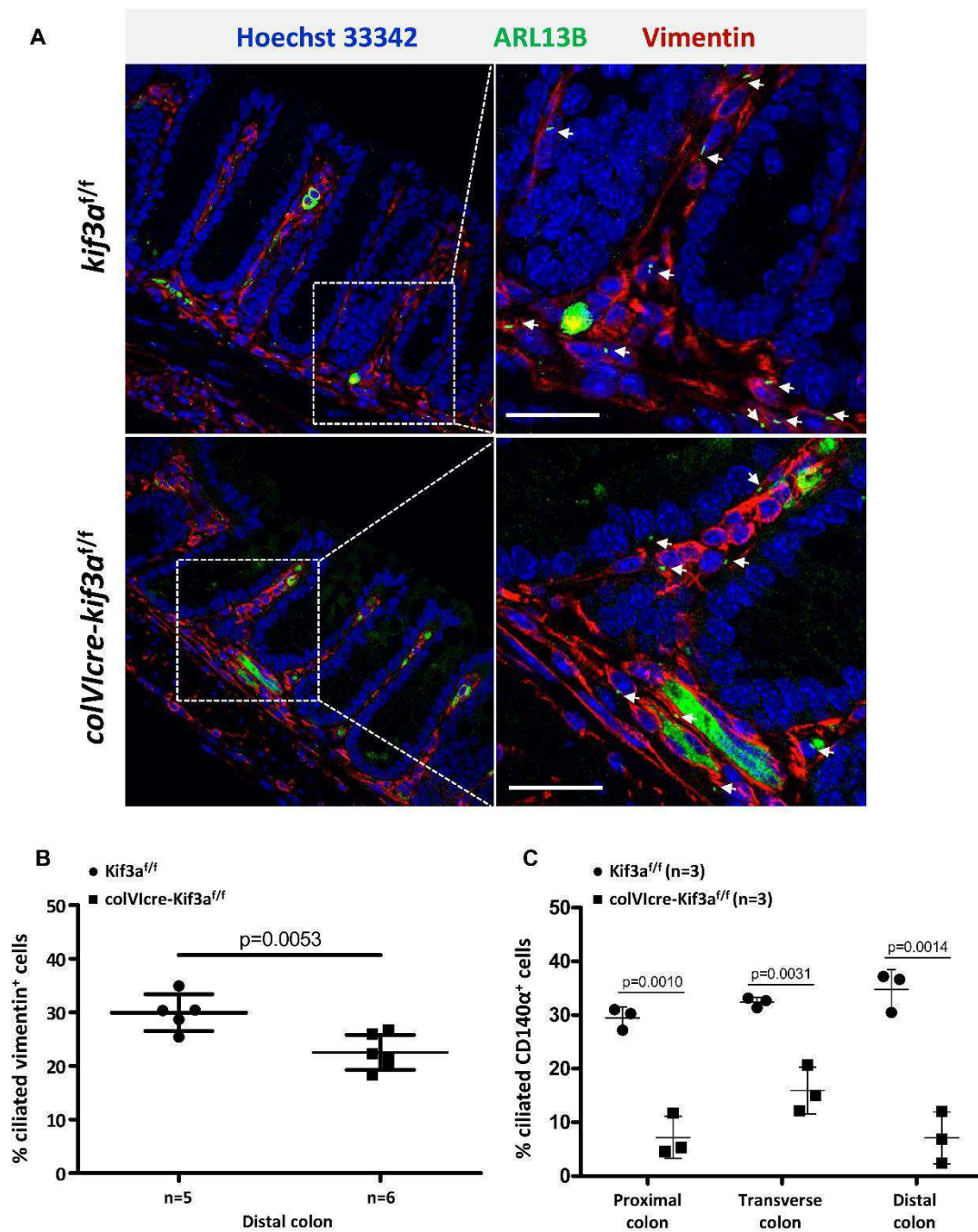


(A) Protocol for isolation of colonic epithelial cells (CECs) and colonic mesenchymal cells (CMCs). Purity of isolated cells (freshly isolated CECs and CMCs at passage 6) was determined by FACS.

(B) Detection of null signals for *Kif3a*-deletion in organs and isolated cells from control and mutant mice. In mutant mice, null band was only detected in tail, colon and CMCs, not spleen, liver and CECs.

(C) Double staining of  $\alpha$ SMA (green) and vimentin (red) of CMCs at different passages. K: *kif3a<sup>fl/fl</sup>* mice, KC: *colVI-kif3a<sup>fl/fl</sup>* mice. All scale bars represent 40  $\mu$ m.

Figure 24 Validation of *colVI-kif3a<sup>fl/fl</sup>* mice on intact tissues



(A) Double staining of ARL13B (green) and vimentin (red) in colon from control and mutant mice. All scale bar represent 20  $\mu$ m.

(B) Quantification of PC in vimentin positive cells from distal colon in control (n=5) and mutant (n=6) mice. 10 images were taken for each mouse.

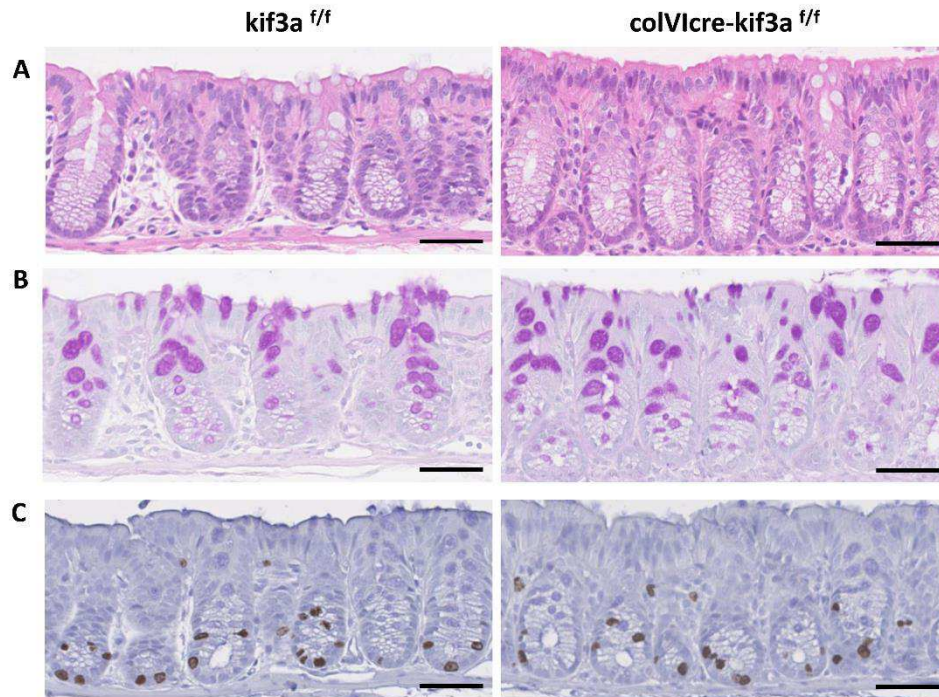
(C) Quantification of PC in vimentin positive cells from three parts of colon in control (n=3) and mutant (n=3) mice. 10 images were taken for each part of colon per mouse.

### **3.6. Phenotype of mice deficient for PC in intestinal mesenchymal cells**

*ColVCre-Kif3a<sup>flx/flx</sup>* and *ColVCre-Ift88<sup>flx/flx</sup>* mice were both fertile, born at expected mendelian ratio. By histological analysis, there is no apparent alteration in colon from *ColVCre-Kif3a<sup>flx/flx</sup>* mice (Figure 25A and 25B). Besides, proliferation of epithelial cells in *ColVCre-Kif3a<sup>flx/flx</sup>* mic was also similar to control animals as measured by BrdU incorporation (Figure 25C). However, we observed a weight loss in *ColVCre-Kif3a<sup>flx/flx</sup>* mice compared to control animals (Figure 14 A) at 7 months of age. Colons of mutant mice were also shorter (Figure 14 A). We kept a small cohort of mice for aging, and we observed the weight loss in *ColVCre-Kif3a<sup>flx/flx</sup>* mice after 4 months (Figure 26B) in spite of the fact that food and water intake were only slightly different in mutant mice (Figure 26C and 26D). At 12 month of age, *ColVCre-Kif3a<sup>flx/flx</sup>* mice displayed in average a 10 g lower weight to controls. Mice were sacrificed for further analysis of brown adipocytes (BAT), gonadal white adipocytes (gWAT), and inguinal white adipocytes (iWAT) (Figure 26E). Weight of iWAT was significantly decreased in *ColVCre-Kif3a<sup>flx/flx</sup>* mice indicating that aging *ColVCre-Kif3a<sup>flx/flx</sup>* mice may have an altered metabolism (Figure 26F). The colVCre-promoter has been described to be active in different cell types of mesenchymal origin such as synovial fibroblasts and adipocytes (Armaka et al., 2008b). Additional studies involving larger cohorts of

mice are necessary to decipher the weight loss in aging *ColVIcre-Kif3a<sup>flx/flx</sup>* mice. In the following experiments we used mice at the age of 8-12 weeks.

**Figure 25** Histological analysis of *colVI-kif3a<sup>ff</sup>* mice.



Mice were sacrificed 3 hours after BrdU injection.

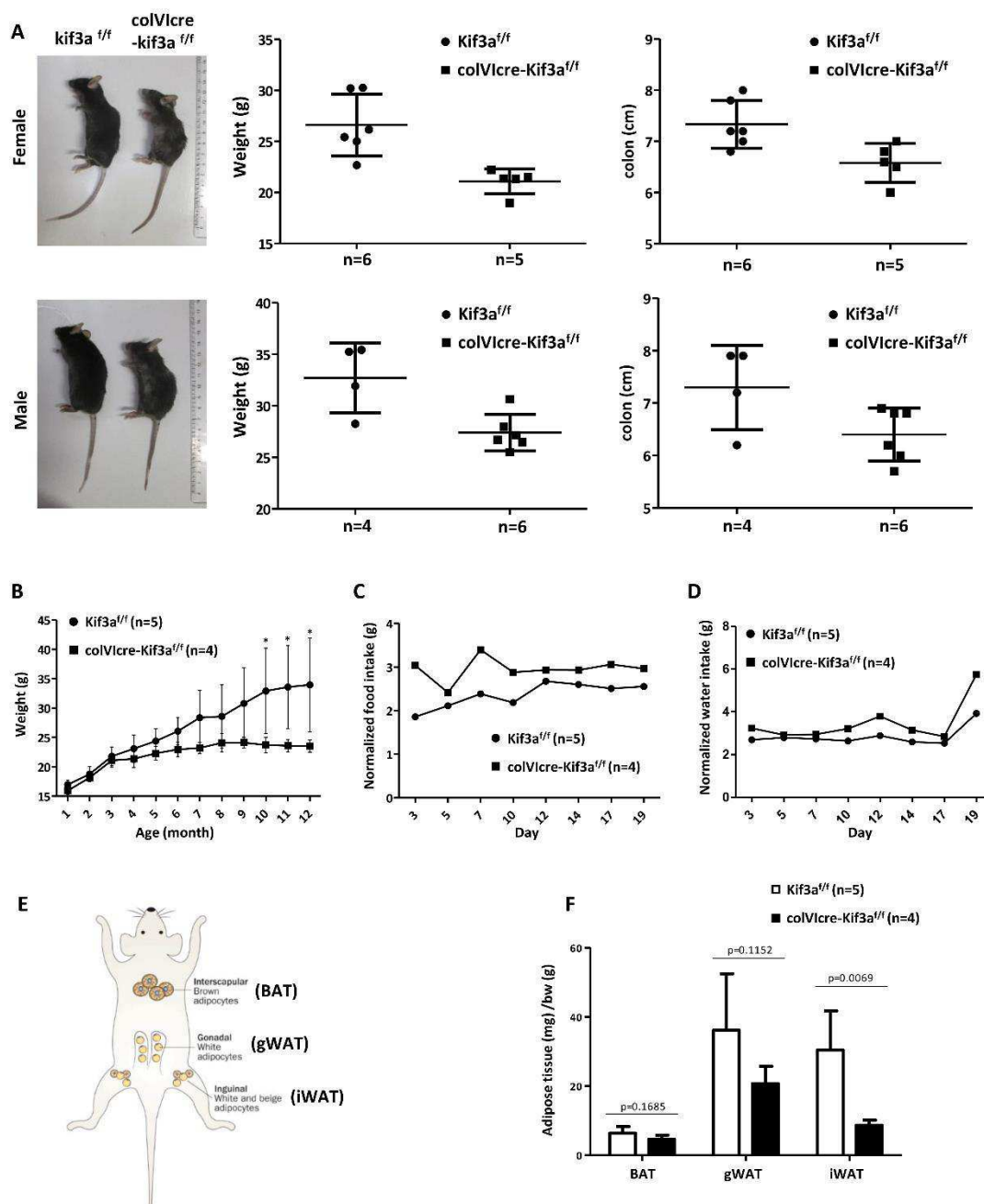
(A) Hematoxylin and eosin staining

(B) Periodic acid–Schiff (PAS) staining

(C) BrdU staining



**Figure 26** Weight loss of *colVI-kif3a<sup>fl/fl</sup>* mice.



(A) Representative photo, weight, and colon size of control (n=6) and mutant (n=5) mice at 7 months of age.

(B) Body weight changes in 4 to 12-month-old control (n=5) and mutant (n=4) mice.

(C) Food intake is presented as the quantity of ingested food normalized to 20g of body weight per day. Food was weighted every 2 days for 19 days for control (n=5) and mutant (n=4) 12 months old mice.

(D) Water intake is presented as the quantity of ingested food normalized to 20g of body weight per day. Water was weighted every 2 days for 19 days for control (n=5) and mutant (n=4) 12 month old mice.

(E) Illustration of brown adipocytes (BAT), Gonadal white adipocytes (gWAT) and inguinal white adipocytes (iWAT) in mouse (Bartelt and Heeren, 2014).

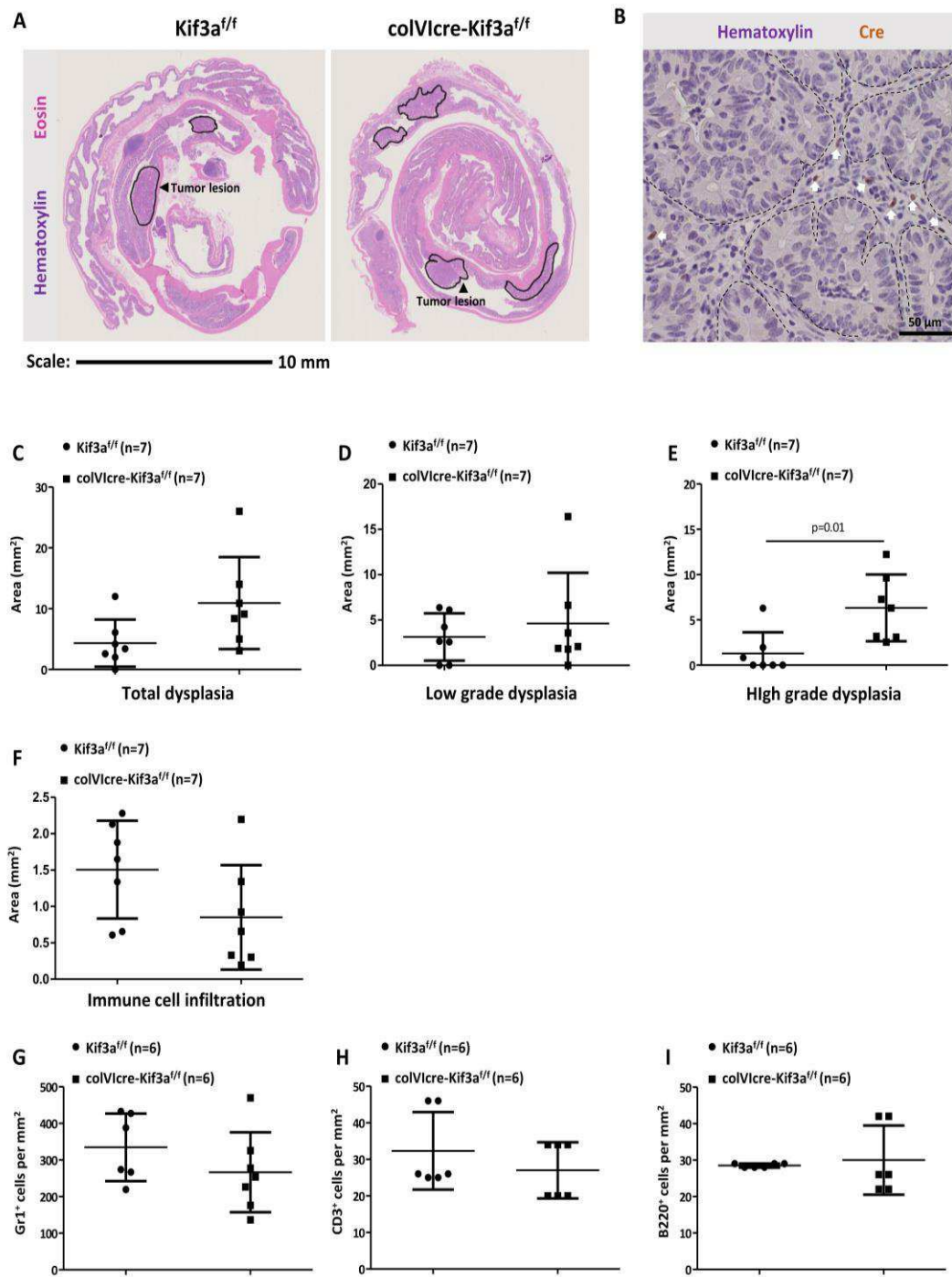
(F) BAT, gWAT and iWAT to body weight (bw) ratios were determined in 12-month-old control (n=5) and mutant (n=4) mice. Results are presented as the mean  $\pm$ SD of adipose tissue (mg)/bw (g).



### ***3.7. Decreased number of PC in colonic mesenchymal cells promotes CAC***

To test whether the decreased number of PC in colons of *ColVIcre-Kif3a<sup>flx/flx</sup>* alters their susceptibility to induced carcinogenesis, mice were exposed to the AOM/DSS protocol (see Figure 18). Female *ColVIcre-Kif3a<sup>flx/flx</sup>* mice displayed an increased incidence of dysplasia in particular a higher number of high grade dysplasia compared to *Kif3a<sup>flx/flx</sup>* mice (Figures 27C-E). This suggests that the decreased number of PC in colons of *ColVIcre-Kif3a<sup>flx/flx</sup>* rather promotes both tumor formation initiation and progression. Notably, the expression of the cre-recombinase correlated with the location of the tumor lesions in the *ColVIcre-Kif3a<sup>flx/flx</sup>* mice suggesting that the decreased number of PC in colonic mesenchymal cells indeed promotes tumor development (Figure 27B). No overall difference in infiltration of immune cells (granulocytes, T and B cells) was detectable (Figure 27F-I). Interestingly, only about 50% of the male *ColVIcre-Kif3a<sup>flx/flx</sup>* mice survived the AOM/DSS treatment (Figure 28A). This observation was associated with a significant lower weight of *ColVIcre-Kif3a<sup>flx/flx</sup>* mice at different time points during the protocol (Figure 28B).

**Figure 27 Decreased number of PC in colonic mesenchymal cells promotes CAC**



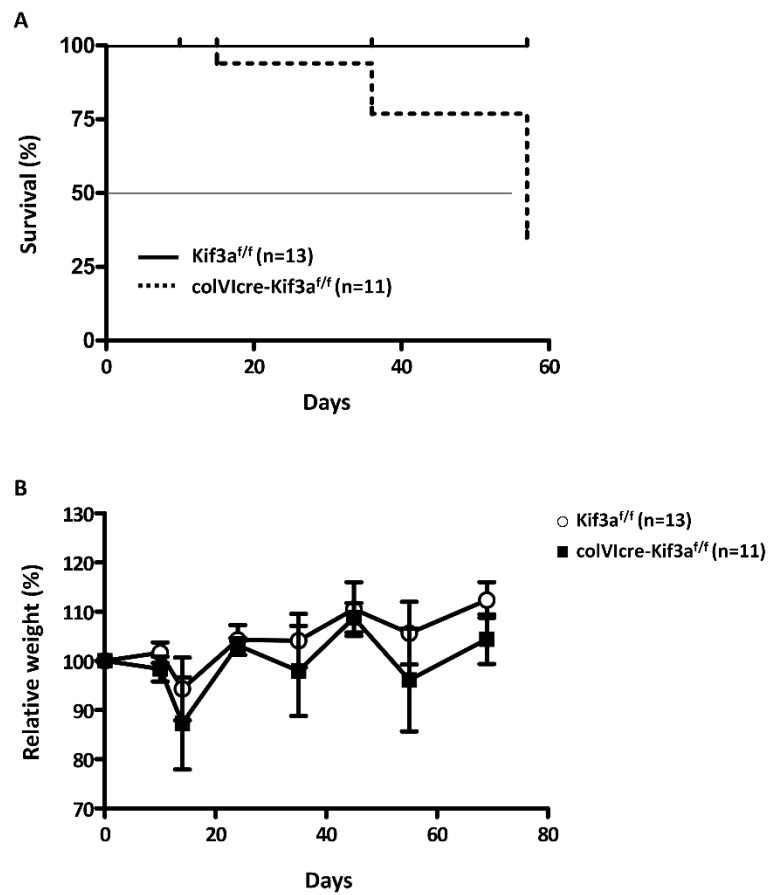
(A) Representative images of hematoxylin and eosin staining of colon sections taken from mice at the end of the AOM/DSS protocol (see Figure 18). Tumor lesions are labeled by black lines.

(B) Identification of CRE expression by immunohistochemistry. Epithelial cells are labeled by black lines, and CRE positive cells (brown) are indicated by white arrows.

(C-F) Total areas of total dysplasia, low grade dysplasia, high grade dysplasia, and immune cell infiltration in control (n=7) and mutant (n=7) mice. Results are presented as the mean  $\pm$  SD of areas (mm<sup>2</sup>).

(G-I) Quantification of Gr1, CD3 and B220 positive cells in colon from control (n=6) and mutant mice (n=6). Results are presented as the mean  $\pm$  SD of positive cells.

**Figure 28 Male mutant mice were more susceptible to AOM/DSS**



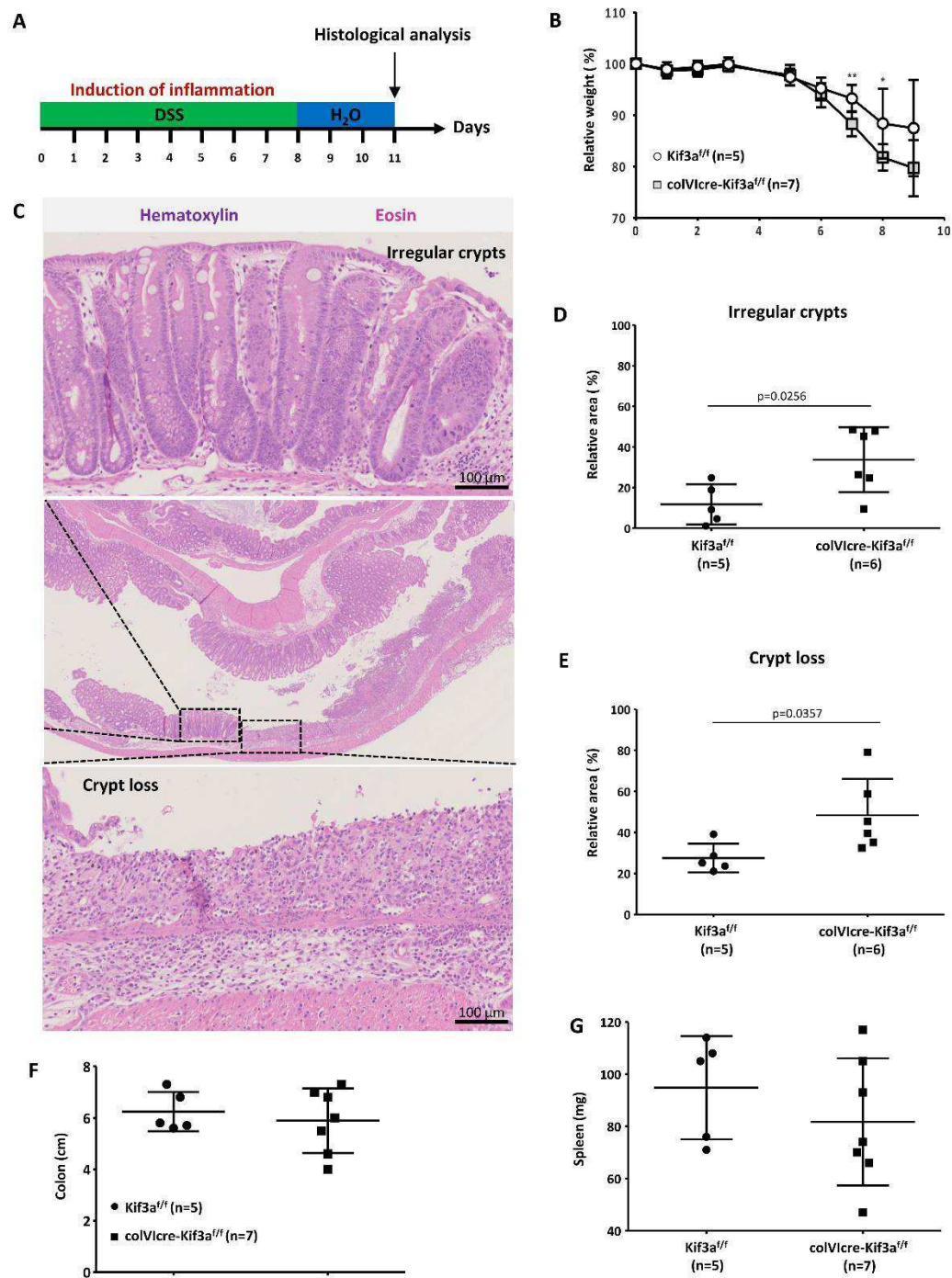
(A) Survival curve of male control (n=13) and mutant (n=11) mice. Mutant mice died at day 15, 36 and 57.

(B) Body weight strongly changes in male control (n=13) and mutant (n=11) mice at day 14, 35 and 55.

### ***3.8. Decreased number of PC in colonic mesenchymal cells promotes DSS-induced colitis***

To test the impact of decreased numbers of colonic PC in inflammation *ColVIcre-Kif3a<sup>flx/flx</sup>* and control mice were treated for one week with DSS, a commonly used animal model for acute colitis (Wirtz et al., 2007) (Hao et al., 2015). In fact, *ColVIcre-Kif3a<sup>flx/flx</sup>* mice displayed a moderate, but significant higher weight loss compared to *Kif3a<sup>flx/flx</sup>* mice at days 7, 8 and 9 after the start of the protocol (Figure 29A). According to the increased weight loss (Figure 29B), colon of *ColVIcre-Kif3a<sup>flx/flx</sup>* mice displayed larger areas of crypt loss and irregularities (Figure 29C-E). Colon length (Figure 29F) and spleen weight (Figure 29G) were comparable between the two cohorts of mice.

**Figure 29 Decreased number of PC in colonic mesenchymal cells promotes DSS-induced colitis**



(A) The experimental timeline for DSS-induced colitis.

(B) Weight loss of control (n=5) and mutant (n=7) mice during experiment.

(C) Representative images of irregular crypt and crypt loss in a control mouse.

(D, E) Quantification of irregular crypts and crypt loss of control (n=5) and mutant (n=7) mice.

(F, G) Size of colon and weight of spleen of control (n=5) and mutant (n=7) mice.

### **3.9. *ColVCre-Kif3a<sup>flx/flx</sup>* colonic mesenchymal cells display an altered molecular signature**

The ciliary membrane contains receptors for morphogens of the Wnt, Hedgehog (Hh) and Notch pathway, as well as other growth factors. We therefore explored whether either of these pathways is altered due to the decreased number of ciliated colonic mesenchymal cells in *ColVCre-Kif3a<sup>flx/flx</sup>* mice that could explain their increased susceptibility to DSS-induced colitis and AOM/DSS-induced colon carcinogenesis.

For this, we performed RNAseq gene profiling of purified colonic mesenchymal cells to screen for altered transcript expression levels. This analysis displayed an elevated expression for several genes involved in Notch and WNT signaling (Annex Table 1). We are presently validating the differential mRNA expression levels for several genes of either pathway by qPCR. In addition, we will test for elevated expression levels of Hes1 (to confirm altered Notch signaling) and increased nuclear location for beta-catenin (to confirm an elevated activation of Wnt signaling) by IHC in colons of *ColVCre-Kif3a<sup>flx/flx</sup>* mice.

Interestingly, we also detected elevated transcript levels for genes, which have been associated with cancer-associated fibroblasts (CAFs)(Shiga et al., 2015) (Kalluri, 2016)( Annex Table 1). These are fibroblasts within the microenvironment of tumors contributing to the tumor development. In spite of the distinct transcript expression profile in colonic mesenchymal cells, Hematoxylin and eosin staining of colons from *ColVCre-Kif3a<sup>flx/flx</sup>* mice appear to have no major alterations (Figure 25A).

We next analyzed the transcriptome of the distal parts of colons (i.e. those with the highest lesion incidence) from DSS-treated mice. Upregulated transcripts in ColVIcre-Kif3a<sup>flx/flx</sup> mice showed an inflammatory signature (Annex Table 2) corresponding to the increased lesion size observed in those mice (Figure 29D,29E). There was a striking upregulation of IL-6,  $\gamma$ -IFN and interferon-responsive genes. We are presently testing whether the colons of DSS-treated ColVIcre-Kif3a<sup>flx/flx</sup> mice released significantly higher levels of proinflammatory cytokines IL-6,  $\gamma$ -Interferon, TNF $\alpha$  *ex vivo* using CBA technique (see material and methods). Interestingly, several genes involved in tumorigenesis and cell cycle were upregulated as well, reflecting the incidence of dysplasia observed in DSS-treated ColVIcre-Kif3a<sup>flx/flx</sup> mice. To better characterize cell-specific alterations we isolated colonic mesenchymal cells and epithelial cells of DSS-treated mice for RNAseq analysis. This analysis is presently ongoing.

We also performed RNAseq analysis of distal parts of colons of AOM/DSS treated animals. The analysis, however, was not conclusive. We therefore plan to repeat this experiment and to perform RNAseq on isolated tumor lesions. Interestingly, however, among the ten highest hits of upregulated genes in colons of ColVIcre-Kif3a<sup>flx/flx</sup> mice was the TNF family member APRIL, our group previously identified to be a promoter of CRC in APC<sup>min</sup> and AOM/DSS treated mice(Lascano et al., 2012).

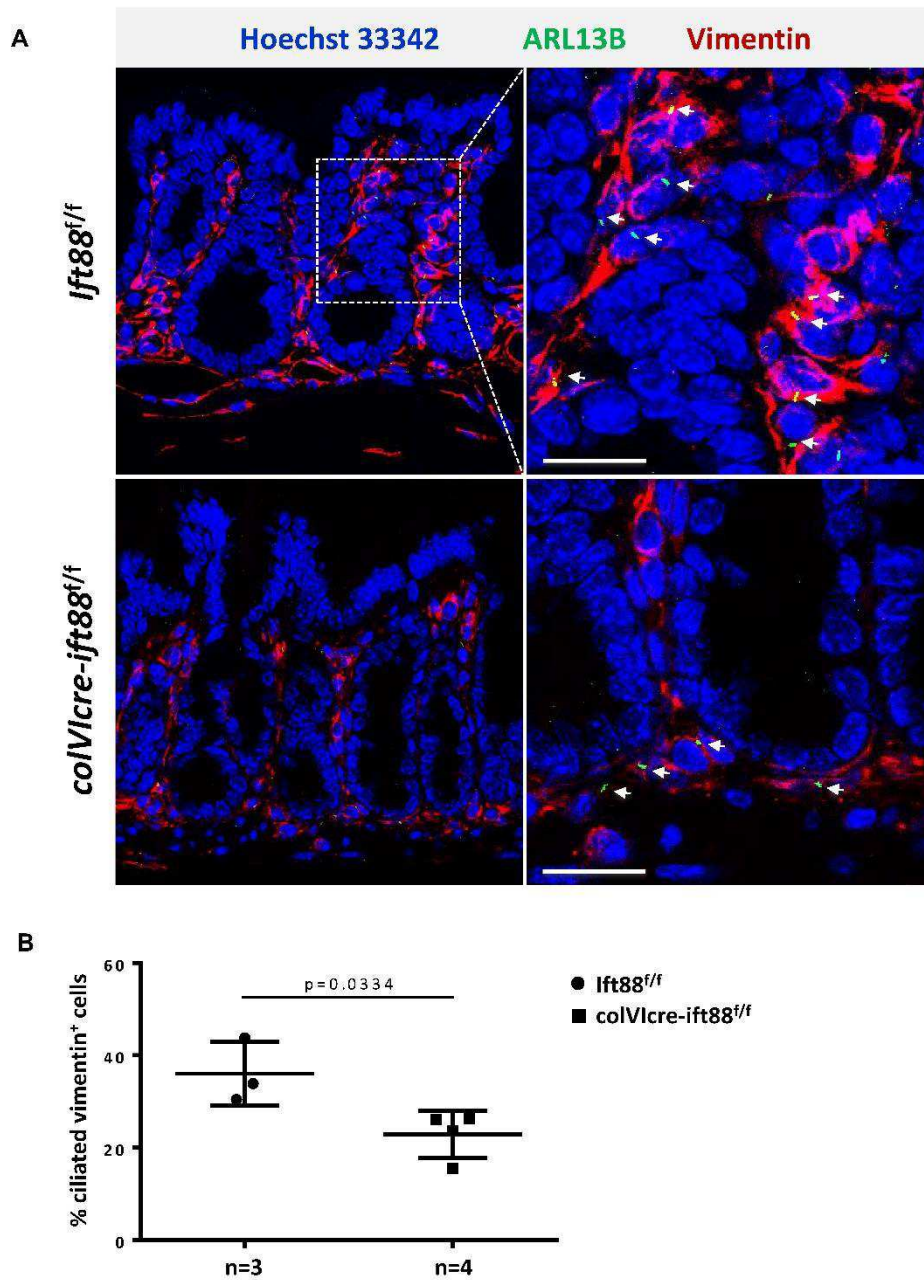
### ***3.10. ColVCre-Ift88<sup>flx/flx</sup> display less colonic PC and increased susceptibility to DSS-induced colitis***

Our analysis of *ColVCre-Kif3a<sup>flx/flx</sup>* mice revealed a link between PC expression on colonic mesenchymal cells and susceptibility to DSS-induced colitis and AOM/DSS-induced carcinogenesis. To validate these observations I employed conditional knockout mice for the intraflagellar transport protein 88 (*Ift88<sup>flx/flx</sup>*) that is also required to constitute PC (Haycraft et al., 2007b).

As expected, decreased number of PC in vimentin<sup>+</sup> colonic cells were detected in mutant mice (Figure 30). Importantly, *ColVCre-Ift88<sup>flx/flx</sup>* were more susceptible to DSS-induced colitis (Figure 31A), as manifested by elevated weight loss (Figure 31B), decreased colon size (Figure 31C) and spleen weight (Figure 31D).



Figure 30 *ColVlcre-IFT88<sup>flx/flx</sup>* mice display less colonic PC compared to control mice

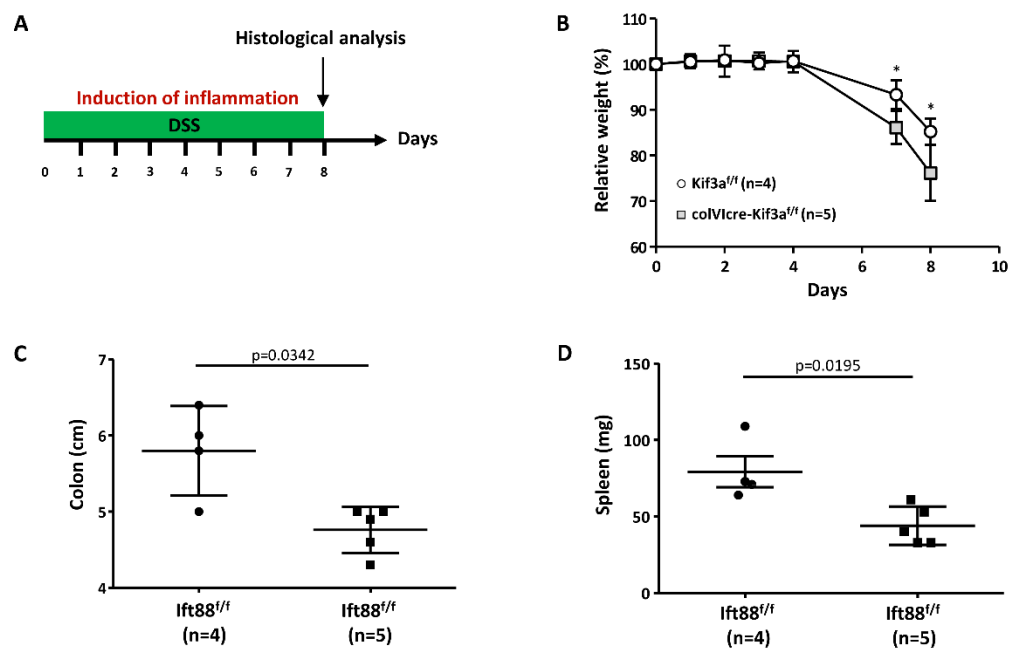


(A) Double staining of ARL13B (green) and vimentin (red) in colon from control and mutant mice.

White arrow heads indicate PC. All scale bars represent 20  $\mu$ m.

(B) Quantification of PC in vimentin positive cells from distal colon in control (n=3) and mutant mice (n=4). 10 images were taken for each mouse.

**Figure 31** *ColVCre-IFT88<sup>flx/flx</sup>* display increased susceptibility to DSS-induced colitis



(A) The experimental time line for DSS-induced colitis.

(B) Weight loss of control (n=4) and mutant (n=5) mice during DSS treatment.

(C-D) Mutant mice (n=5) had smaller colon and spleen compared with control mice (n=4) after 8-day DSS treatment.

## 4. Discussion

Our group previously described an unexpected role of the tubulin glycosylase TTLL3 in the regulation of colon homeostasis and tumorigenesis (Rocha et al., 2014b). This observation was associated with a significantly decreased number of Primary cilia (PC) in TTLL3 deficient colons. The aim of my PhD project was to further explore the role of PC colon carcinogenesis using established mouse models for PC.

Various reports associate PC with tumorigenesis, but their role in tumor development appears to be dual. Reduced numbers of PC have been described for breast and pancreatic cancer, as well as melanoma (reviewed in (Cao and Zhong, 2015)), whereas PC were reported to be maintained in about half of the tested biopsies medulloblastoma and BCC patients (Han et al., 2009b) (Wong et al., 2009b). The latter is underlined by the observation in mouse models that, depending on the nature of the oncogenic initiating event, ciliary ablation can be required or block medulloblastoma as well as BCC tumor formation (Han et al., 2009b)(Wong et al., 2009b). Distinct roles for PC in tumor formation is also suggested by an analysis of the ciliary gene expression in eight different cancers using the *The Cancer Gene Atlas (TCGA)* dataset (Shpak et al., 2014b). Ciliary genes were found to be upregulated in kidney renal clear cell carcinoma, lung squamous cell carcinoma, lung and rectal adenocarcinoma, but downregulated in glioblastoma, ovarian

cancer, breast and colon adenocarcinoma. I analyzed PC expression in colons of mice exposed to the CAC model, in which colon carcinogenesis is chemically induced. This analysis showed that numbers of PC decreased during colon carcinogenesis in the CAC mouse model. Notably, a recent report described a correlation between the frequency of colonic PC and disease outcome in CRC patients (Dvorak et al., 2016). The authors found a significant longer overall survival in CRC patients with higher frequency of PC concurring with our observations made in mice. We initiated collaborations with clinicians to analyze the presence of PC by immunohistochemistry in biopsies of colon carcinoma patients. So far, I only could analyze two patient samples, in which the tumor was separately located in sigmoid colon and rectum. On these two samples, PC were nearly undetectable on adjacent non-neoplastic colon mucosa, but highly expressed in the tumor area. More samples need to be analyzed in the future to allow conclusions.

I observed that PC are detectable only on subsets of vimentin<sup>+</sup> or CD140α<sup>+</sup> colonic mesenchymal cells. To our knowledge this is the first description of PC on colonic stromal cells. To investigate consequences of the deletion of PC in colonic mesenchymal cells, we crossed the two commonly used mouse strains to study PC, i.e. *Kif3a*<sup>flx/flx</sup> and *Ift88*<sup>flx/flx</sup>, with *ColVCre* transgenic mice, targeting mesenchymal cells including

subsets of colonic mesenchymal cells (Armaka et al., 2008a) (Koliaraki et al., 2015a). In addition to their role in PC formation, KIF3a and IFT88 may promote cilia-independent functions, such as spindle orientation or mother centriole appendage formation (Kodani et al., 2013b)(Delaval et al., 2011b). Therefore, we decided to study both mutant mice deficient of PC to allow a conclusion whether a potential phenotype is are truly cilia-dependent.

The number of PC was significantly lower in *ColVIcre-Kif3a<sup>flx/flx</sup>* as well as *ColVIcre-Ift88<sup>flx/flx</sup>* mice compared to control animals, in agreement with the requirement of Kif3a and Ift88 for maintenance of PC. To study the consequences of the deletion of PC in colonic mesenchymal cells animals were exposed to chemically induced colon carcinogenesis. *ColVIcre-Kif3a<sup>flx/flx</sup>* mice showed an elevated incidence of high grade dysplasia suggesting that the reduction of PC on colonic mesenchymal cells rather promotes then initiates tumor progression.

Weight loss was observed in aging *ColVIcre-Kif3a<sup>flx/flx</sup>* mice and these mice had smaller inguinal white adipocytes. This is probably due to the fact that the *colVI* promoter is active in various mesenchymal cell types (joint synovial fibroblasts, articular chondrocytes and myocytes, skin keratinocytes and dermal fibroblasts and the muscle layer around arteries of the heart) (Armaka et al., 2008a), which might cause altered

metabolism during aging process. As weight loss became evident in aged mice we used less than 4 month old mice for the *in vivo* experimentation.

*ColVCre-Kif3a<sup>flx/flx</sup>* mice also showed weight loss when they were exposed to chemically induced colitis (DSS). Area of irregular crypts and crypt loss were significantly higher in mutant mice. These findings on *ColVCre-Kif3a<sup>flx/flx</sup>* mice were confirmed by the analysis of *ColVCre-Ift88<sup>flx/flx</sup>* animals. *ColVCre-Ift88<sup>flx/flx</sup>* mice also showed smaller colon and spleen size. Interestingly, the male *ColVCre-Kif3a<sup>flx/flx</sup>* mice appear more susceptible to DSS treatment. These findings suggest that the downregulation of PC on colonic mesenchymal cells promote colitis.

To identify on which molecular level PC-negative colonic mesenchymal cells promote more advanced dysplasia, we performed RNA-seq analysis on isolated colonic mesenchymal cells from *ColVCre-Kif3a<sup>flx/flx</sup>* and control mice. This revealed an upregulation of various genes characteristic for Wnt and Notch signaling in *ColVCre-Kif3a<sup>flx/flx</sup>* mice derived fibroblasts. Interestingly, these displayed also an upregulation of various genes characteristic for cancer-associated fibroblasts (CAFs) such as vimentin,  $\alpha$ SMA, Fibroblast-Specific Protein-1 (S100A4), platelet derived growth factor receptor- $\alpha$  and  $\beta$  (PDGFR  $\alpha$  and  $\beta$ ) (Koliaraki et al., 2015b). Different cellular origins for CAFs have been described. These include

resident myofibroblasts and fibroblasts, as well as endothelial or epithelial cells (Shiga et al., 2015) (Koliaraki et al., 2015b). It is tempting to speculate that the accumulation of CAF markers in *ColVIcre-Kif3a<sup>flx/flx</sup>* mice supports the idea that resident fibroblasts are at the origin of CAFs.

RNAseq analysis of the distal part of colon derived from DSS-treated *ColVIcre-Kif3a<sup>flx/flx</sup>* mice showed an upregulation of inflammation associated genes, which is consistent with the increased irregular crypts and crypt loss found in mutant mice. However, the analysis of distal parts of colons from AOM/DSS treated *ColVIcre-Kif3a<sup>flx/flx</sup>* mice was not conclusive. This is likely due to the mixture of tumor lesions and tissue areas without dysplasia.

Therefore, during writing of this thesis we started to validate the RNAseq data by qPCR and to generate RNA from isolated colonic mesenchymal cells and epithelial cells from DSS treated *ColVIcre-Kif3a<sup>flx/flx</sup>* and control mice to monitor the cell type specific molecular changes. In addition, we started to validate increased WNT activity (by staining for nuclear beta-catenin) and Notch signaling (by staining for HSE-1). Besides, we plan to perform RNAseq on isolated tumor lesions from AOM/DSS experiment *ColVIcre-Kif3a<sup>flx/flx</sup>*.

Colonic mesenchymal cells are well established to cooperate with



epithelial cells during colon carcinogenesis (Vermeulen et al., 2010). Colonic mesenchymal cells can also modulate inflammation, maintain the stem cell niche, promote angiogenesis, regulate synthesis and remodeling of the extracellular matrix (ECM) in colon carcinogenesis (Reviewed in Koliaraki et al., 2017). For example, two recent interesting articles described different roles for colonic mesenchymal cells during CAC in mice (Pallangyo et al., 2015) (Koliaraki et al., 2015a). In both studies the role of IKK $\beta$  in CAC was investigated upon tissue specific deletion of subsets of stromal cells in the colon using either collagenase1a2 (*colla2*)- or *colVI*-promoter driven recombination. In the former model tumor promotion was observed, while the latter resulted in decreased tumor initiation. A possible explanation for these findings might be the targeting of stromal subsets, which are not identical and have different functions. Interestingly, while IKK $\beta$ -deletion upon *colVI*-promoter driven recombination appears to regulate tumor initiation, we observed that *colVI*-promoter driven deletion of PC rather appears to affect tumor progression, instead of initiation.

Previous work of our group (Rocha et al., 2014b) led to the hypothesis that reduced numbers of PC in the colon promoted colon carcinogenesis. My work shows that decreased numbers of PC indeed promote chemically induced colon carcinogenesis in mice using the CAC model. This suggest the possibility of restoration of PC for CAC therapy.

Our previous work(Rocha et al., 2014b) also showed the link between deficient tubulin glycyrase and reduced numbers of PC in the colon. This would suggest that targeting deglycyases has therapeutic potential, but deglycyase(s) have not yet been identified. However, several PTM *of tubulin play an important* role in the maintenance of PC. Thus, the modulation of enzymes katalyzing those PTMs may have the potential for restoration of PC, eg. the  $\alpha$ -tubulin deacetylase, histone deacetylase 6 (HDAC6) (Hubbert et al., 2002). Inhibition of HDAC6 have been shown to restore ciliary expression and suppressed tumor development in a cholangiocarcinoma (CCA) model (Gradilone et al., 2013). In fact, several HDAC inhibitors have already been approved for cancer therapy (Table 1). For example, loss of PC is observed in pancreatic ductal adenocarcinoma (PDAC) cells, interestingly, inhibition of HDAC2 by trichostatin A (TSA) , or depletion of HDAC 2 by siRNA both restored PC formation in PDAC *cells*(Kobayashi et al., 2016). Besides, the group of Johannes V. Swinnen has screened a library of clinically evaluated compounds to identify their ability to restore PC in cancer cells (Khan et al., 2016). 118 compounds, including microtubule modulator Docetaxel, were able to stimulate PC expression in pancreatic ductal cancer cells. A selection of the most potent compounds (Clofibrate, Gefitinib, Sirolimus, Imexon and Dexamethasone) significantly increased the percentage of ciliated cells in a panel of cancer cell lines (pancreas, lung, kidney and breast).

I could demonstrate *in vivo* that PC are downregulated during colon carcinogenesis. Though this findings still need confirmation on biopsies of CRC patients, my findings obtained in mouse models support the idea to restore PC as a novel therapeutic strategy for PC negative/low tumors.

**Table 1 The list of HDAC inhibitors approved for cancer treatment**

<b>Inhibitor</b>	<b>Trade name</b>	<b>Treatment</b>	<b>Approval</b>
Vorinostat	Zolinza	Cutaneous T cell lymphoma	U.S. FDA 2006
Romidepsin	Istodax	Cutaneous T cell lymphoma	U.S. FDA 2009
Belinostat	Beleodaq	Peripheral T-cell lymphoma	U.S. FDA 2014
Chidamide	Epidaza	Peripheral T-cell lymphoma	China FDA 2014
Panobinostat	Farydak	Multiple myeloma	U.S. FDA 2015

Source :

1. <https://www.fda.gov/downloads/drugs/guidancecomplianceregulatoryinformation/lawsactsandrules/ucm428333.pdf>
2. <http://www.sfda.gov.cn/WS01/CL0103/115469.html>

## 5. Material and Methods

### *Patient samples*

Untreated human samples from colorectal adenomas, adenocarcinoma, and matched normal adjacent colorectal tissues were collected by the surgical oncology and stored in the University of Chieti, Italy (permission N° A10-024). According to Italian regulations, patients were informed of research performed with the biological specimens obtained during their treatment and did not express opposition. Disease stage of CRC was based on 7<sup>th</sup> revised edition of the AJCC Colorectal Cancer.

### *Animal experimentation*

Mouse experiments were performed in strict accordance with the guidelines of the European Community (86/609/EEC) and the French National Committee (87/848) for care and use of laboratory animals. To study PC we used *Kif3a<sup>flx/flx</sup>* and *Ift88<sup>flx/fl</sup>* mice which have been previously described (Marszalek et al., 1999b)(Haycraft et al., 2007b). Tissue specific knock-out mice were obtained by crossing with villin-cre mice (el Marjou et al., 2004) and ColVI cre-transgenic strains. The latter was obtained by G. Koliass (Armaka et al., 2008a)(Koliaraki et al., 2015a). Mice were maintained on C57BL/6 genetic background, and experimental groups contained littermates that were caged together according to gender. Genotyping was done as described before

(Marszalek et al., 1999b)(Haycraft et al., 2007b)(el Marjou et al., 2004)(Armaka et al., 2008a). ColVICre-*Kif3a*<sup>flx/flx</sup> and ColVICre-*Ift88*<sup>flx/fl</sup> mice were fertile, born at expected mendelian ratio and displayed no overt intestinal phenotype (data not shown). Mice used for the experiments described were used at age of 8-12 weeks. Some of the mutant mice cohorts used had a 10% lower weight than controls at beginning of treatments. Partial recombination of the floxed alleles was also detectable in the heart of ColVICre-*Kif3a*<sup>flx/flx</sup> mice, but those animals presented no indication for heart dysfunction (data not shown).

### ***DNA extraction by proteinase K for genotyping***

725  $\mu$ L Tail Buffer (50 mM Tris-HCL, pH 8, 10 Mm EDTA, 100 mM NaCl, 0.5% SDS) and 25  $\mu$ L 20 mg/ml Proteinase K(#EU0090, EUROMEDEX) were mixed with a piece of mouse tail in an Eppendorf tube and digested at 50  $^{\circ}$ C (with moderate agitation) overnight. After vortexing samples, 250  $\mu$ L saturated NaCl were added to each tube and vortexed again. Samples were centrifuged for 15 minutes at 12,000 rpm at room temperature. 750  $\mu$ L of the supernatant were carefully removed without touching the pallet and transferred it to a new tube. 500  $\mu$ L isopropanol were then added to each tube to precipitated DNA and samples were vortexed again. Samples were centrifuged for 20 minutes at 12,000 rpm at room temperature. The supernatant was discarded and the

remaining pellet was dried with an Eppendorf centrifugal vacuum concentrator 5301. Pellets were resuspended in 50  $\mu$ L MilliQ water and vortexed. The concentration was measured using Nanodrop and adjusted to a final concentration of 40ng/ $\mu$ L. 1  $\mu$ L of those samples were taken for PCR and remaining samples were kept at 4  $^{\circ}$ C.

### ***HotSHOT DNA extraction for genotyping***

DNA extraction by proteinase K is a commonly used protocol to isolate genomic DNA, but relatively time intensive. After searching and discussing with colleagues at our campus, I discovered a new protocol named as “HotSHOT” (hot sodium hydroxide and tris). This protocol allows to acquire genomic DNA in one hour. Briefly, 100  $\mu$ L of lysis buffer (25 mM NaOH and 0.2 mM EDTA) are added into an Eppendorf tube containing mouse tail (2-3 mm long). After incubation at 95  $^{\circ}$ C for 20 min, the tubes are placed on ice for 20 min. Then 100  $\mu$ L Neutralization Buffer (40 mM Tris-HCl) are added and the tubes are vortexed. 2  $\mu$ L from the top of the solution is taken for PCR. Remaining sample were kept at 4  $^{\circ}$ C.

### ***Polymerase chain reaction (PCR)***

PCR was performed as described below(Figure 32), using GoTaq® Flexi DNA Polymerase (#M8305, Promega) and GoTaq® Hot Start



Polymerase (#MM5005, Promega). Details of primers were shown in Table 1.

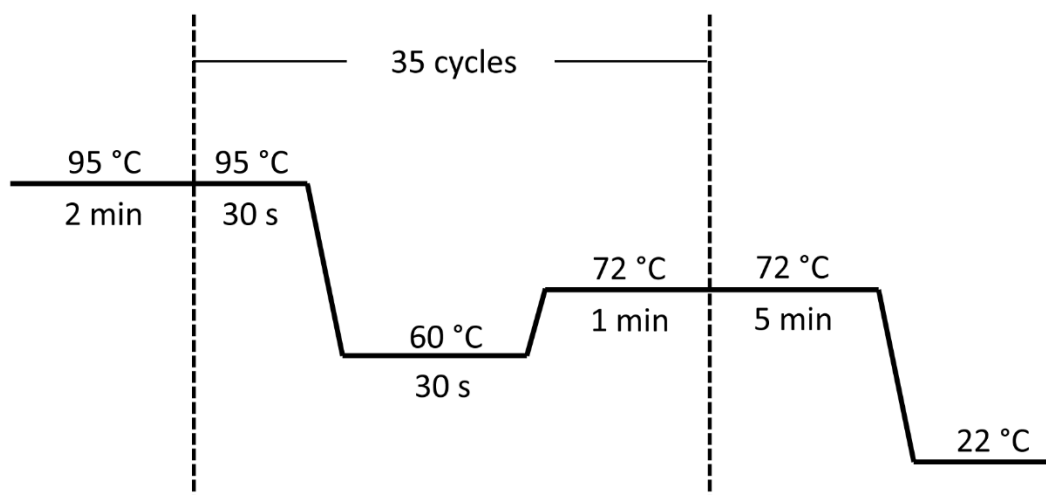


Figure 32 PCR cycling parameters.

## ***Immunohistochemistry***

The entire colon was prepared according to the Swiss roll procedure, and fixed with formalin and embedded in paraffin. Immunohistochemistry was performed on 4- $\mu$ m sections.

Tissue slides were deparaffinized and rehydraed at roome temperature, by washing with xylene(2 x 5 min), 100 % ethanol (5 min), 96% ethanol (3 min), 70% ethanol (3 min) and dH<sub>2</sub>O (5 min). Antigen retrieval was performed by 10 mM sodium citrate buffer (pH=6, T0050, DIAPATH) for 20 minutes at 100 °C in the water bath. After cooling down for 20 min, slides were incubated by 0.3% hydrogen (#H1009, Sigma) for 10 min, then Avidin/Biodin (#SP-2001, *Vector Laborarories*) for 15min. After

blocking with 2.5 % goat serum (#S-1012, *Vector Laboratories*) for 1h at RT, samples were incubated with primary antibody (Table 1) overnight at 4 °C, then biotinylated antibodies (*Vector Laboratories*) for 45 min at room temperature. Peroxidase substrate kit (#SK-4100, *Vector Laboratories*) or ImmPRESS™ HRP Anti-Rabbit IgG Polymer Detection Kit (#MP-7401, *Vector Laboratories*) *were used for detection.*

### ***Detection of PC on intact tissue***

Previously in our lab, PC were detected on colon using frozen sections, prepared by Tissue-Tek® O.C.T. Compound (#4583, SAKURA). PC were detected using an anti-ARL13B antibody (Table 1) previously established as a marker for PC (Figure 33).

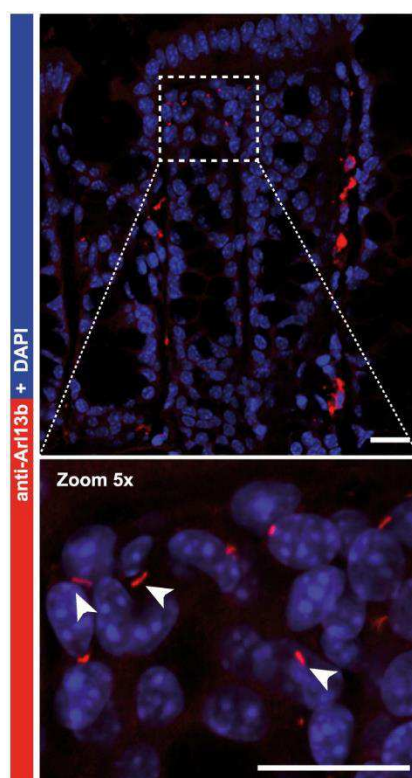


**Figure 33 Detection of PC in colon using ARL13B antibody. Scale bar: 20µm(Rocha et al., 2014a)**

To allow detection of PC I established a new protocol, which combined the work of Nadia B. Hassounah (Hassounah et al., 2013a) and a protocol from Cell Signaling Technology (<https://www.cellsignal.com/contents/resources-protocols/immunofluorescence-genera-protocol/if>). After this protocol was proven to work on kidney, which are known for high expression levels of PC (Figure 34), I decided to detect PC on colon using 4-  $\mu$ m paraffin sections.

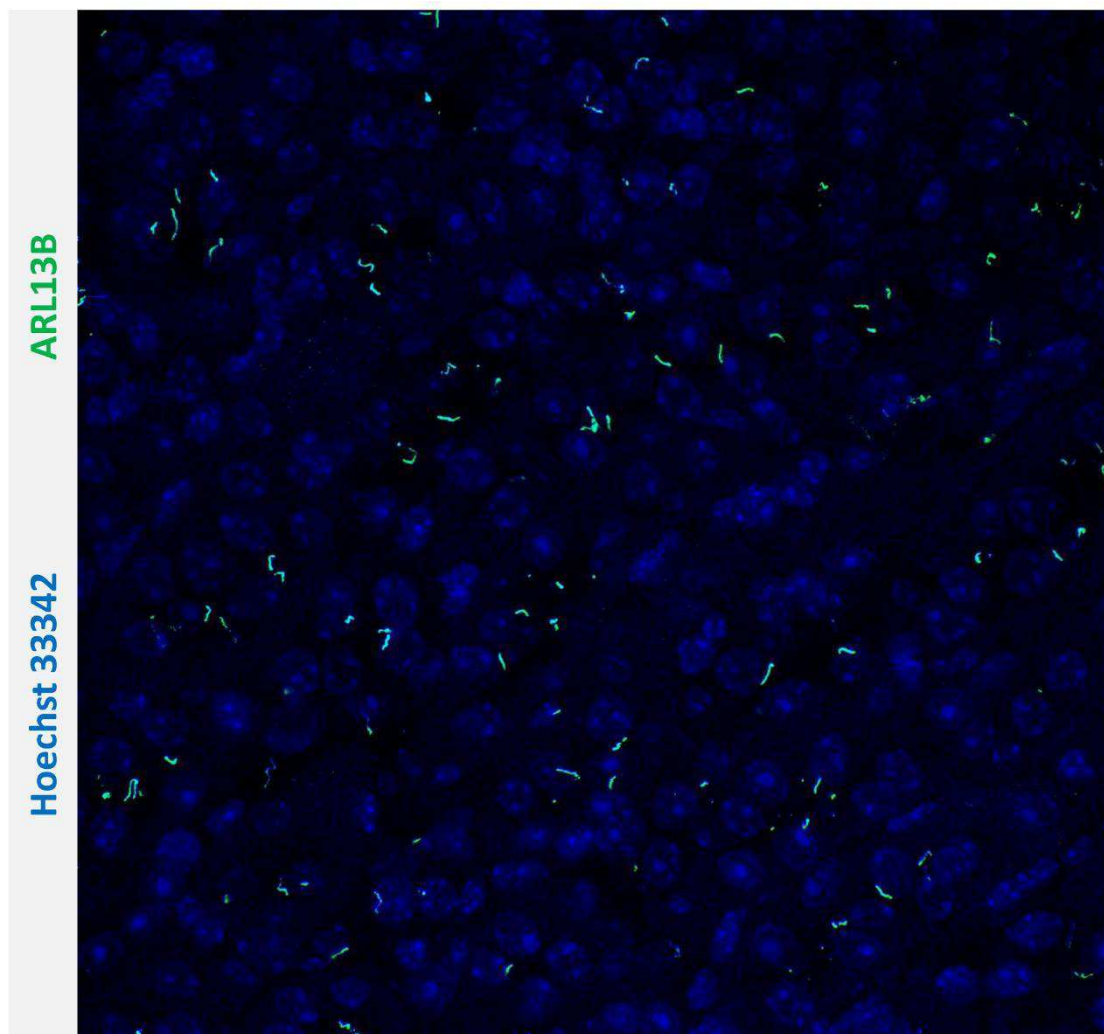


**Figure 34** Detection of PC in kidney using paraffin sections.

First, the entire colon was prepared in the same way as mentioned in immunohistochemistry section. Tissue slides were deparaffinized and rehydrated at room temperature, by washing with xylene(2 x 5 min), 100 % ethanol (5 min), 96% ethanol (3 min), 70% ethanol (3 min) and dH<sub>2</sub>O (5 min). Antigen retrieval was performed by 1mM EDTA for 25 minutes at 100 °C in the water bath. After incubation with blocking buffer (5% goat serum/0.3% Triton X-100) for 1h at RT, slides *were incubated with anti-ARL13B and/or anti-cell markers (E-cadherin, Vimentin, αSMA, CD140α) (Table 1) overnight at 4°C. After washing with PBS for three times*, slides were incubated with *secondary* antibodies labeled with Alexa 488 or Alexa 568 (Thermo Fisher Scientific, dilution 1/1000). After washing with PBS for three times, DNA was stained with 0.2 µg/ml Hoechst 33342. Primary antibodies, secondary antibodies, and Hoechst 33342 were all diluted by Blocking Buffer. Slides were mounted with coverslips (#0102242, Marienfeld-Superior), using Prolong Gold Antifade Mountant (#P36930, Thermo Fisher Scientific).

### ***BrdU incorporation proliferation assay***

For proliferation studies, 12-week-old mice were intraperitoneally injected with 100 µg/g Bromodeoxyuridine (BrdU; B9285, Sigma) in PBS. Colons were dissected 2 h or 5 days of injection. Colons were flushed with 10 ml of cold PBS, followed by formalin solution

(DiaPATH F0046; MM France). Incorporation of BrdU in proliferating intestinal epithelial cells was detected with anti-BrdU antibody (Biolegend), and the tissue was counterstained with Hematoxylin. The number of BrdU-positive cells per crypt and crypt segment was quantified of at least three animals per condition.

### ***AOM/DSS model, tumor histology and histological grading of tumors***

For colitis-associated carcinogenesis, mice were intraperitoneally injected with azoxymethane (AOM, 6.25 mg/kg), followed by three cycles of 2.5% (w/v) dextrane sodium sulphate (DSS) administered in the drinking water (Figure 4). In between the cycles the mice received no treatment for 2 weeks. For histological analysis the entire colon was prepared according to the Swiss roll procedure, fixed with formalin and embedded in paraffin. 4 µm sections were stained with hematoxylin and eosin, Alcan blue, periodic acid–Schiff (PAS) stain or deparaffinized and subsequently incubated with the primary antibody described below. Histological grading of AOM/DSS-induced tumors was determined with blinded genotype according to the described classification of intestinal neoplasia (Washington et al., 2013).

### ***Isolation of colonic epithelial cells (CECs) and mesenchymal cells (CMCs)***

The Protocol for isolation of CECs and CMCs were modified according to Roulis's publication. (Roulis et al., 2014). Briefly, the colon was isolated from mouse, flushed with PBS/2% FBS, and then opened longitudinally and processed as follows. The colon were cut into small pieces and incubated with CEC buffer (PBS/2% FBS/1 mM EDTA/1 mM DTT) at 37 °C for 45 minutes under continuous shaking to releases CEC. For the isolation of CMCs, the colon was incubated with CEC buffer for 75 min to eliminate CECs, then washed by PBS/2% FBS, and further processed by treatment with 3 mg/ml Collagenase type I (#C7657, Sigma) and 0.1 mg/ml Dispase (#LS0002100, PAN-Biotech) in DMEM for 30 min at 37 °C. Cells were filtered through a 70-µm strainer, washed with PBS/2% FBS and subsequently analyzed. Purity was validated by FACS performed on a FACSCalibur (BD), using the surface markers EpCAM, CD45, CD90.2 (Table 1).

### ***Microscopy and imaging***

Histological slides were scanned using Nanozoomer 2.0 HT scanner with a 40x objective, and visualized with the ndpi viewer. Fluorescent images were acquired on a inverted Confocal LSM780 (Zeiss) using the ZEN software. Images were processed with ImageJ. Images were assembled

and adjusted with Adobe Illustrator. Counting of PC was performed using Z-stack acquisition. Co-staining with fibroblast markers was confirmed on distinct layers.

### ***RNA-seq***

RNA was extracted from homogenized mouse organs or from cells using TRIzol reagent following the standard protocol. RNA-seq analysis was performed by BGI (China; [www.BGI.com](http://www.BGI.com)). Briefly, 2-3 µg of RNA per sample was provided to BGI to purify mRNA via oligo (dT) magnetic beads and to generate subsequently a cDNA library for sequencing. Bioinformatics analysis of raw data (taking in account an average of 44 million clean reads per sample) was performed by BGI as well. Altered gene expression was provided as log2 of ratio of FPKM values derived from ColVIcre-Kif3a<sup>flx/flx</sup> and Kif3a<sup>flx/flx</sup> mice. Poisson distribution method was used to calculate significance of differential gene expression.

### ***Quantitative real-time PCR***

Transcript levels were first determined using pooled RNA samples using RNAseq analysis. Differentially expressed transcripts were then validated by qPCR in single samples. qPCR (quantitative real-time PCR) was performed using SYBR Green (Roche) with the primers. Briefly, 1 µg of RNA was used to generate 20 µl of complementary DNA, following which the complementary DNA samples were diluted and then subjected



to 45 cycles of PCR at 95 °C for 10 s and 60 °C for 15 s. Internal controls used were GUS ( $\beta$ -glucuronidase), HPRT (hypoxanthine guanine phosphoribosyl transferase 1) and TBP (TFIID TATA box binding protein). Reactions were performed on a LightCycler 480 (Roche) machine. Data are shown as relative units where control bands were given a value of 1 and experimental values as fold change over control following normalization with the three housekeeping genes. All the experiments were performed in duplicate and at least three times.

### ***Measurement of cytokine production in ex vivo colons***

Colons from DSS-treated mice were isolated, washed with PBS and taken in culture in DMEM (10% FCS) for 24 h. Supernatants were analyzed for cytokine production by cytometric bead array technology (CBA; Becton Dickinson). Detection limits were IL-6: 5pg/ml, MCP-1:52.7pg/ml, IL-10: 17.5pg/ml, IFN $\gamma$ : 2.5pg/ml, TNF: 7.3 pg/ml, IL12 p70: 10.7 pg/ml.

### ***Statistical analysis***

Statistical analysis was performed by two-tailed unpaired t-test followed by Mann-Whitney post-test and t-test unpaired test followed by Dunn post-test using GraphPad Prism version 5.

**Table 1. Primers for genotyping**

Mouse strain	Primer	Sequence (5'-3')
<b>Ift88 WT</b>	ift88-1	GCCTCCTGTTTCTTGACAACAGTG
	ift88-2	GGTCCTAACAAGTAAGCCCAGTGTT
<b>Ift88 KO</b>	ift88-1	GCCTCCTGTTTCTTGACAACAGTG
	ift88-3	CTGCACCAGCCATTTCCTCTAAGTCATGTA
<b>Kif3a WT</b>	kif3a-1	AGGGCAGACGGAAGGGTGG
	kif3a-2	TCTGTGAGTTTGTGACCAGCC
<b>Kif3a KO</b>	kif3a-1	AGGGCAGACGGAAGGGTGG
	kif3a-3	TGGCAGGTCAATGGACGCAG
<b>Villin-cre Tg</b>	villin-1	CAAGCCTGGCTCGACGGCC
	villin-2	CGCGAACATCTTCAGGTTCT
<b>colVI-cre Tg</b>	colVI-1	ATTACCGGTCGATGCAACGAGT
	colVI-2	CAGGTATCTCTGACCAGAGTCA

WT: wild type, KO: knock out, Tg: Transgenic

**Table 2 The list of antibodies**

<b>Antigen</b>	<b>Company</b>	<b>Clone/reference</b>	<b>Concentration</b>	<b>Dilution used</b>
Arl13b	Neuromab	N295B/6675-287	1mg/ml	1/1000
alphaSMA	ebioscience	1A4/14-9760	0.5mg/ml	1/500
B220	BD	553086	0.5mg/ml	1/800
CD140 $\alpha$	Cell Signaling Technology	D1E1E/3174	not provided by supplier	1/400
CD3	Thermo Fisher Scientific	sp7/RM-9107	not provided by supplier	1/400
CD45-PE	Biolegend	30-F11/103105	0.2 mg/ml	1/100
CD90.2-FITC	BD	30-H12/553013	0.5 mg/ml	1/50
Cre	Cell Signaling Technology	D7L7L/15036	not provided by supplier	1/125
E-cadherin	Cell Signaling Technology	24E10/3195	not provided by supplier	1/500
EpCAM-APC	Biolegend	G8.8/118213	0.2 mg/ml	1/50
$\gamma$ -tubulin	Sigma	AK-15/T3320	8mg/ml	1/1000
Gr-1	Biolegend	RB6-8C5/108403	0.5mg/ml	1/100
Vimentin	Cell Signaling Technology	D21H3/5741	not provided by supplier	1/100

## 6. Reference

- 1) Armaka, M., Apostolaki, M., Jacques, P., Kontoyiannis, D.L., Elewaut, D., and Kollias, G. (2008a). Mesenchymal cell targeting by TNF as a common pathogenic principle in chronic inflammatory joint and intestinal diseases. *J. Exp. Med.* 205, 331–337.
- 2) Armaka, M., Apostolaki, M., Jacques, P., Kontoyiannis, D.L., Elewaut, D., and Kollias, G. (2008b). Mesenchymal cell targeting by TNF as a common pathogenic principle in chronic inflammatory joint and intestinal diseases. *J. Exp. Med.* 205, 331–337.
- 3) Barker, N. (2014). Adult intestinal stem cells: critical drivers of epithelial homeostasis and regeneration. *Nat. Rev. Mol. Cell Biol.* 15, 19–33.
- 4) Barker, N., Ridgway, R.A., van Es, J.H., van de Wetering, M., Begthel, H., van den Born, M., Danenberg, E., Clarke, A.R., Sansom, O.J., and Clevers, H. (2009). Crypt stem cells as the cells-of-origin of intestinal cancer. *Nature* 457, 608–611.
- 5) Bartelt, A., and Heeren, J. (2014). Adipose tissue browning and metabolic health. *Nat. Rev. Endocrinol.* 10, 24–36.
- 6) Basten, S.G., and Giles, R.H. (2013). Functional aspects of primary cilia in signaling, cell cycle and tumorigenesis. *Cilia* 2, 6.
- 7) Bolt, A.B., Papanikolaou, A., Delker, D.A., Wang, Q.-S., and Rosenberg, D.W. (2000). Azoxymethane induces KI-ras activation in the tumor resistant AKR/J mouse colon. *Mol. Carcinog.* 27, 210–218.
- 8) Bosch Grau, M., Gonzalez Curto, G., Rocha, C., Magiera, M.M., Marques Sousa, P., Giordano, T., Spassky, N., and Janke, C. (2013). Tubulin glycyloses and glutamylases have distinct functions in stabilization and motility of ependymal cilia. *J. Cell Biol.* 202, 441–451.
- 9) Brink, G.R. van den (2007). Hedgehog Signaling in Development and Homeostasis of the Gastrointestinal Tract. *Physiol. Rev.* 87, 1343–1375.
- 10) Cao, M., and Zhong, Q. (2015). Cilia in autophagy and cancer. *Cilia* 5, 4.

- 11) Clement, D.L., Mally, S., Stock, C., Lethan, M., Satir, P., Schwab, A., Pedersen, S.F., and Christensen, S.T. (2013). PDGFR $\alpha$  signaling in the primary cilium regulates NHE1-dependent fibroblast migration via coordinated differential activity of MEK1/2–ERK1/2–p90RSK and AKT signaling pathways. *J Cell Sci* 126, 953–965.
- 12) Corbit, K.C., Shyer, A.E., Dowdle, W.E., Gaulden, J., Singla, V., and Reiter, J.F. (2008). Kif3a constrains  $\beta$ -catenin-dependent Wnt signalling through dual ciliary and non-ciliary mechanisms. *Nat. Cell Biol.* 10, 70–76.
- 13) De Filippo, C., Caderni, G., Bazzicalupo, M., Briani, C., Giannini, A., Fazi, M., and Dolara, P. (1998). Mutations of the Apc gene in experimental colorectal carcinogenesis induced by azoxymethane in F344 rats. *Br. J. Cancer* 77, 2148–2151.
- 14) Delaval, B., Bright, A., Lawson, N., and Doxsey, S. (2011a). The cilia protein IFT88 is required for spindle orientation in mitosis. *Nat. Cell Biol.* 13, 461–468.
- 15) Delaval, B., Bright, A., Lawson, N.D., and Doxsey, S. (2011b). The cilia protein IFT88 is required for spindle orientation in mitosis. *Nat. Cell Biol.* 13, 461–468.
- 16) Doobin, D.J., Kemal, S., Dantas, T.J., and Vallee, R.B. (2016). Severe NDE1-mediated microcephaly results from neural progenitor cell cycle arrests at multiple specific stages. *Nat. Commun.* 7, 12551.
- 17) Dummer, A., Poelma, C., DeRuiter, M.C., Goumans, M.-J.T.H., and Hierck, B.P. (2016). Measuring the primary cilium length: improved method for unbiased high-throughput analysis. *Cilia* 5, 7.
- 18) Dumontet, C., and Jordan, M.A. (2010). Microtubule-binding agents: a dynamic field of cancer therapeutics. *Nat. Rev. Drug Discov.* 9, 790–803.
- 19) Dvorak, J., Hadzi Nikolov, D., Dusek, L., Filipova, A., Richter, I., Buka, D., Ryska, A., Mokry, J., Filip, S., Melichar, B., et al. (2016). Prognostic significance of the frequency of primary cilia in cells of small bowel and colorectal adenocarcinoma. *J. BUON Off. J. Balk. Union Oncol.* 21, 1233–1241.
- 20) Erdman, S.H., Wu, H.D., Hixson, L.J., Ahnen, D.J., and Gerner, E.W. (1997). Assessment of mutations in ki-ras and p53 in colon cancers

from azoxymethane- and dimethylhydrazine-treated rats. *Mol. Carcinog.* *19*, 137–144.

- 21) Es, J.H. van, Geest, N. de, Born, M. van de, Clevers, H., and Hassan, B.A. (2010). Intestinal stem cells lacking the Math1 tumour suppressor are refractory to Notch inhibitors. *Nat. Commun.* *1*, 18.
- 22) van Es, J.H., van Gijn, M.E., Riccio, O., van den Born, M., Vooijs, M., Begthel, H., Cozijnsen, M., Robine, S., Winton, D.J., Radtke, F., et al. (2005). Notch/ $\gamma$ -secretase inhibition turns proliferative cells in intestinal crypts and adenomas into goblet cells. *Nature* *435*, 959–963.
- 23) Ezratty, E., Stokes, N., Chai, S., Shah, A., Williams, S., and Fuchs, E. (2011). A role for the primary cilium in Notch signaling and epidermal differentiation during skin development. *Cell* *145*, 1129–1141.
- 24) Fearon, E.R., and Vogelstein, B. (1990). A genetic model for colorectal tumorigenesis. *Cell* *61*, 759–767.
- 25) Fre, S., Huyghe, M., Mourikis, P., Robine, S., Louvard, D., and Artavanis-Tsakonas, S. (2005). Notch signals control the fate of immature progenitor cells in the intestine. *Nature* *435*, 964–968.
- 26) Gerdes, J.M., Davis, E.E., and Katsanis, N. (2009). The Vertebrate Primary Cilium in Development, Homeostasis, and Disease. *Cell* *137*, 32–45.
- 27) Gradilone, S.A., Radtke, B.N., Bogert, P.S., Huang, B.Q., Gajdos, G.B., and LaRusso, N.F. (2013). HDAC6 inhibition restores ciliary expression and decreases tumor growth. *Cancer Res.* *73*, 2259–2270.
- 28) Han, Y.-G., Spassky, N., Romaguera-Ros, M., Garcia-Verdugo, J.-M., Aguilar, A., Schneider-Maunoury, S., and Alvarez-Buylla, A. (2008). Hedgehog signaling and primary cilia are required for the formation of adult neural stem cells. *Nat. Neurosci.* *11*, 277–284.
- 29) Han, Y.-G., Kim, H.J., Dlugosz, A.A., Ellison, D.W., Gilbertson, R.J., and Alvarez-Buylla, A. (2009a). Dual and opposing roles of primary cilia in medulloblastoma development. *Nat. Med.* *15*, 1062–1065.
- 30) Han, Y.-G., Kim, H.J., Dlugosz, A.A., Ellison, D.W., Gilbertson, R.J., and Alvarez-Buylla, A. (2009b). Dual and opposing roles of primary cilia in medulloblastoma development. *Nat. Med.* *15*, 1062–1065.

- 31) Han, Y.-G., Kim, H.J., Dlugosz, A.A., Ellison, D.W., Gilbertson, R.J., and Alvarez-Buylla, A. (2009c). Dual and opposing roles of primary cilia in medulloblastoma development. *Nat. Med.* *15*, 1062–1065.
- 32) Hao, X.P., Lucero, C.M., Turkbey, B., Bernardo, M.L., Morcock, D.R., Deleage, C., Trubey, C.M., Smedley, J., Klatt, N.R., Giavedoni, L.D., et al. (2015). Experimental colitis in SIV-uninfected rhesus macaques recapitulates important features of pathogenic SIV infection. *Nat. Commun.* *6*, 8020.
- 33) Hassounah, N.B., Nagle, R., Saboda, K., Roe, D.J., Dalkin, B.L., and McDermott, K.M. (2013a). Primary Cilia Are Lost in Preinvasive and Invasive Prostate Cancer. *PLOS ONE* *8*, e68521.
- 34) Hassounah, N.B., Nagle, R., Saboda, K., Roe, D.J., Dalkin, B.L., and McDermott, K.M. (2013b). Primary cilia are lost in preinvasive and invasive prostate cancer. *PloS One* *8*, e68521.
- 35) Haycraft, C.J., Zhang, Q., Song, B., Jackson, W.S., Detloff, P.J., Serra, R., and Yoder, B.K. (2007a). Intraflagellar transport is essential for endochondral bone formation. *Development* *134*, 307–316.
- 36) Haycraft, C.J., Zhang, Q., Song, B., Jackson, W.S., Detloff, P.J., Serra, R., and Yoder, B.K. (2007b). Intraflagellar transport is essential for endochondral bone formation. *Dev. Camb. Engl.* *134*, 307–316.
- 37) Ho, L., Ali, S.A., Al-Jazrawe, M., Kandel, R., Wunder, J.S., and Alman, B.A. (2013). Primary cilia attenuate hedgehog signalling in neoplastic chondrocytes. *Oncogene* *32*, 5388–5396.
- 38) Hubbert, C., Guardiola, A., Shao, R., Kawaguchi, Y., Ito, A., Nixon, A., Yoshida, M., Wang, X.-F., and Yao, T.-P. (2002). HDAC6 is a microtubule-associated deacetylase. *Nature* *417*, 455–458.
- 39) Janke, C. (2014). The tubulin code: Molecular components, readout mechanisms, and functions. *J. Cell Biol.* *206*, 461–472.
- 40) Jemal, A., Bray, F., Center, M.M., Ferlay, J., Ward, E., and Forman, D. (2011). Global cancer statistics. *CA. Cancer J. Clin.* *61*, 69–90.
- 41) Kalluri, R. (2016). The biology and function of fibroblasts in cancer. *Nat. Rev. Cancer* *16*, 582–598.
- 42) Khan, N.A., Willemarck, N., Talebi, A., Marchand, A., Binda, M.M., Dehairs, J., Rueda-Rincon, N., Daniels, V.W., Bagadi, M., Raj,



- D.B.T.G., et al. (2016). Identification of drugs that restore primary cilium expression in cancer cells. *Oncotarget* 7, 9975–9992.
- 43) Kim, S., and Tsiokas, L. (2011). Cilia and cell cycle re-entry. *Cell Cycle* 10, 2683–2690.
  - 44) Kim, S., Zaghloul, N.A., Bubenshchikova, E., Oh, E.C., Rankin, S., Katsanis, N., Obara, T., and Tsiokas, L. (2011). Nde1-mediated inhibition of ciliogenesis affects cell cycle re-entry. *Nat. Cell Biol.* 13, 351–360.
  - 45) Klapholz-Brown, Z., Walmsley, G.G., Nusse, Y.M., Nusse, R., and Brown, P.O. (2007). Transcriptional Program Induced by Wnt Protein in Human Fibroblasts Suggests Mechanisms for Cell Cooperativity in Defining Tissue Microenvironments. *PLOS ONE* 2, e945.
  - 46) Kobayashi, T., and Dynlacht, B.D. (2011). Regulating the transition from centriole to basal body. *J. Cell Biol.* 193, 435–444.
  - 47) Kobayashi, T., Nakazono, K., Tokuda, M., Mashima, Y., Dynlacht, B.D., and Itoh, H. (2016). HDAC2 promotes loss of primary cilia in pancreatic ductal adenocarcinoma. *EMBO Rep.* e201541922.
  - 48) Kodani, A., Salomé Sirerol-Piquer, M., Seol, A., Manuel Garcia-Verdugo, J., and Reiter, J.F. (2013a). Kif3a interacts with Dynactin subunit p150Glued to organize centriole subdistal appendages. *EMBO J.* 32, 597–607.
  - 49) Kodani, A., Salomé Sirerol-Piquer, M., Seol, A., Garcia-Verdugo, J.M., and Reiter, J.F. (2013b). Kif3a interacts with Dynactin subunit p150 Glued to organize centriole subdistal appendages. *EMBO J.* 32, 597–607.
  - 50) Koliarakis, V., Pasparakis, M., and Kollias, G. (2015a). IKK $\beta$  in intestinal mesenchymal cells promotes initiation of colitis-associated cancer. *J. Exp. Med.* 212, 2235–2251.
  - 51) Koliarakis, V., Pasparakis, M., and Kollias, G. (2015b). IKK $\beta$  in intestinal mesenchymal cells promotes initiation of colitis-associated cancer. *J. Exp. Med.* 212, 2235–2251.
  - 52) Koliarakis, V., Pallangyo, C.K., Greten, F.R., and Kollias, G. (2017). Mesenchymal Cells in Colon Cancer. *Gastroenterology* 152, 964–979.
  - 53) Kosinski, C., Li, V.S.W., Chan, A.S.Y., Zhang, J., Ho, C., Tsui, W.Y., Chan, T.L., Mifflin, R.C., Powell, D.W., Yuen, S.T., et al. (2007).

Gene expression patterns of human colon tops and basal crypts and BMP antagonists as intestinal stem cell niche factors. *Proc. Natl. Acad. Sci. U. S. A.* *104*, 15418–15423.

- 54) Kurahashi, M., Nakano, Y., Peri, L.E., Townsend, J.B., Ward, S.M., and Sanders, K.M. (2013). A novel population of subepithelial platelet-derived growth factor receptor  $\alpha$ -positive cells in the mouse and human colon. *Am. J. Physiol. - Gastrointest. Liver Physiol.* *304*, G823–G834.
- 55) Lancaster, M.A., Schroth, J., and Gleeson, J.G. (2011). Subcellular spatial regulation of canonical Wnt signalling at the primary cilium. *Nat. Cell Biol.* *13*, 700–707.
- 56) Lascano, V., Zabalegui, L.F., Cameron, K., Guadagnoli, M., Jansen, M., Burggraaf, M., Versloot, M., Rodermond, H., van der Loos, C., Carvalho-Pinto, C.E., et al. (2012). The TNF family member APRIL promotes colorectal tumorigenesis. *Cell Death Differ.* *19*, 1826–1835.
- 57) Magiera, M.M., and Janke, C. (2013). Investigating Tubulin Posttranslational Modifications with Specific Antibodies. In *Methods in Cell Biology*, J.J.C. and L. Wilson, ed. (Academic Press), pp. 247–267.
- 58) Magiera, M.M., and Janke, C. (2014). Post-translational modifications of tubulin. *Curr. Biol.* *24*, R351–R354.
- 59) el Marjou, F., Janssen, K.-P., Chang, B.H.-J., Li, M., Hindie, V., Chan, L., Louvard, D., Chambon, P., Metzger, D., and Robine, S. (2004). Tissue-specific and inducible Cre-mediated recombination in the gut epithelium. *Genes. N. Y. N* 2000 *39*, 186–193.
- 60) Marszalek, J.R., Ruiz-Lozano, P., Roberts, E., Chien, K.R., and Goldstein, L.S.B. (1999a). Situs inversus and embryonic ciliary morphogenesis defects in mouse mutants lacking the KIF3A subunit of kinesin-II. *Proc. Natl. Acad. Sci. U. S. A.* *96*, 5043–5048.
- 61) Marszalek, J.R., Ruiz-Lozano, P., Roberts, E., Chien, K.R., and Goldstein, L.S. (1999b). Situs inversus and embryonic ciliary morphogenesis defects in mouse mutants lacking the KIF3A subunit of kinesin-II. *Proc. Natl. Acad. Sci. U. S. A.* *96*, 5043–5048.
- 62) Medema, J.P., and Vermeulen, L. (2011). Microenvironmental regulation of stem cells in intestinal homeostasis and cancer. *Nature* *474*, 318–326.

- 63) Menzl, I., Lebeau, L., Pandey, R., Hassounah, N.B., Li, F.W., Nagle, R., Weihs, K., and McDermott, K.M. (2014). Loss of primary cilia occurs early in breast cancer development. *Cilia* 3, 7.
- 64) Miyoshi, Y., Nagase, H., Ando, H., Horii, A., Ichii, S., Nakatsuru, S., Aoki, T., Miki, Y., Mori, T., and Nakamura, Y. (1992). Somatic mutations of the APC gene in colorectal tumors: mutation cluster region in the APC gene. *Hum. Mol. Genet.* 1, 229–233.
- 65) Morin, P.J., Sparks, A.B., Korinek, V., Barker, N., Clevers, H., Vogelstein, B., and Kinzler, K.W. (1997). Activation of beta-catenin-Tcf signaling in colon cancer by mutations in beta-catenin or APC. *Science* 275, 1787–1790.
- 66) Moser, A.R., Pitot, H.C., and Dove, W.F. (1990). A dominant mutation that predisposes to multiple intestinal neoplasia in the mouse. *Science* 247, 322–324.
- 67) Pallangyo, C.K., Ziegler, P.K., and Greten, F.R. (2015). IKK $\beta$  acts as a tumor suppressor in cancer-associated fibroblasts during intestinal tumorigenesis. *J. Exp. Med.* 212, 2253–2266.
- 68) Powell, D.W., Pinchuk, I.V., Saada, J.I., Chen, X., and Mifflin, R.C. (2011). Mesenchymal Cells of the Intestinal Lamina Propria. *Annu. Rev. Physiol.* 73, 213–237.
- 69) Qiu, N., Xiao, Z., Cao, L., Buechel, M.M., David, V., Roan, E., and Quarles, L.D. (2012). Disruption of Kif3a in osteoblasts results in defective bone formation and osteopenia. *J. Cell Sci.* 125, 1945–1957.
- 70) Rocha, C., Papon, L., Cacheux, W., Sousa, P.M., Lascano, V., Tort, O., Giordano, T., Vacher, S., Lemmers, B., Mariani, P., et al. (2014a). Tubulin glycyloses are required for primary cilia, control of cell proliferation and tumor development in colon. *EMBO J.* 33, 2247–2260.
- 71) Rocha, C., Papon, L., Cacheux, W., Marques Sousa, P., Lascano, V., Tort, O., Giordano, T., Vacher, S., Lemmers, B., Mariani, P., et al. (2014b). Tubulin glycyloses are required for primary cilia, control of cell proliferation and tumor development in colon. *EMBO J.* 33, 2247–2260.
- 72) Rogowski, K., Juge, F., van Dijk, J., Wloga, D., Strub, J.-M., Levilliers, N., Thomas, D., Br é M.-H., Van Dorsselaer, A., Gaertig,

- J., et al. (2009). Evolutionary Divergence of Enzymatic Mechanisms for Posttranslational Polyglycylation. *Cell* 137, 1076–1087.
- 73) Roulis, M., Nikolaou, C., Kotsaki, E., Kaffe, E., Karagianni, N., Koliarakis, V., Salpea, K., Ragoussis, J., Aidinis, V., Martini, E., et al. (2014). Intestinal myofibroblast-specific Tpl2-Cox-2-PGE2 pathway links innate sensing to epithelial homeostasis. *Proc. Natl. Acad. Sci. U. S. A.* 111, E4658–E4667.
- 74) Sato, T., van Es, J.H., Snippert, H.J., Stange, D.E., Vries, R.G., van den Born, M., Barker, N., Shroyer, N.F., van de Wetering, M., and Clevers, H. (2011). Paneth cells constitute the niche for Lgr5 stem cells in intestinal crypts. *Nature* 469, 415–418.
- 75) Schneider, L., Clement, C.A., Teilmann, S.C., Pazour, G.J., Hoffmann, E.K., Satir, P., and Christensen, S.T. (2005). PDGFRalpha signaling is regulated through the primary cilium in fibroblasts. *Curr. Biol. CB* 15, 1861–1866.
- 76) Shiga, K., Hara, M., Nagasaki, T., Sato, T., Takahashi, H., and Takeyama, H. (2015). Cancer-Associated Fibroblasts: Their Characteristics and Their Roles in Tumor Growth. *Cancers* 7, 2443–2458.
- 77) Shpak, M., Goldberg, M.M., and Cowperthwaite, M.C. (2014a). Cilia Gene Expression Patterns in Cancer. *Cancer Genomics - Proteomics* 11, 13–24.
- 78) Shpak, M., Goldberg, M.M., and Cowperthwaite, M.C. (2014b). Cilia gene expression patterns in cancer. *Cancer Genomics Proteomics* 11, 13–24.
- 79) Sjöblom, T., Jones, S., Wood, L.D., Parsons, D.W., Lin, J., Barber, T.D., Mandelker, D., Leary, R.J., Ptak, J., Silliman, N., et al. (2006). The Consensus Coding Sequences of Human Breast and Colorectal Cancers. *Science* 314, 268–274.
- 80) Smits, R., Kartheuser, A., Jagmohan-Changur, S., Leblanc, V., Breukel, C., de Vries, A., van Kranen, H., van Krieken, J.H., Williamson, S., Edelmann, W., et al. (1997). Loss of Apc and the entire chromosome 18 but absence of mutations at the Ras and Tp53 genes in intestinal tumors from Apc1638N, a mouse model for Apc-driven carcinogenesis. *Carcinogenesis* 18, 321–327.

- 81) Sohn, O.S., Fiala, E.S., Requeijo, S.P., Weisburger, J.H., and Gonzalez, F.J. (2001). Differential Effects of CYP2E1 Status on the Metabolic Activation of the Colon Carcinogens Azoxymethane and Methylazoxymethanol. *Cancer Res.* *61*, 8435–8440.
- 82) Spassky, N., Han, Y.-G., Aguilar, A., Strehl, L., Besse, L., Laclef, C., Romaguera Ros, M., Garcia-Verdugo, J.M., and Alvarez-Buylla, A. (2008). Primary cilia are required for cerebellar development and Shh-dependent expansion of progenitor pool. *Dev. Biol.* *317*, 246–259.
- 83) Stewart, B., and Wild, C. (2014). World Cancer Report 2014. (WHO), pp. 392–393.
- 84) Suzuki, R., Kohno, H., Sugie, S., and Tanaka, T. (2004). Sequential observations on the occurrence of preneoplastic and neoplastic lesions in mouse colon treated with azoxymethane and dextran sodium sulfate. *Cancer Sci.* *95*, 721–727.
- 85) Tanaka, T. (2012). Development of an Inflammation-Associated Colorectal Cancer Model and Its Application for Research on Carcinogenesis and Chemoprevention. *Int. J. Inflamm.* *2012*, e658786.
- 86) Tanaka, T., Kohno, H., Suzuki, R., Yamada, Y., Sugie, S., and Mori, H. (2003a). A novel inflammation-related mouse colon carcinogenesis model induced by azoxymethane and dextran sodium sulfate. *Cancer Sci.* *94*, 965–973.
- 87) Tanaka, T., Kohno, H., Suzuki, R., Yamada, Y., Sugie, S., and Mori, H. (2003b). A novel inflammation-related mouse colon carcinogenesis model induced by azoxymethane and dextran sodium sulfate. *Cancer Sci.* *94*, 965–973.
- 88) Umberger, N.L., and Caspary, T. (2015). Ciliary transport regulates PDGF-AA/ $\alpha\alpha$  signaling via elevated mammalian target of rapamycin signaling and diminished PP2A activity. *Mol. Biol. Cell* *26*, 350–358.
- 89) Vermeulen, L., De Sousa E Melo, F., van der Heijden, M., Cameron, K., de Jong, J.H., Borovski, T., Tuynman, J.B., Todaro, M., Merz, C., Rodermond, H., et al. (2010). Wnt activity defines colon cancer stem cells and is regulated by the microenvironment. *Nat. Cell Biol.* *12*, 468–476.

- 90) Walther, A., Johnstone, E., Swanton, C., Midgley, R., Tomlinson, I., and Kerr, D. (2009). Genetic prognostic and predictive markers in colorectal cancer. *Nat. Rev. Cancer* 9, 489–499.
- 91) Washington, M.K., Powell, A.E., Sullivan, R., Sundberg, J.P., Wright, N., Coffey, R.J., and Dove, W.F. (2013). Pathology of rodent models of intestinal cancer: progress report and recommendations. *Gastroenterology* 144, 705–717.
- 92) Waters, A.M., and Beales, P.L. (2011). Ciliopathies: an expanding disease spectrum. *Pediatr. Nephrol. Berl. Ger.* 26, 1039–1056.
- 93) van de Wetering, M., Sancho, E., Verweij, C., de Lau, W., Oving, I., Hurlstone, A., van der Horn, K., Batlle, E., Coudreuse, D., Haramis, A.-P., et al. (2002). The  $\beta$ -Catenin/TCF-4 Complex Imposes a Crypt Progenitor Phenotype on Colorectal Cancer Cells. *Cell* 111, 241–250.
- 94) Wirtz, S., Neufert, C., Weigmann, B., and Neurath, M.F. (2007). Chemically induced mouse models of intestinal inflammation. *Nat. Protoc.* 2, 541–546.
- 95) Wong, S.Y., Seol, A.D., So, P.-L., Ermilov, A.N., Bichakjian, C.K., Epstein, E.H., Dlugosz, A.A., and Reiter, J.F. (2009a). Primary cilia can both mediate and suppress Hedgehog pathway-dependent tumorigenesis. *Nat. Med.* 15, 1055–1061.
- 96) Wong, S.Y., Seol, A.D., So, P.-L., Ermilov, A.N., Bichakjian, C.K., Epstein, E.H., Dlugosz, A.A., and Reiter, J.F. (2009b). Primary cilia can both mediate and suppress Hedgehog pathway-dependent tumorigenesis. *Nat. Med.* 15, 1055–1061.
- 97) Yuan, K., Frolova, N., Xie, Y., Wang, D., Cook, L., Kwon, Y.-J., Steg, A.D., Serra, R., and Frost, A.R. (2010). Primary Cilia Are Decreased in Breast Cancer: Analysis of a Collection of Human Breast Cancer Cell Lines and Tissues. *J. Histochem. Cytochem.* 58, 857–870.

## 7. Annex

### 7.1. RNA seq analysis

**Table 1. Deregulated transcripts in colonic mesenchymals of DSS-treated *ColVIcre-Kif3a<sup>flx/flx</sup>* mice display an inflammatory signature.**

CAF-related						
symbol	gene ID	R7-FPKM	R8-FPKM	log2(R8/R7)	Up-Down-Regulation	P-value
TGFBetaR3	21809	13,08	19,87	0,6	Up	1,58E-34
Hif3a	53417	0,49	0,74	0,6	Up	0,0138038
Hgfac	54426	30,52	45,55	0,58	Up	2,93E-26
Igf1r	16001	5,15	7,69	0,58	Up	6,21E-25
Igfbp5	54426	113,42	168,46	0,57	Up	5,34E-243
Megf6	230971	2	2,95	0,56	Up	2,36E-06
Vegfc	22341	15,63	22,58	0,53	Up	6,61E-05
Egfl7	353156	42,9	61,67	0,52	Up	2,43E-19
Tnxb	81877	60,23	83,81	0,48	Up	1,48E-143
P4htm	74443	3,06	4,15	0,44	Up	0,0234874
Vtn	22370	8,85	11,79	0,41	Up	0,000355708
Fgf3	14174	10,05	13,33	0,41	Up	2,83E-09
TGFBeta3	21809	10,3	13,61	0,4	Up	1,87E-07
S100a4	20198	31,25	40,2	0,36	Up	0,00217732
ANGPT2	11601	70,31	89,79	0,35	Up	7,91E-33
S100a14	66166	41,78	52,91	0,34	Up	9,59E-07
Mif	17319	71,95	90,36	0,33	Up	1,27E-05
Hif1a	15251	26,03	32,39	0,32	Up	1,91E-14
Fgf1	14164	26,35	32,77	0,32	Up	4,19E-15
Acta2	11475	719,21	872,63	0,28	Up	1,35E-145
TGFBeta2	21808	11,87	13,91	0,23	Up	0,000260554
Cxcr4	12767	26,17	30,72	0,23	Up	0,000724454
FN1	14268	231,13	263,9	0,19	Up	6,30E-67
TGFBeta1	21803	45,63	52,11	0,19	Up	5,50E-05
Tgfb1i1	21804	34,42	39,25	0,19	Up	3,37E-06
Loxl2	94352	63,93	72,13	0,17	Up	2,25E-11
S100a11	20195	373,17	406,02	0,12	Up	0,000758274
CTGF	14219	58,89	64,08	0,12	Up	0,0025235
Cxcl12	20315	216,8	220,04	0,02	Up	3,32E-05
S100a6	20200	764,22	721,16	-0,08	Down	9,96E-05
Tnc	21923	168,79	157,94	-0,1	Down	1,75E-11
Egfr	13649	11,67	10,71	-0,12	Down	0,00398372
EGFR	13649	11,67	10,71	-0,13	Down	0,00398372
S100a10	20194	331,27	296,93	-0,16	Down	6,29E-06
Cxcl1	14825	62,11	55,13	-0,17	Down	0,00900196
Postn	50706	724,72	634,97	-0,19	Down	8,35E-73
Areg	11839	111,03	96,39	-0,2	Down	3,52E-06
Ptgs2	19225	73,51	60,96	-0,27	Down	1,03E-21
Fgf9	14180	3,37	2,62	-0,36	Down	0,00925678
IL6	16193	9,83	7,21	-0,45	Down	0,0046274

Wnt						
symbol	gene ID	R7-FPKM	R8-FPKM	log2(R8/R7)	Up-Down-Regulation	P-value
Fzd10	93897	0,23	0,6	1,38	Up	0,0028
Cldn4	12740	18,26	35,66	0,97	Up	4,16E-41
TCF15	21407	2,27	4,03	0,83	Up	0,00477702
FOXD3	15221	2,49	4,28	0,78	Up	9,24E-06
FOXC1	17300	1,01	1,7	0,75	Up	0,000393402
Sox18	20672	13,83	22,61	0,71	Up	1,26E-14
Gja5	14613	2,64	4,32	0,71	Up	1,89E-06
Wnt6	22420	1,49	2,41	0,69	Up	0,005
Hgfac	54426	30,52	45,55	0,58	Up	2,93E-26
Sox17	20671	4,47	6,47	0,53	Up	7,51E-07
Sox7	20680	9,59	13,61	0,51	Up	2,32E-10
Tcf7l1	21415	13,97	19,72	0,5	Up	2,16E-12
Epha2	13836	24,95	35,15	0,5	Up	7,34E-28
Cldn5	12741	21,33	29,73	0,48	Up	6,15E-09
Jag2	16450	5,13	7	0,45	Up	5,95E-06
Gja4	14612	9,81	13,36	0,45	Up	7,03E-05
Fzd6	14368	3,54	4,7	0,41	Up	0,0006
FgfR3	14184	10,05	13,33	0,41	Up	2,83E-09
Fzd4	14366	10,17	13,4	0,4	Up	9,75E-08
Sox10	20665	9,22	12,14	0,4	Up	1,45E-05
Mmp28	118453	7,33	9,39	0,36	Up	0,00014083
FOXQ1	15220	5,89	7,56	0,36	Up	0,001436524
Tcf3	21423	15,02	19,15	0,35	Up	7,67E-08
FO XK1	17425	9,74	12,35	0,34	Up	2,25E-10
FgfR1	14182	26,35	32,77	0,32	Up	4,19E-15
Jund	16478	264,92	329,43	0,32	Up	1,15E-78
Fzd8	14370	5,6	6,9	0,3	Up	0,005
Junb	16477	862,09	1057,51	0,3	Up	1,86E-139
Cdk9	107951	15,3	18,61	0,28	Up	1,20E-05
EphB	270190	28,79	34,64	0,27	Up	1,73E-10
LRP5	16973	30,49	36,45	0,26	Up	4,63E-12
Fzd7	14369	8,15	9,67	0,24	Up	0,00096
FOXO3	56484	11,76	13,93	0,24	Up	0,00235394
cyclin D2	12444	37,5	43,67	0,22	Up	6,10E-12
Cldn3	12739	156,89	181,07	0,21	Up	1,02E-09
FOXO1	56458	12,23	14,13	0,21	Up	0,00027157
FN1	14268	231,13	263,9	0,19	Up	6,30E-67
Ephb3	13845	9,24	10,46	0,18	Up	0,0184601
Sox13	20668	15,84	17,89	0,18	Up	0,00546508
Mmp15	17388	30,2	33,88	0,17	Up	6,63E-05
Foxp1	108655	19,83	22,32	0,17	Up	8,36E-06
Tcf7l2	21416	8,89	9,9	0,16	Up	0,0523714
Grem2	23893	28,73	32,15	0,16	Up	0,000401988
Foxp4	74123	31,93	35,77	0,16	Up	9,24E-05
Dickkopf2	56811	23,55	19,94	0,13	Down	0,00026
Sox9	20682	16,13	17,59	0,13	Up	0,034205



<b>DKK3</b>	50781	69,69	75,66	0,12	Up	0,000156213
<b>Ets2</b>	23872	85,31	92,45	0,12	Up	2,64E-05
<b>Tcf4</b>	21413	26,76	28,53	0,09	Up	0,00840246
<b>LRP6</b>	16974	17,96	16,66	-0,11	Down	0,00422294
<b>cyclin M4</b>	94220	42,23	38,55	-0,13	Down	0,00023917
<b>cyclin A2</b>	12428	13,5	11,6	-0,22	Down	0,0078215
<b>Wn5a</b>	22418	23,55	19,94	-0,24	Down	8,62E-06
<b>Wnt4a</b>		14,82	12,5	-0,25	Down	0,00027
<b>TCF7</b>	21414	13,35	10,5	-0,35	Down	6,02E-05
<b>cdk1</b>	12534	5,77	4,16	-0,47	Down	0,000295818
<b>Cldn8</b>	54420	17,03	12,34	-0,47	Down	2,71E-08

<b>Notch</b>						
<b>symbol</b>	<b>gene ID</b>	<b>R7-FPKM</b>	<b>R8-FPKM</b>	<b>log2(R8/R7)</b>	<b>Up-Down-Regulation</b>	<b>P-value</b>
<b>Hes1</b>	15205	168,68	184,71	0,13	Up	1,70E-05
<b>Krt36</b>	16673	3,75	7,2	0,94	Up	1,73E-08
<b>Krt23</b>	94179	4,15	6,49	0,65	Up	0,000194761
<b>DLL4</b>	54485	13,66	20,89	0,61	Up	1,04E-21
<b>Notch4</b>	18132	4,83	7,34	0,6	Up	7,33E-15
<b>HEY1</b>	15231	6,3	9,43	0,58	Up	9,53E-07
<b>Notch3</b>	18131	15,63	22,58	0,53	Up	2,06E-40
<b>Dtx1</b>	14357	6,24	8,44	0,44	Up	3,60E-06
<b>FOSL1</b>	16598	24,8	32,85	0,41	Up	8,56E-09
<b>Fosl1</b>	14283	24,8	32,85	0,41	Up	8,56E-09
<b>Hes6</b>	55927	24,23	30,56	0,34	Up	4,28E-05
<b>Sta5a</b>	20850	4,86	5,85	0,27	Up	0,01910266
<b>Krt18</b>	16668	262,51	311,66	0,25	Up	9,42E-24
<b>DLL1</b>	13388	12,87	15,09	0,23	Up	0,001122266
<b>PINK1</b>	68934	61,45	69,01	0,17	Up	2,30E-05
<b>Fos</b>	14281	1208,07	1329,24	0,14	Up	1,33E-47
<b>Fosb</b>	14282	838,12	881,2	0,07	Up	4,48E-17
<b>Stat3</b>	20848	48,93	51,23	0,07	Up	0,0421854
<b>NEDD4</b>	17999	198,03	205,17	0,05	Up	0,0005
<b>Notch1</b>	18128	16,61	19,57	0,024	Up	2,21E-10
<b>Krt4</b>	16882	1356,94	1309,2	-0,05	Down	2,01E-07
<b>Stat1</b>	20846	19,63	14,23	-0,46	Down	9,38E-19

Genes were grouped according to their annotations for cancer associated fibroblasts (CAFs), Wnt and Notch signaling. RNA was isolated from fibroblasts of distal parts of colons from 4 month old ColVIcre-*Kif3a*<sup>flx/flx</sup> (R8) and control (R7) mice , pooled and analyzed by RNA seq as described in the material and methods section.

FPKM represents gene expression corrected to gene length and sequencing discrepancy and the log2 of (FPKMs of R8/R7) represents the value of differentially expressed genes.

**Table 2. Upregulated transcripts in colons of DSS-treated *ColVIcre-Kif3a<sup>flx/flx</sup>* mice display an inflammatory signature.**

Colitis					
Symbol	geneID	R5-FPKM	R6-FPKM	log2 (R6/R5)	P-value
Pla2g4b	211429	0,01	0,43	5,43	4E-08
Metrn1	210029	22,36	29,99	0,42	6E-11
Myo7a	17921	1,89	2,9	0,62	1E-06
Cancer related					
Symbol	geneID	R5-FPKM	R6-FPKM	log2 (R6/R5)	P-value
Fgf23	64654	0,08	0,76	3,25	5E-07
Fosb	14282	2,01	14,89	2,89	1E-140
Ceacam12	67315	1,49	6,63	2,15	3E-12
Ido1	15930	21,23	78,23	1,88	7E-174
Oip5	70645	0,78	2,18	1,48	9E-05
Pttg1	30939	13,15	27,71	1,08	6E-13
Adm	11535	7,11	14,3	1,01	8E-13
Shcbl1	20419	3,44	6,21	0,85	1E-07
Chrdl2	69121	9,18	16,17	0,82	2E-11
Hif1a	15251	47,09	81,23	0,79	2E-147
Fam3b	52793	114,5	195,98	0,78	3E-63
Bcl3	12051	31,08	52,78	0,76	1E-36
Tacc3	21335	6,95	11,68	0,75	2E-12
Ereg	13874	2,39	5,9	1,30	7E-23
Gch1	14528	11,88	19,58	0,72	2E-19
Higd1a	56295	34,84	49,6	0,51	5E-18
Nme1	18102	32	49,15	0,62	1E-16
Pttg1	30939	13,15	27,71	1,08	6E-13
Adm	11535	7,11	14,3	1,01	8E-13
Tacc3	21335	6,95	11,68	0,75	2E-12
Ceacam12	67315	1,49	6,63	2,15	3E-12
Chrdl2	69121	9,18	16,17	0,82	2E-11
Ranbp1	19385	84,38	110,57	0,39	2E-11
Plagl2	54711	14,99	19,23	0,36	2E-11
Rab22a	19334	24,83	34,16	0,46	4E-11
Dirc2	224132	10,31	14,04	0,45	2E-10
Fos	14281	47,55	58,76	0,31	5E-10
Mtmr7	54384	8,29	11,74	0,50	2E-08
Cdcp1	109332	17,33	21,75	0,33	4E-08
Myeov2	66915	94,37	125,93	0,42	5E-08
Ect2	13605	3,9	5,87	0,59	5E-07
Rab21	216344	30,83	38,13	0,31	3E-06
Racgap1	26934	9,29	12,52	0,43	4E-06
Rhof	23912	14,99	19,44	0,38	1E-05
Fgfr1op	75296	3,92	5,85	0,58	1E-05
Gadd45g	23882	8,14	13,02	0,68	2E-05
Depdc1a	76131	2,39	3,88	0,70	2E-05
Oip5	70645	0,78	2,18	1,48	9E-05

inflammation and immune responses					
Symbol	geneID	R5-FPKM	R6-FPKM	log2 (R6/R5)	P-value
Il6	16193	0,45	3,21	2,83	4E-10
Ifng	15978	0,59	3,56	2,59	1E-10
Tgtp1	21822	5,14	30,2	2,55	1E-184
Ccl7	20306	2,37	13,01	2,46	2E-25
Ifit2	15958	7,01	37,51	2,42	1E-302
Gm17757	100417829	0,95	4,72	2,31	2E-41
Ccl2	20296	2,42	11,85	2,29	4E-19
Igtp	16145	15,61	73,72	2,24	5E-281
Cxcl9	17329	4,33	18,89	2,13	6E-97
Cxcl1	14825	2,46	9,52	1,95	2E-15
Socs1	12703	4,61	17,59	1,93	2E-34
Gzma	14938	2,46	8,98	1,87	1E-12
Cxcl10	15945	8,86	31,69	1,84	2E-51
Cxcl5	20311	7,68	27,3	1,83	2E-65
Irgm2	54396	12,67	44,3	1,81	5E-221
Ifi47	15953	8,99	30,27	1,75	1E-71
Gbp4	17472	3,45	11,07	1,68	5E-65
Marco	17167	1,35	4,23	1,65	8E-12
Tgtp2	100039796	6,67	20,86	1,64	6E-74
Irgm1	15944	23,86	73,68	1,63	5E-199
Gbp2	14469	39,93	113,45	1,51	6E-304
Gata3	14462	0,62	1,73	1,48	2E-07
Gzmb	14939	2,35	6,48	1,46	7E-11
Ifit3b	667370	3,16	8,56	1,44	5E-19
Ifi202b	26388	1,14	3,01	1,40	1E-06
Tifa	211550	21,37	55,27	1,37	1E-113
Il18bp	16068	5,83	13,96	1,26	9E-18
Gm4841	225594	2,62	6,15	1,23	2E-15
Nlrc5	434341	1,88	4,35	1,21	3E-25
Ripk3	56532	13,94	31,66	1,18	1E-46
Il11	16156	2,61	5,76	1,14	3E-09
Tnfrsf8	21941	2,34	5,06	1,11	8E-07
Tnfsf10	22035	4,97	10,71	1,11	2E-37
Ifi205	226695	5,92	12,61	1,09	8E-15
Gbp5	229898	6,69	14,04	1,07	1E-28
Cd38	12494	61,14	127,88	1,06	5E-245
Ly6c1	17067	49,64	102,81	1,05	3E-54
Nr4a1	15370	4,59	9,47	1,04	3E-16
Chil1	12654	3,85	7,91	1,04	1E-09
Socs3	12702	22,88	46,53	1,02	2E-77
Batf2	74481	14,64	29	0,99	2E-24
Stat1	20846	19,65	38,54	0,97	1E-110
Pbk	52033	5,95	11,43	0,94	3E-11
Tnfrsf1b	21938	14,73	28,13	0,93	1E-72
Plat	18791	7,88	15,02	0,93	3E-21
Nfkbiz	80859	26,7	50,16	0,91	7E-91

Egr1	13653	13,93	25,91	0,90	1E-39
Irf8	15900	29,54	53,9	0,87	7E-71
Birc5	11799	15,72	28,67	0,87	3E-10
Ptk6	20459	10,7	19,5	0,87	1E-21
Casp4	12363	38,02	69,02	0,86	2E-45
Ccr5	12774	2,82	5,07	0,85	5E-08
Lbp	16803	4,47	7,99	0,84	4E-10
Tnf	21926	4,98	8,84	0,83	4E-08
Snx10	71982	10,29	18,1	0,81	4E-20
Ccl8	20307	46,3	80,53	0,80	6E-17
Ifit1	15957	9,2	15,78	0,78	3E-17
Rtp4	67775	15,33	26,24	0,78	8E-17
Steap4	117167	22,84	38,83	0,77	4E-46
Selp	20344	2,46	4,17	0,76	1E-06
Ly6g	546644	84,93	141,2	0,73	1E-44
Slpi	20568	65,99	109,56	0,73	1E-33
Cd274	60533	5,12	11,33	1,15	2E-31
Casp7	12369	72,78	97,64	0,42	1E-30
Gbp5	229898	6,69	14,04	1,07	1E-28
Ctsc	13032	24,6	32,18	0,39	1E-28
Psmb10	19171	69,18	101,03	0,55	5E-27
Ccl7	20306	2,37	13,01	2,46	2E-25
Nlr5	434341	1,88	4,35	1,21	3E-25
Serp1	28146	86,75	110,19	0,35	5E-25
Batf2	74481	14,64	29	0,99	2E-24
Tnfaip3	21929	19,53	27,98	0,52	5E-24
Ifitm3	66141	170,51	234,77	0,46	4E-23
Stat2	20847	9,99	15,92	0,67	4E-22
Ptk6	20459	10,7	19,5	0,87	1E-21
Plat	18791	7,88	15,02	0,93	3E-21
Ccl2	20296	2,42	11,85	2,29	4E-19
Il18bp	16068	5,83	13,96	1,26	9E-18
Nox1	237038	24,69	35,21	0,51	1E-17
Appl1	72993	9,08	12,9	0,51	2E-17
Ifit1	15957	9,2	15,78	0,78	3E-17
Il4ra	16190	17,66	23,72	0,43	4E-17
Ccl8	20307	46,3	80,53	0,80	6E-17
Hsd17b12	56348	68,23	87,77	0,36	7E-17
Rtp4	67775	15,33	26,24	0,78	8E-17
Gm4841	225594	2,62	6,15	1,23	2E-15
Cxcl1	14825	2,46	9,52	1,95	2E-15
Skap2	54353	42,58	58,26	0,45	3E-15
Ifi205	226695	5,92	12,61	1,09	8E-15
Nab1	17936	14,33	19,35	0,43	9E-15
Trafd1	231712	20,29	28,87	0,51	3E-14
Mall	228576	61,88	77,76	0,33	1E-13
Gzma	14938	2,46	8,98	1,87	1E-12
Icam1	15894	9,22	14,69	0,67	2E-12
Tnfrsf1a	21937	46,22	58,52	0,34	3E-12

Ly75	17076	5,18	8	0,63	3E-12
Ifit1bl2	112419	8,59	13,05	0,60	3E-12
Marco	17167	1,35	4,23	1,65	8E-12
Capn13	381122	30,67	39,45	0,36	2E-11
Pbk	52033	5,95	11,43	0,94	3E-11
Smad1	17125	16,02	21,82	0,45	5E-11
Gzmb	14939	2,35	6,48	1,46	7E-11
Ifng	15978	0,59	3,56	2,59	1E-10
Tlr4	21898	7,45	9,85	0,40	2E-10
Cd47	16423	22,03	30,53	0,47	2E-10
Il6	16193	0,45	3,21	2,83	4E-10
Lbp	16803	4,47	7,99	0,84	4E-10
Chil1	12654	3,85	7,91	1,04	1E-09
Irf9	16391	21,24	28,14	0,41	2E-09
Il11	16156	2,61	5,76	1,14	3E-09
Plgrkt	67759	69,65	90,55	0,38	4E-09
Thy1	21838	21,94	30,06	0,45	5E-09
Cyr61	16007	6,8	11,2	0,72	6E-09
Noxo1	71893	32,91	40,99	0,32	3E-08
Tnf	21926	4,98	8,84	0,83	4E-08
Ccr5	12774	2,82	5,07	0,85	5E-08
Ifitm1	68713	32	46,84	0,55	7E-08
Traf4	22032	13,91	18,25	0,39	2E-07
Igsf5	72058	34,75	44,01	0,34	2E-07
Gata3	14462	0,62	1,73	1,48	2E-07
Tnfrsf8	21941	2,34	5,06	1,11	8E-07
Noxa1	241275	15,58	21,52	0,47	9E-07
Tec	21682	7,93	11,29	0,51	1E-06
Selp	20344	2,46	4,17	0,76	1E-06
Ifi202b	26388	1,14	3,01	1,40	1E-06
Ccr1	12768	5,32	7,96	0,58	1E-06
Mif	17319	73,43	93,97	0,36	6E-06
Ikzf1	22778	2,97	4,49	0,60	9E-06
Pla2g4f	271844	8,14	10,91	0,42	1E-05
Nmi	64685	27,8	35,41	0,35	1E-05
Mydgf	28106	56,12	69,33	0,30	1E-05
Il33	77125	5,61	8,2	0,55	1E-05
Cxcl16	66102	15,27	19,44	0,35	1E-05
Ifi204	15951	5,16	7,77	0,59	1E-05
Ncf2	17970	12,02	14,98	0,32	2E-05
Tcf7	21414	4,5	6,81	0,60	2E-05
Tlr3	142980	9,37	11,65	0,31	5E-05

**cell cycle and regulation**

Symbol	geneID	R5-FPKM	R6-FPKM	log2 (R6/R5)	P-value
Saxo1	75811	0,38	1,36	1,84	8E-05
Mmp3	17392	6,21	14,16	1,19	1E-20
Dynlt1b	21648	10,62	21,62	1,03	3E-11
Mmp13	17386	5,18	10,22	0,98	1E-16

Cenpu	71876	1,88	3,66	0,96	3E-06
Ccne1	12447	1,74	3,37	0,95	6E-05
Cdc45	12544	1,86	3,56	0,94	1E-05
Nuf2	66977	3,28	6,06	0,89	2E-08
Rilpl2	80291	8,79	16,19	0,88	6E-11
E2f8	108961	3,11	5,57	0,84	2E-10
E2f2	242705	5,7	10,11	0,83	4E-21
sept-01	54204	6,62	11,54	0,80	4E-08
Nek2	18005	5,15	8,62	0,74	3E-11
Ankrd22	52024	4,83	8,08	0,74	2E-06
Capn12	60594	27,52	45,97	0,74	2E-46
Kif22	110033	6,37	10,63	0,74	4E-09
Aurkb	20877	5,61	9,35	0,74	9E-08
Tuba4a	22145	37,61	58,22	0,63	1E-32
Anxa4	11746	141,56	178,83	0,34	4E-31
Pak1	18479	31,07	45,17	0,54	5E-29
Casp8	12370	48,17	67,56	0,49	7E-29
Itga3	16400	35,78	46,93	0,39	9E-27
Plekham1	353047	17,03	24,72	0,54	1E-26
Pls1	102502	79,26	97,74	0,30	5E-26
Mapk13	26415	178,04	219,66	0,30	3E-22
E2f2	242705	5,7	10,11	0,83	4E-21
Capg	12332	54,71	78,8	0,53	5E-21
Mmp3	17392	6,21	14,16	1,19	1E-20
Snx10	71982	10,29	18,1	0,81	4E-20
Lamc2	16782	25,38	32,94	0,38	5E-19
Ccna2	12428	19,02	27,77	0,55	2E-17
Bnip3	12176	27,48	40,82	0,57	5E-17
Cdc42se1	57912	25,19	35,25	0,48	5E-17
Stx7	53331	54,89	69,85	0,35	7E-17
Mmp13	17386	5,18	10,22	0,98	1E-16
Nme1	18102	32	49,15	0,62	1E-16
Nr4a1	15370	4,59	9,47	1,04	3E-16
Nsf	18195	18,17	25,13	0,47	5E-16
Cdc25a	12530	10,8	16,16	0,58	8E-15
Tuba1c	22146	40,74	54,43	0,42	8E-15
Stk40	74178	23,16	30,91	0,42	9E-15
Ckap4	216197	21,41	29,63	0,47	9E-15
Mapk6	50772	35,81	44,23	0,30	2E-14
Itgav	16410	11,15	14,84	0,41	3E-14
Vmp1	75909	35,32	45,65	0,37	5E-14
Pcna	18538	59,63	79,63	0,42	1E-13
Mapklip11	218975	27,69	34,52	0,32	4E-13
Ralgapa2	241694	12,82	15,96	0,32	6E-13
Rmdn3	67809	31,97	42,01	0,39	5E-12
Incenp	16319	11,06	16,11	0,54	7E-12
Dynlt1b	21648	10,62	21,62	1,03	3E-11
Kif11	16551	7,36	10,59	0,52	3E-11
Arhgap17	70497	25,11	32,36	0,37	3E-11

Nek2	18005	5,15	8,62	0,74	3E-11
Rilpl2	80291	8,79	16,19	0,88	6E-11
Cend1	12443	24,66	30,97	0,33	8E-11
E2f8	108961	3,11	5,57	0,84	2E-10
Sh3kbp1	58194	7,65	11,09	0,54	6E-10
Akt3	23797	5,59	8,25	0,56	8E-10
Tapbp1	213233	22,18	29,86	0,43	1E-09
Cdc20	107995	11,6	17,86	0,62	1E-09
Tapbp1	213233	22,18	29,86	0,43	1E-09
Cdc20	107995	11,6	17,86	0,62	1E-09
Rangap1	19387	26,62	33,45	0,33	3E-09
Kif22	110033	6,37	10,63	0,74	4E-09
Pla2g2a	18780	31,81	46,55	0,55	5E-09
Vps37b	330192	17	22,74	0,42	1E-08
Osmr	18414	5,73	8,12	0,50	2E-08
Nuf2	66977	3,28	6,06	0,89	2E-08
Dynlt1a	100310872	9,66	12,63	0,39	3E-08
Hbegf	15200	8,83	13,1	0,57	3E-08
Fas	14102	10,83	16,15	0,58	3E-08
Pla2g4b	211429	0,01	0,43	5,43	4E-08
sept-01	54204	6,62	11,54	0,80	4E-08
Muc1	17829	7,77	11,87	0,61	5E-08
Vps29	56433	32,14	44,19	0,46	9E-08
Aurkb	20877	5,61	9,35	0,74	9E-08
Dynlt1f	100040531	19,23	29,76	0,63	1E-07
Prc1	233406	8,73	12,23	0,49	1E-07
Shcbl1	20419	3,44	6,21	0,85	1E-07
Aurka	20878	6,57	10,57	0,69	2E-07
Cdk1	12534	6,17	9,2	0,58	3E-07
Cdca3	14793	19,94	27,3	0,45	3E-07
Epha4	13838	2,17	3,37	0,64	3E-07
Nrarp	67122	7,04	10,37	0,56	4E-07
Cks2	66197	31,73	45,59	0,52	4E-07
S100a4	20198	26,24	41,33	0,66	5E-07
Ccnbl1	268697	8,58	12,41	0,53	5E-07
Fgf23	64654	0,08	0,76	3,25	5E-07
Hspe1	15528	70,88	89,29	0,33	6E-07
S100a8	20201	96,59	128,13	0,41	7E-07
Tpx2	72119	7,28	9,84	0,43	7E-07
Arpin	70420	24,61	30,71	0,32	2E-06
Adamts1	11504	2,2	3,5	0,67	2E-06
Anln	68743	3,9	5,48	0,49	2E-06
Mmp10	17384	6,12	9,76	0,67	2E-06
Ankrd22	52024	4,83	8,08	0,74	2E-06
Cenpu	71876	1,88	3,66	0,96	3E-06
Plaur	18793	11,5	16,66	0,53	3E-06
Nlrc4	268973	13,41	16,71	0,32	3E-06
Sdf2l1	64136	27,28	36,26	0,41	3E-06
Shf	435684	6,56	10,46	0,67	4E-06

Pard6b	58220	7,89	10,56	0,42	6E-06
Bub1b	12236	5,71	7,87	0,46	9E-06
Cdc45	12544	1,86	3,56	0,94	1E-05
Lamtor3	56692	27,55	35,38	0,36	1E-05
Cdc25b	12531	5,12	7,35	0,52	2E-05
Kif23	71819	7,59	9,99	0,40	3E-05
Ccnf	12449	3,09	4,76	0,62	4E-05
Ccnb2	12442	12,86	17,49	0,44	4E-05
Ncoa7	211329	7,12	10,72	0,59	5E-05
Ccncl	12447	1,74	3,37	0,95	6E-05
Gmnn	57441	11,82	17,34	0,55	7E-05
Kif4	16571	3,74	5,11	0,45	8E-05
Saxo1	75811	0,38	1,36	1,84	8E-05
Cemip	80982	0,99	1,58	0,67	8E-05
Emb	13723	4,65	6,72	0,53	9E-05
Tbc1d1	57915	6,45	8,04	0,32	9E-05

#### Fibroblasts

Symbol	geneID	R5-FPKM	R6-FPKM	log2 (R6/R5)	P-value
Areg	11839	11,49	29,48	1,36	2E-34
Ereg	13874	2,39	5,9	1,30	7E-23

#### Cell death

Symbol	geneID	R5-FPKM	R6-FPKM	log2 (R6/R5)	P-value
Cd274	60533	5,12	11,33	1,15	2E-31
Parp14	547253	18,07	29,84	0,72	1E-73
Cox5a	12858	242,57	322,42	0,41	9E-28
Parp12	243771	36,72	49,87	0,44	3E-24
Apaf1	11783	5,78	9,02	0,64	1E-17
Cox7a2	12866	188,64	233,36	0,31	2E-13
Uqcr11	66594	327,73	403,7	0,30	2E-12
Pdcd10	56426	49,52	62,09	0,33	9E-11
Birc5	11799	15,72	28,67	0,87	3E-10
Cnot6	104625	14,46	18,04	0,32	9E-09
Cstb	13014	94,61	120,18	0,35	1E-07
Osgin1	71839	5,54	8,18	0,56	8E-05

RNA was isolated from distal parts of colons from DSS-treated ColVICre-*Kif3a*<sup>flx/flx</sup> (R6) and control (R5) mice display and analyzed by RNA seq as described in the material and methods section.

FPKM represents gene expression corrected to gene length and sequencing discrepancy and the log2 of (FPKM of R6/R5) represents the value of differentially expressed genes. Genes were selected for a log2 of (FPKM of R6/R5) value above 0,3 and filtered for a p-value below 1E-04.



## 7.2. CV

### Personal Information

**Nationality:** P. R. China

**Gender:** Male

**Date of Birth:** Dec. 24, 1987    **Phone:** 06 17 11 58 17    **E-mail:** ruizhi.tang@igmm.cnrs.fr

**Postal Address:** IGMM, 1919 Route de Mende, 34293 Montpellier, France

**Personal website:** <https://fr.linkedin.com/pub/ruizhi-tang/9b/93/a50>

### Education

**Sept. 2013-Present:** PhD candidate in Sciences Chimiques et Biologiques pour la Santé  
Université de Montpellier

**Sept. 2010-Nov. 2012:** M.S. in Biochemistry and Molecular Biology, University of Science  
and Technology of China (USTC)

**Sept. 2006-Jul. 2010:** B.S in Biotechnology, Inner Mongolia University (IMU)

### Research Experience

● **Sept. 2013-Present:** Graduate research at L'institut de Génétique Moléculaire de  
Montpellier, France

**Advisor:** DR2 Michael Hahne

**Thesis:** The role of PC in colon homeostasis and tumor development

● **Sept. 2010-Nov. 2012:** Graduate research in School of Life Sciences, USTC, China

**Advisor:** Prof. Jun Wang

**Thesis:** Mixed micellar nanoparticles for tumor associated macrophage targeted delivery

● **Sept. 2007-Jul. 2010:** Undergraduate research in School of Life Sciences, IMU, China

**Advisor:** Prof. Wanjin Xing

**Thesis:** Distribution of PDIA3 transcript and protein in rat testis and sperm cells

## Awards

- [1] Outstanding Student Leaders of University of Science and Technology of China in 2011
- [2] Outstanding Graduates of Inner Mongolia Autonomous Region in 2010
- [3] Outstanding Student Leaders of Inner Mongolia University in 2007, 2008, 2009
- [4] The First Prize of Excellent Student Scholarship in 2007, 2008, 2009 and 2010

## Publications

- [1] Tian-Meng Sun, Yu-Cai Wang, Feng Wang, Jin-Zhi Du, Cheng-Qiong Mao, Chun-Yang Sun, **Rui-Zhi Tang**, Yang Liu, Jing Zhu, Yan-Hua Zhu, Xian-Zhu Yang, Jun Wang\*. Cancer stem cell therapy using doxorubicin conjugated to gold nanoparticles via hydrazone bonds. *Biomaterials*, 2014; 35(2): 836-845.
- [2] Xi-Qiu Liu, Meng-Hua Xiong, Hong-Xia Wang, Xiao-Ting Shu, **Rui-Zhi Tang**, Jun Wang\*. Therapeutic Delivery of siRNA Silencing HIF-1 Alpha with Micellar Nanoparticles Inhibits Hypoxic Tumor Growth. *Molecular Pharmaceutics*, 2012; 9(10): 2863–2874.
- [3] Zhao XJ, **Tang RZ** (co-first author), Wang ML, Guo WL, Liu J, Xing WJ\*. Distribution of PDIA3 transcript and protein in rat testis and sperm cells. *Reproduction in Domestic Animals*, 2013 Feb; 48(1):59-63

## Social activities

**Jan. 2017-Present:** President of L'association des Etudiants et Chercheurs Chinois de L'université de Montpellier

**Sept. 2011-Jul. 2012:** Vice president of Graduate Student Union in School of Life Sciences, USTC

**Sept. 2006-Jul. 2010:** Class president in School of Life Sciences, IMU

## **Courses taken during my PhD (provided by the University of Montpellier or the Doctoral School of Montpellier (CBS2))**

FLE - Français Langue Etrangère, 2014

Preparing a research project and taking notes on scientific literature, 2014

Cancer biology seminars, 2014

Writing a scientific paper step by step, 2015

Formation de niveau 1 en experimentation animale, 2015

France-BioImaging Advanced Training course (FBI-AT), 2016

Dépot électronique de la thèse : présentation générale et aspects juridiques, 2016

## **Conferences**

*IGMM internal seminars* in 2014, 2015 and 2016, oral presentations

*Journée scientifique IGMM*, 2014, poster presentation

*Doctoral school (CBS2)* 2015, oral presentation

*Les 2<sup>èmes</sup> Journées du Réseau France Microtubules*, 2015, oral presentation

*Cilia 2016* (EMBO conference), poster presentation

*Cilia & Centrosomes* (Cold Spring Harbor Asia meeting), oral and poster presentation

### **7.3. Involvement in other projects during my PhD**

#### **Participation in other projects in our group:**

1) The role of cyclin A2 in CRC:

I trained Yuchen Guo, a PhD student in our group who started one year later, to isolate colon from mice, colonic mesenchymal cells and epithelial cells, immunohistochemical methods and related methods.

2) The role of the anti-apoptotic protein BAG3 (BCL2 Associated Athanogene 3) in CRC:

I helped to establish BAG3<sup>flx/flx</sup> cre-villin mice.

3) Generation of agonistic monoclonal antibodies against TNF-receptors BCMA and TACI:

I trained Yuchen Guo, PhD student in our group, to generate monoclonal antibodies.